Sasol Advanced Fuels Laboratory

UNIVERSITY OF CAPE TOWN

Investigation of combustion image analysis by the two-colour method as a technique for comparing diesel fuels

Author:

Adrian Velaers

Supervised by:

Mr Paul Schaberg, Dr Andy Yates and Mr André Swarts

A dissertation submitted to the Department of Mechanical Engineering, University of Cape Town, in partial fulfilment of the requirements for the degree of Master of Science in Engineering

Cape Town, South Africa
31 March 2006

Declaration

1. I know the meaning of plagiarism and declare that all the work in the document, save for that which is properly acknowledged, is my own.

2. I have used the Harvard convention for citation and referencing. Each significant contribution to, and quotation in this project from the works of other people has been attributed, and has been cited and referenced.

3. I have not allowed, and will not allow anyone to copy my work with the intention of passing it off as his or her own work.

Signature _____

Acknowledgements

This project was initiated and sponsored by:

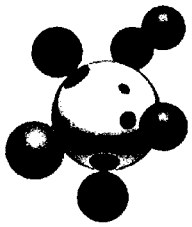

Sasol Technology Fuels Research funded this project and is gratefully acknowledged.

The writer wishes to thank the following people for their tremendous help in making this project successful:

Mr Paul Schaberg – Project supervisor, SAFL

Dr Andy Yates – Project co-supervisor, SAFL

Mr André Swarts – Project co-supervisor, SAFL

Mr Geoff Miller – Assistance with the combustion bomb, Sasol

Mr Murangi Ratshikuni – Assistance in this project which has followed on from his M.Sc Project, Sasol

Mr Etienne Eccles – Electrical engineering assistance with the combustion bomb trigger circuit

Mr Peter Werlberger – Support with the AVL Visioscope, AVL

Terms of reference

In March 2004, Mr Paul Schaberg of the Sasol Advanced Fuels Laboratory at UCT initiated this project. Sasol has invested in considerable equipment to facilitate direct imaging of diesel combustion, both in an engine and a constant volume bomb. Furthermore it has acquired a propriety software system to scientifically analyse such images. It is envisaged that this equipment be used as a research tool to compare fuels and to better understand diesel combustion. In order to successfully achieve this, the method of combustion imaging and image analysis needs to be mastered and understood.

The specific instructions of the Sasol Advanced Fuels Laboratory were to:

1) Modify the cylinder head of the Hydra engine to accommodate a modern water cooled pressure transducer and ensure that by this the load of the engine can be accurately metered and controlled.
2) Master the technique of capturing the highest quality images possible in the Hydra engine.
3) Research and understand how the software system analyses the images.
4) Asses the limitations and benefits of the method with the equipment available.
5) Develop an experimental procedure to compare two diesel fuels with slightly different fuel properties.
6) Conduct experiments to test and reveal what the method is capable of.
7) Complete the development of the SAFL constant volume combustion bomb.
8) Develop a system for capturing images in the combustion bomb.
9) Use the combustion bomb to verify testing done in the Hydra engine.
10) Draw conclusions on the effectiveness of the method and make recommendations for improvements and future tests.

Abstract

This project involves an investigation of combustion image analysis by the two-colour method as a technique for comparing diesel fuels. The purpose is to master the technique of combustion imaging in both an engine and a Combustion Bomb, with a view to determine the suitability of the two-colour method for fuel comparisons. To evaluate the abilities of the method, an intensive range of testing was conducted on two diesel fuels with slightly different fuel properties.

Sasol has invested in considerable means to facilitate combustion imaging and analysis in a diesel engine and a Combustion Bomb. A Ricardo Hydra single cylinder research engine was modified for endoscopic optical access of the AVL VisioScope system which was acquired. Furthermore a Combustion Bomb was designed and built for a wide range of fuel testing and primarily for excellent optical access to combustion events. The AVL VisioScope includes proprietary software that uses the two-colour method for analysis of combustion images to determine the diesel flame temperature and soot concentration.

The reference fuel is a conventional diesel fuel which is blended to meet current European specifications. The model fuel is a synthetic, highly paraffinic diesel fuel with no aromatics or sulphur and a high cetane number. These two fuels are expected to have slightly different combustion properties and the analysis of the combustion images will reveal to what extent the two-colour method can expose these differences.

To compliment the engine testing, the two fuels were compared using the Combustion Bomb. Initially this involved the relocation and some additional development to commission the bomb in a suitably operational condition. Once the bomb was operating reliably, a range of tests were conducted on the two test fuels in an effort to simulate the engine conditions as far as possible. The Combustion Bomb allows direct optical access to the entire injector flame area, thus providing considerably better images than in the engine where only part of the combustion chamber is visible.

It is envisaged that the method can be used to gain valuable insight into the combustion characteristics of different fuels. Furthermore the knowledge of in-cylinder combustion phenomena can be better understood.

A considerable amount of combustion images and data were collected from both the engine and the Combustion Bomb and was analysed to extract data representing flame temperature and soot concentration for each image. This was done in the best possible way that the available software could achieve, although a newer version can offer greater image analysis potential. The results were compared for the two fuels and some differences were revealed.

The model fuel has a high cetane number and is therefore expected to ignite earlier than the reference fuel. In all tests this effect was clearly shown and quantified by the optical two-colour image results.

The optical flame temperature results also revealed differences between the two fuels over the time period from start of combustion to well beyond the end of injection. The model fuel exhibits a higher initial flame area at high temperature due to earlier combustion, but quickly drops below the reference fuel during injection. This effect was noticed in the engine tests and verified by the Combustion Bomb results. Interestingly this apparent deviation in the flame temperature at this point was reflected in the engine pressure trace for the model fuel. The Combustion Bomb revealed that after injection stops the model fuel tends to burn with higher temperature areas for a longer time than the reference fuel. This indicates better combustion in the after burn phase which should result in lower soot emissions, as revealed in some other literature with similar model fuels. The engine results did not pick up this phenomenon as clearly due to the turbulence and swirl that is present in the engine.

The optical temperature results from the Combustion Bomb are particularly interesting as they seem to show the effect of the different phases of diesel combustion. High initial temperature areas reflect the premixed combustion phase after which the flame area above threshold temperatures drops before rising to a peak during the diffusion combustion phase. As injection stops the flame area at high temperature rises and drops gradually as the fuel burns, representing the after burn phase. The results show that collectively over the range of images captured, the reference fuel has a higher number of pixels at high temperature than the model fuel. This result was found in both the engine tests and the Combustion Bomb. The potential for more detailed analysis than this exists if direct access to the processed image data was possible, but this was not possible with the available system.

Based on the foregoing information and results, the following conclusions were drawn:

- This technique has proved to be effective for the purpose of comparing different fuels as significant differences were established in the results. Some of these differences can be explained by the fuel properties of the two test fuels, while some other differences observed hold possible new insight into in-cylinder combustion phenomena not yet fully understood.
- The optical results indicated that the reference fuel exhibited higher collective flame temperature areas over the combustion range; however the flame area at high temperature of the model fuel was found to be slightly higher after injection stops.
- The results obtained from the engine and the combustion bomb concur by demonstrating similar trends with respect to the difference between the two test fuels. The combustion bomb results verify the engine results to a large extent and hold additional useful information.
- The method of extracting the numerical image results used in this project contains little value compared to what can potentially be achieved with improved software abilities. The results presented are heavily dependant on flame area and reveal no spatial information of the flame structure. A more detailed fuel comparison could be achieved if the raw data assigned to each processed image pixel could be accessed.
- Engine results were further limited by soot deposits on the endoscope widow.

While this project has been successful in achieving what it set out to do, it has highlighted areas that need to be improved to realise the potential of this method to compare and characterise different fuels more effectively using this technique.
A number of recommendations have been made to further improve the systems in place to improve the quality of the images and the data generated.

Table of contents

List of figures

List of tables

Nomenclature

ATDC – After top dead centre

BMEP – Brake mean effective pressure

BTDC – Before top dead centre

CAD – Crank angle degrees

CCD – Charge coupled display

CN – Cetane number

CO – Carbon monoxide

CO_2 – Carbon dioxide

ECU – Engine control unit

FMEP – Frictional mean effective pressure

HC - Hydrocarbon

IMEP – Indicated mean effective pressure

K – Temperature in degrees Kelvin

KL – A factor derived from optical results representing soot concentration

LEMF – Low emission model fuel

NOx – Nitrous oxides

Pixel – One unit of a CCD array

PM – Particulate matter

SAFL – Sasol Advanced Fuels Laboratory

SFC – Specific fuel consumption

SOI – Start of injection

SOC – Start of combustion

TDC – Top dead centre

UCT – University of Cape Town

1. Introduction

Photography of combustion within an engine is a specialised operation that has been undertaken by only a few laboratories throughout the world. Many different methods have been attempted, including the construction of glass engines, but the only method that does not directly interfere with the combustion process as it would occur in a standard engine is endoscopy.

Capturing the images is half the story though; the analysis of the images is where the real science comes in. The two-colour method has been used to determine flame temperature from luminosity for many years. (Agnew, 1961) The method has been refined over time and has been the subject of a number of different research endeavours where measurement of flame temperature is of interest.

Engine testing specialists, AVL, have to some extent been the pioneers in offering combustion chamber endoscopy as a commercially available technology. They have developed a complete system to capture images and analyse them by means of the two-colour method. The system is called the AVL VisioScope and in conjunction with their propriety ThermoVision software it can offer detailed insight into flame temperature and soot concentration information for images taken of diesel combustion. (AVL, 2001)

Sasol has invested in the abovementioned apparatus and this project is a thorough investigation of combustion imaging by means of an endoscope system and image analysis using the two-colour method. The focus of the investigation is specifically to gauge its suitability as a tool for comparing the combustion characteristics of different diesel fuels.

Sasol is a world leader in the production synthetic fuels from coal and gas. Intensive research is encouraged to gain a better understanding about the differences of these fuels in an effort to further improve fuel quality and gain associated benefits.
The focus of fuel research in recent times has been on exhaust emissions where exhaust gasses are analysed in every last detail. A less exact science, but one of considerable interest is in-cylinder emission formation. It is envisaged that with a sound understanding of this method and confidence in its results, it can be used to gain valuable insight in the field of in-cylinder combustion research.

1.1. Problem definition

With a view to detailed comparisons of fuels, the system and method needs to be mastered and fully understood. This project follows on from previous work which was to equip the Hydra test engine to conform to the specifications of a modern high pressure common rail diesel engine with electronic engine management. The engine was also modified to allow for optical access of the endoscopes. The next logical step is to rigorously test the method and optimise its use. With a well documented and sound understanding of the system as a whole, it can then become a valuable research tool.

1.2. Objectives

- **Optimise the equipment available to obtain the best possible combustion images**

A good image is a direct view of a complete injection plume. The endoscope needs to be positioned in an area that minimises soot fouling and gets the best possible viewing angle. The procedure of optimised image capture needs to be recorded and used for the comparative testing procedure.

- **Set up an experimental procedure to conduct tests of two different fuels**.

This needs to be done in such a way that it covers a large range of operation without introducing an unmanageable number of variables.

- **Analyse the range of image data by the two-colour method and make comparisons in a logical way that will reveal the useful information that the system can offer.**

- **Apply the system to investigate other interesting optical research topics**

Testing will include images using flash light illumination to look at injector spray and start of combustion phenomena for a visual comparison.

- **Compliment the engine results by similar testing on the Combustion Bomb**

The process to incorporate the VisioScope to work with the bomb needs to be established, and similar comparative testing conducted. The objective is to use these results to add value and hopefully verify the results of the engine testing. Comparisons between applying the two-colour method to the engine and Combustion Bomb can be drawn.

1.3. Layout of document

This document is structured in a way that allows the reader to use it as a manual for further testing. The following section includes a detailed overview of the theory behind the methodology. A broader overview of the effect of fuel properties is then given in an effort to be able to discuss the results in this context.

In **Chapter 3**, the relevant literature is surveyed, looking particularly at development and use of the two-colour method in fuel testing. Literature on combustion imaging and comparative fuel testing is briefly discussed where relevant.

Chapter 4 describes the apparatus used in detail and how it is best set up.
From this point on the chapters are structured in two parts, looking first at the Hydra Engine and then at the Combustion Bomb in each case. This is done such that the two fields of research can compliment each other within the same chapter.

The experimental procedure followed is detailed in **Chapter 5** which begins with various procedures used and testing conducted to optimise the final test procedure.

The main results are presented in **Chapter 6** and then discussed in **Chapter 7** with a view to explain differences observed with respect to the fuel properties. The extent to which this can tie up with conventional wisdom and other test results will determine the success of the method.

A number of conclusions and recommendations for future work are made. The appendices include operating instructions and design modifications made to the specific systems used in this project.

2. Theoretical background

2.1. Overview of diesel combustion

The combustion of diesel fuel in a direct injection, compression ignition engine can be summarised as follows: Fuel is injected directly into the cylinder at very high pressure through a multi hole electronically controlled injector. This process results in a finely atomised spray plume of diesel droplets entering the cylinder which contains air at high pressure and temperature. The liquid fuel vaporises and mixes with air to form zones of flammable fuel mixtures. Auto-ignition occurs in these premixed regions and a diffusion flame develops. This is also referred to as the onset of sooting combustion as soot is formed and then burned in the diffusion flame.

Recent laser sheet diagnostic testing in DI diesel engines have been used to develop a better understanding of diesel combustion which is different to early models based on steady spray combustion in furnaces and gas turbines. (Dec, 1997) The three main phases of diesel combustion can be described with greater insight using the Dec model.

Ignition delay: This is defined as the time taken between start of injection (SOI) and the start of combustion. (SOC) During this ignition delay period a certain amount of fuel entrains hot cylinder air leading to vaporisation around the periphery of the liquid spray plume. The amount of premixed fuel prior to auto-ignition is determined by the length of the ignition delay. This is indicated by the cetane number of the fuel.

Premixed Combustion: The premixed air-fuel mixture ignites as it enters the flammability limits of the fuel. The fuel is partially oxidised in a rich premixed reaction. Hydroxyl (OH) radicals are released in the premixed burn, but the flame has a low luminosity and can be viewed by chemiluminescence. This mixture burns rapidly resulting in high heat release rates and rates of pressure rise that are characteristic of this phase.

Mixing Controlled Combustion: Once the premixed fuel has been consumed, the heat release rate is controlled by the rate at which a mixture becomes available for combustion. A turbulent diffusion flame forms around the products of the premixed phase which begins the transition to the mixing controlled phase. This results in the ignition of locally rich mixtures and consequently the formation and combustion of larger soot particles. This occurs at the jet

periphery and the soot concentration increases throughout the vortex region at the head of the jet. The burning of carbon particles at high temperature releases a large amount of radiation which is visible as an orange flame of varying brightness.

The Dec model is based on combustion during injection. The organised structure of this model falls away after injection stops and this is often referred to as the after burn phase. Most of the soot is burned with the fuel at the diffusion flame; however the soot that is not burned here becomes an exhaust emission. NOx emissions originate in the high temperature regions of the diffusion flame where both oxygen and nitrogen are present. NOx can also form in post combustion hot gas regions. (Ferguson. 2001)

A study by Musculus and Cicone (2005) presented imaging of low temperature diesel combustion. This is summarised in the following figure which illustrates the start of diesel combustion very well. It shows that mixing is least complete at the head of the spray where OH is deficient and the fuel mixture is rich, hence soot combustion initiates there. This puts the 'sooting flame' into perspective which is relevant as it will be referred to extensively in following sections of this document.

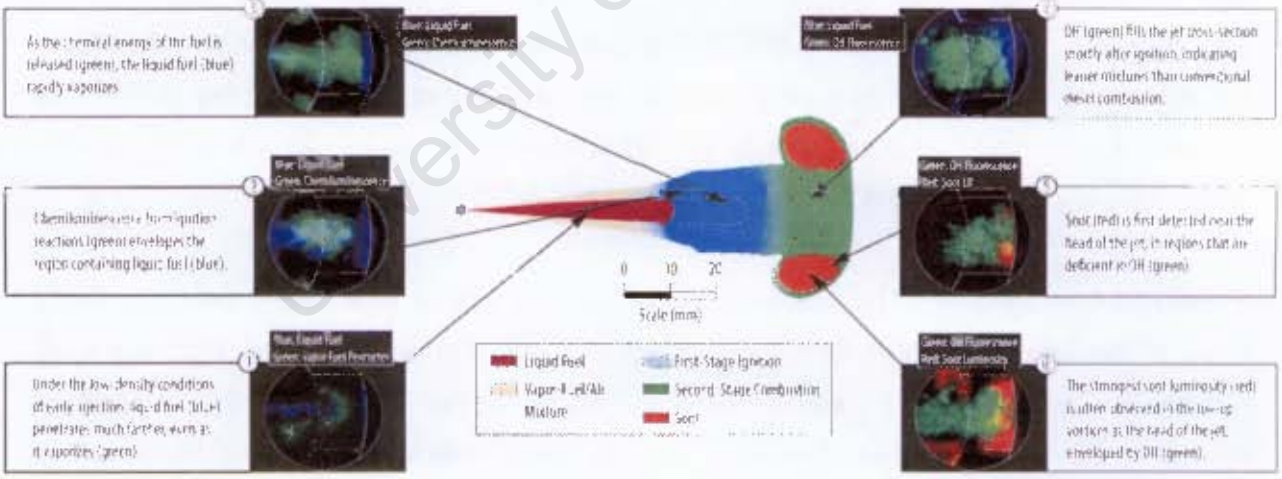

Figure 2-1: Schematic model of a diesel flame from various optical techniques

2.2. Theory of the two-colour method

The focus of this project is to evaluate the method of extracting scientific data pertaining to physical properties using only the radiation exposed to a CCD camera. The method has been used and refined over many years and has been put together in a software package by engine testing specialists, AVL. It is important to understand the basic theory upon which the system operates in order to better understand the results that are revealed in the end.

The software is based upon the two-colour method which has been researched extensively over many years and by many accounts shown to be a very effective way of determining flame temperature from the radiation of soot particles during combustion. This section describes the details of the method as researched by Matsui et al (1979), Bakenhus and Reitz (1999), Zhao (2001) and (AVL, 2001)

The method is entirely based on flames arising from the combustion of soot particles. After diesel injection there is an ignition delay phase, followed by thermal ignition. Diesel combustion thereafter involves the formation and combustion of soot particles which is a diffusion process. In oxygen deficient zones, carbon is released as soot which is oxidised again in the after-burn phase.
In a sooting diesel flame the two-colour method uses the measured thermal radiation of soot particles to calculate the temperature of soot particles within the flame. The method therefore actually determines the temperature of the soot particles and makes the assumption that this is equal to the gas temperature. The credibility of this assumption has been researched extensively by Millikan (1961) and as a start this is described briefly below.

Relationship between soot particle temperature and combustion gasses

Soot samples from a diesel flame examined under an electron microscope show that the soot is made up of agglomerates of individual spherical particles with a diameter in the order of 50nm. The gas temperature can be calculated assuming that the continuous flow equation holds for heat transfer between the particles and gas even though the mean free path of the gas molecules within the flame is about one tenth of the soot particle diameter. Also that the there is no surface chemical reaction. The following equation is used to calculate the temperature of soot particles (T_p) within a gas of temperature (T_g).

$$C_p \frac{\pi}{6} d^3 \gamma_p \frac{t}{dt} T_p = \pi d^2 \frac{2\gamma_g}{d} (T_g - T_p) - \pi d^2 \varepsilon \sigma (T_p^4 - T_w^4) \qquad \text{(Equation 2-1)}$$

Where: d = particle diameter

C_p = specific heat of particle

γ_p = specific gravity of particle

T_w = cylinder temperature

λ_g = Heat conductivity of the gas

σ = Stefan-Boltzmann constant

ε = emissivity of the particle

t = time

When the gas and soot particles are in thermal equilibrium, the right hand side of the equation becomes zero. If the emissivity is assumed to be 1, $T_g - T_p = 0.3K$.
Similarly, Schack (1925) also showed that the temperature difference is less than 1K for particles of 300nm diameter in a gas of temperature 1873K, by determining the total emissivity of the soot particle from the scattering theory. It was also shown that if there is no surface reaction of the soot particle, it may be assumed that the soot particles immediately approach the temperature of the surrounding gas.
Millikan (1961) went further to show by another method that in the case where surface reaction is present, the temperature obtained from the radiation of soot particles coincided with that of the gas temperature.

By all accounts it can be assumed with confidence that due to the small particle sizes within a sooting flame, the soot particle temperature is approximately the same as the combustion gas temperature.

Soot temperature measurement

The principle behind the Two-Colour method is to detect the radiation of the soot particles at two different wave lengths. The temperature can then be determined by using two equations to eliminate an unknown factor of flame emissivity.

Every body emits electromagnetic radiation due to its finite temperature. The intensity of this radiation varies with wavelength and depends on the temperature of the body. A description of monochromatic black body radiance was devised by M. Planck in 1900 and further

developed by Einstein based on the quantum light theory. The equation for black body radiance below is suitable for temperatures under 3000K, where its accuracy has been shown to be within 1%.

$$N_o(\lambda,T) = C_1\lambda^{-5}\exp\left(-\frac{C_2}{\lambda T}\right) \qquad \text{(Equation 2-2)}$$

Where: λ = Wavelength (μm)

T = Absolute Temperature (K)

C_1 = Planck's first constant

= 3.7418 x 10^{-16} Wm^2

C_2 = Planck's second constant

= 1.4388 x 10^{-2} mK

If ε_λ denotes the monochromatic emissivity of the flame (a non-black body), the monochromatic radiance of the flame is described below:

$$N(\lambda,T) = \varepsilon_\lambda N_o(\lambda,T) = \varepsilon_\lambda C_1\lambda^{-5}\exp\left(-\frac{C_2}{\lambda T}\right) \qquad \text{(Equation 2-3)}$$

To represent the effective monochromatic radiance of a non-black body in terms of the monochromatic radiance of a black body, an apparent temperature, T_a, is introduced. T_a is defined as the temperature of a black body that will emit the same radiation intensity as a non-black body at temperature T.

$$N(\lambda,T) = N_o(\lambda,T_a) = C_1\lambda^{-5}\exp\left(-\frac{C_2}{\lambda T_a}\right) \qquad \text{(Equation 2-4)}$$

At this point the empirical correlation devised by Hottel and Broughton (1932) for the monochromatic emissivity of soot particles in a diesel flame is introduced.

$$\varepsilon_\lambda = 1-\exp\left(-\frac{KL}{\lambda^\alpha}\right) \qquad \text{(Equation 2-5)}$$

K is an absorption co-efficient which is nearly proportional to the number density of soot particles. L is the geometric thickness of the flame in the direction of the light axis of the flame detection system.

Together it is known as the KL factor which is a good description of soot concentration.
α is an empirical constant within a specific range of wavelength and is dependant on the physical and optical properties of the soot in the flame. Fuel type may have an influence on the value of α. However, if the two wavelengths are selected in the visible range, the value of α is less critical to the flame temperature and KL value calculations. (Zhao, 2001)

Equations (2-3) and (2-5) are combined to give the following equation for KL:

$$KL = -\lambda^{\alpha} \ln\left[1 - \exp\left\{-\frac{C_2}{\lambda_2}\left(\frac{1}{T_a} - \frac{1}{T}\right)\right\}\right] \qquad \text{(Equation 2-6)}$$

By measuring the brightness temperature of the flame (T_{a1},T_{a2}) at two wavelengths (λ_1,λ_2), they can be substituted into equation 6. The measurement of the brightness temperature is usually calibrated for a specific apparatus using a tungsten lamp which glows at a known temperature. In fact the purpose of the two-colour system is to provide instantaneous measurements of the two brightness temperatures at the two chosen wavelengths.
The unknown factor KL is thus eliminated and the absolute temperature T can be solved from the following equation:

$$\left[1 - \exp\left\{-\frac{C_2}{\lambda_1}\left(\frac{1}{T_{a1}} - \frac{1}{T}\right)\right\}\right]^{\lambda_1^{\alpha 1}} = \left[1 - \exp\left\{-\frac{C_2}{\lambda_2}\left(\frac{1}{T_{a2}} - \frac{1}{T}\right)\right\}\right]^{\lambda_2^{\alpha 2}} \qquad \text{(Equation 2-7)}$$

In the case of the AVL ThermoVision software, this process is applied over each pixel in the 640 x 480 pixel image. The result is 307200 temperature readings for each image taken. These data can be represented in a temperature image or tabled as number of pixels at various temperature steps. Unfortunately it cannot be accessed directly in ThermoVision V1.1.

Calculation of soot concentration

The image processing procedure involves a first step of calibrating each pixel to determine the brightness temperatures at the two wavelengths. The absolute temperature of each pixel is then calculated. Using those results, the absolute temperature is substituted back into equation 2-6 to determine KL. The KL factor is then used directly as a description of soot concentration.

Specifications of the AVL VisioScope

Some key specifications of the AVL VisioScope used in this project are listed: (AVL, 2001)

Analysis Method: Two Colour Method

Wavelengths: Red and green channels – (both in visible range)

Model: Locally homogeneous and thermal distribution as soot density along the optical penetration depth is assumed

Measurement Range: 1800K – 3000K

Measurement Resolution: approx. 5K

Image size: 640 x 480 pixels

Measurement Accuracy: Absolute accuracy for the specified calibration temperatures:

$$\Delta T_{abs} = abs(T_{cal} - T_{meas}) < 140K$$

Limitations of the two-colour method

A critical analysis based on the theory presented here reveals some limitations of the method and these must be considered to better understand the results.

The images are a representation of the luminosity emitted by the combustion of soot particles. Any combustion reactions prior to sooting combustion cannot be detected by this method. Furthermore the analysis is based upon knowledge of soot particle combustion and this is then assumed be representative of the flame.

The images are a representation of the surface exposed to the view of the camera. The images cannot represent the entire volume of the flame and are dependant on the position of the endoscope window. In an engine the endoscope protrudes into the combustion chamber and is immersed in the flame, while images in the Combustion Bomb are taken from further away. In all cases one must be aware that the system cannot detect a temperature gradient

along the optical penetration depth. The flame is a volume radiator as opposed to a surface radiator and is assumed to be homogenous. This assumption is a limitation of the method because the non-uniformity of temperature and soot concentration in reality will influence the physical meaning of the measured temperature and KL results of this technique. A large temperature gradient along the optical penetration depth of the flame would result in erroneous results due to this assumption.

The line of sight thickness of the burnt gas region cannot be directly measured from the image, but it is inferred from the flame brightness. Optical thickness is identified in terms of local brightness and hence local sooting on the viewing window will reduce its transmissivity and can cause lower resulting temperatures and KL values. This remains the most significant limitation of this method which can only work properly as long as the optical access is kept clean.

It must be noted however that in equation 2-7 the true flame temperature is mainly determined by the ratio of flame radiation at the two wavelengths. Equation 2.6 shows that the KL factor is directly proportional to the absolute amount of flame radiation. It follows that a drop in transmissivity due to soot deposits would have a much greater effect on the KL results that it would have on the flame temperature results.

Similarly the effect of wall reflections would affect the accuracy of the KL values more than the temperature values. However if the wavelengths are in the visible range, the effect of wall reflections are reduced.

In general the two-colour method is well suited for good flame temperature measurements, however soot concentration results from this method should be treated with caution. These results are more prone to interference by window sooting and non-uniform soot distributions along the optical path of the measurements.

2.3. Comparison of test fuels

The primary purpose of this project is to investigate combustion imaging as a method for comparing fuels, however the method is best investigated by doing an intensive comparison of two fuels in an effort to extract every piece of information that the method can offer. For the purpose of this project two diesel fuels with slightly different fuel properties were chosen for investigation. The reference fuel is a conventional diesel fuel which is blended to meet current European specifications. The model fuel is a highly paraffinic diesel fuel with no aromatics or sulphur and a high cetane number. The reference fuel EN590 is a blend of coal-to-liquid (CTL) and crude oil based components and the model fuel is entirely synthetic. Where convenient the fuels will from hereon be referred to as 'EN590' and 'LEMF' (Low Emission Model Fuel) for the reference and model fuels respectively.

Table 2-1: Fuel Properties

Fuel Properties	*Units*	*Reference Fuel* *EN590*	*Model Fuel* *LEMF*
Density @ 20 °C	kg/ℓ	0.8297	0.7647
Distillation - Dist D86			
Initial boiling point	°C	180	169
10%	°C	212	187
50%	°C	276	251
95%	°C	350	321
Final boiling point	°C	371	329
Flash Point	°C	60	59
Viscosity @ 40 °C	cSt	2.73	1.97
Cold Filter Plugging Point	°C	-8	-19
Sulphur content	ppm	<10	<1
Cetane number		54.8	74
Carbon content	Mass %	86.2	85
Hydrogen content	Mass %	13.8	15
Hydrogen/Carbon ratio	mol/mol	1.87	2.11
Mono-Aromatic Hydrocarbons	Mass %	25.2	0.14
Bi-Aromatic Hydrocarbons	Mass %	2.4	0
Poly-Aromatic Hydrocarbons	Mass %	0.3	0
Total Aromatic Content	Mass %	27.9	0.14
Net Heating Value	MJ/kg	42.75	43.81

Both fuels have been analysed intensively and the key properties are listed in the table above and illustrated in a graphic comparison overleaf:

Fuel Property	Relative Comparison
Density (kg/m³)	750 — 850
Viscosity (cSt)	2.0 — 4.5
Heating Value (MJ/kg)	41 — 45
Aromatics Content (% m)	0 — 40
H/C ratio (molar)	1.8 — 2.2
Sulphur Content (ppm)	0 — 50
Cetane Number	50 — 80

Figure 2-2: Fuel Properties

Hydrocarbon fuels are made up of molecules consisting of carbon and hydrogen atoms bonded in various ways. Each carbon atom has the ability to make four bonds, while each hydrogen atom can only make one bond. It follows that a carbon atom can make either single, double or triple bonds, thus resulting in fewer or more hydrogen atoms that are bonded to it. These features and the bond structure result in different fuel properties.

Straight chain hydrocarbons containing no double bonds and are classified as alkanes or paraffins. The cetane molecule in the figure overleaf is an example of a paraffinic fuel structure. The single bonds result in a maximum number of hydrogen atoms for each carbon atom and therefore alkanes have a high hydrogen to carbon (H/C) ratio.

Some fuels contain aromatics which are ring structures with double bonds between the carbon atoms. The figure below shows 1-Methyl Benzene which illustrates the aromatic ring structure and the ability to accommodate additional hydrocarbon chains on the side. Aromatics result in a lower H/C ratio and a higher density compared to paraffins. Aromatics have slightly lower energy content per unit mass, but higher energy content by volume. A ring structure is very stable and hence makes the fuel more resistant to auto-ignition. (Challen et al. 1998)

From the table of fuel properties above, the reference fuel shows a moderate aromatic content where the model fuel is almost entirely paraffinic. This explains why LEMF has a lower density and slightly higher energy content by mass.

The cetane number is a measure of the fuel's propensity to auto-ignite and LEMF has a higher Cetane number due to its linear molecular structure.

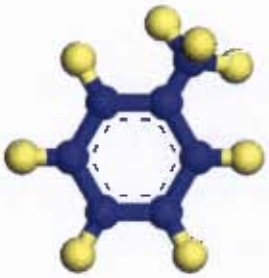

Figure 2-3: 1-Methyl Benzene (C_7H_8)

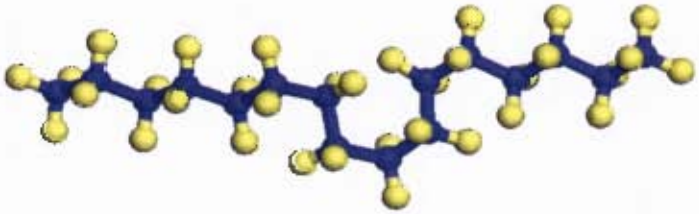

Figure 2-4: Cetane ($C_{16}H_{34}$)

2.4. *The effect of fuel properties on diesel engine operation*

The properties that are responsible for the main differences in the test fuels are discussed here using conventional wisdom. Later on it will be seen if this can be used to explain the differences observed in the optical measurements.

The effect of Fuel Ignition Quality

One of the most significant differences between the test fuels is the Cetane Number (CN). This is a measure of a diesel fuel's ignition quality which is effectively its readiness to auto-ignite. As is standard practise around the world, cetane is measured in a CFR engine with an adjustable compression ratio. In the CFR engine the test fuel is injected 13 crank angle degrees Before Top Dead Centre (BTDC), and the engine's compression ratio is then adjusted until ignition occurs at TDC, resulting in an ignition delay of 13° CA. Reference fuel blends, of known cetane numbers are then tested to find one that also has an ignition delay of 13° CA at the same set compression ratio. The reference fuels used in this test are Cetane (n-hexadecane) with a CN of 100 and heptamethylnonane (HMN) with a CN of 15. The Cetane number of the test fuel is then calculated by: (Heywood, 1988)

$$CN = (vol\ \%)\ hexadecane + 0.15\ (vol\ \%)\ heptamethylnonane$$

In hydrocarbon fuels, short-chain and branched paraffins have a high resistance to auto-ignition resulting in a low cetane number. A high aromatic content would further lower the cetane number. Long chain paraffins auto-ignite readily as shown by n-Hexadecane which

has a cetane of 100. To put this in perspective, commercial diesel fuels typically have a cetane number in the range of 40-55.

In diesel engine combustion, a fuel with a high cetane number would result in a shorter ignition delay. For the same injection timing, combustion will start earlier than it would with a lower cetane fuel. A short ignition delay results in less fuel in the cylinder being available for combustion during the premixed combustion phase. The effect of this is a comparatively lower rate of pressure rise initially. This would result in lower peak combustion pressure and temperature. A lower rate of pressure rise would reduce engine noise and the characteristic diesel knock.

Therefore it can be expected that LEMF should run quieter that EN590 diesel and result in lower peak pressures and temperatures. The rate of heat release should also be comparatively lower. However, given the same injection timing point, a shorter ignition delay would have the effect of advancing the injection timing. Ie: Combustion would start earlier with significant associated effects on ultimate pressure and temperature depending on the reference injection timing point. These effects are not to be confused with the genuine effects of a high cetane number which can only be tested by adjusting the injection timing such that auto-ignition occurs at the same point for the two fuels.

The effect of Fuel Density

An increase in power can be expected for a higher density fuel with the same calorific value, as more fuel mass is effectively injected for the same volume. For the same power output, lower volumetric fuel consumption would result. Many tests have been done to determine the effect of fuel density; in most cases the magnitude and direction have been found to be very dependant on engine design. This implies that engines can be optimised for fuel density. Signer (1996) concluded that there was no evidence of density effects on the combustion process itself.

The density effect therefore comes down to the effect of different resulting energy contents entering the combustion chamber. In the case of our two test fuels, it is apparent that LEMF has a lower density. Therefore, for the same volume of fuel injected, there would be less mass of LEMF fuel than EN590. An associated power loss would be expected, and a lower fuel consumption by mass. However this effect is somewhat offset by the fact that LEMF has a higher energy content.

A study by Kweon et al. (2003) compared a similar model fuel with some standard US diesels. The results reflected lower Specific Fuel Consumption (SFC) for the model fuel. This result was attributed to the fuel's lower density and higher heating value. It was found that this difference in ISFC (indicated specific fuel consumption) was more significant at high engine load. Specific Fuel Consumption is a measure of fuel flow rate per unit of power output. It is an indication of the engines fuel efficiency and therefore is desirable to be low. Expressions for efficiency and SFC are shown below.

$$\eta = \frac{Power_{shaft}}{Power_{fuel}} = \frac{P_{shaft}}{m_f \cdot Q_f} \qquad SFC = \frac{m_f}{P_{shaft}} = \frac{1}{\eta \cdot Q_f}$$

Where: η is overall engine efficiency

m_f is the fuel mass flow rate

Q_f is the energy content of the fuel

The effect of the Hydrogen to Carbon Ratio

The H/C ratio of the fuel has a significant effect on the combustion process and particularly on the mechanisms of soot formation. Soot is formed by the dehydrogenation of organic compounds and polymerisation, leaving carbon particles which agglomerate into larger particles. (Ferguson et al, 2001) As detailed in the previous section, the combustion of soot particles is the primary cause of luminosity and heat radiation in flames. A fuel with a high H/C ratio will have a lower carbon content. It could possibly be expected that such a fuel will burn with a less luminous flame, however only a small portion of the fuel carbon is converted to soot so this effect is unlikely to be very significant. The luminosity of a flame is dependant on the amount of soot formed in the flame, which in turn is dependant on local fuel-air mixing.

Molecular structure also plays a role. For the same H/C ratio, straight chain paraffins produce less soot than corresponding isomers. (Ferguson et al, 2001) Paraffins tend to produce more soot with increasing molecular weight. The fundamental differences in the combustion between fuels of different H/C ratios are best illustrated by considering ideal complete combustion. The equation below shows a fuel reacting with oxygen to form carbon dioxide and water. All of the hydrogen thus becomes water.

$$C_nH_m + xO_2 \rightarrow nCO_2 + \frac{m}{2}H_2O$$

Where: *n* is the number of moles of carbon
m is the number of moles of hydrogen
x is the number of moles of oxygen

An oxygen balance of the above equation is given below:

$$x = n + \frac{m}{4}$$

This can be used to compare fuels of different H/C ratio, for example the combustion reactions for hexane (C_6H_{14}) and benzene (C_6H_6) are shown below. Hexane has a significantly higher H/C ratio.

$$C_6H_{14} + 9\frac{1}{2}O_2 \rightarrow 6CO_2 + 7H_2O$$
$$C_6H_6 + 7\frac{1}{2}O_2 \rightarrow 6CO_2 + 3H_2O$$

It can bee seen that the high H/C ratio results in higher consumption of oxygen and production of water. This would affect various secondary reactions in an engine and emission formation. Most significantly a high H/C ratio would leave less oxygen available for the formation of oxides such as NOx in the flame front.

The effect of Fuel Aromatics Content

Aromatic components in fuels have been found to contribute significantly to the formation of soot and consequently particulate emissions. Compared to olefins and paraffins, aromatics form more soot. (Heywood, 1988)

Azetsu et al. (2003) investigated the Effects of Aromatic Components in Fuel on Flame Temperature and Soot Formation. This research made use of the two-colour method and found that fuels with aromatics produced higher flame temperatures and more soot than fuels with no aromatics.

As LEMF has effectively zero aromatic content and EN590 is contains more than 25% aromatics, it can be expected that similar results should be realised in this study.

2.5. The effect of engine operating parameters

The effect of Engine Load

In a diesel engine the engine load is controlled by the injection duration. At low load the injection duration is very short and most of the fuel is burned in the premixed combustion phase, hence the characteristic diesel knock at idle. As the injection duration increases, the initial combustion and heat release rate remain unchanged, but the mixing controlled combustion phase follows as previously discussed.

An increase in engine load will result in higher temperature and pressure conditions in the combustion chamber due to more fuel being injected. Higher fuel concentration is thus synonymous with higher loads, along with higher soot formation. The increase in soot formation will to some extent be burnt off by the higher combustion temperatures.
(Heywood, 1988)

It is unclear at this point whether the VisioScope will be able to detect the higher temperatures or whether the increased soot deposits will offset this.

The effect of Injection Timing

Injection timing in a diesel engine is a critical parameter affecting engine performance and emissions. After the point of fuel injection into the cylinder, physical and chemical processes occur before combustion initiates. This period is the well documented ignition delay. Some key physical processes are atomisation of the liquid fuel, vaporisation of fuel droplets and the mixing of fuel vapour with air.

Atomisation is improved by high cylinder pressure, while the rate of vaporisation of fuel droplets is also increased by high pressure and temperature inside the cylinder. (Heywood, 1988) Early fuel injection would expose the fuel to relatively lower temperature and pressure in the cylinder, resulting in increased ignition delay. Conversely, if injection timing is retarded, the initial cylinder temperature and pressure are higher resulting in reduced ignition delay. The highest compression temperature and pressure occurs at TDC, however this is too late for fuel injection. According to Heywood (1988), the most favourable conditions for ignition lie before TDC.

The effect of local air-fuel ratio

The overall air-fuel ratio in a diesel engine is usually very lean; however the fuel mixture is not homogenous so the local air-fuel ratios in the area of the fuel spray are significant. This is affected largely by the injector design and fuel pressure, as well as swirl and turbulence in the combustion chamber. Generally locally rich air-fuel mixtures would result in high soot formation and consequently high soot concentration zones. Good mixing and spray atomisation would limit very rich zones and result in cleaner combustion.

Local air-fuel ratio is also dependant on the vaporisation properties and density of the fuel. That is particularly significant in this project as the two fuels being tested would have slightly different mixing properties resulting in a variation in local air-fuel ratios. In the study by Payri et al. (2000) on the characterisation of similar test fuels to this project, non-evaporating spray characteristics in terms of spray tip penetration, spray cone angle and droplet diameter were investigated. It was concluded that no significant differences in the spray were found between the model and reference fuels.

Given that the sprays are similar, the evaporation properties, namely the distillation temperatures could affect the local air-fuel ratio. The model fuel could be expected to vaporise faster due to its lower energy requirement for complete vaporization.

The difference in density between the two fuels amounts to approximately 8%. Thus the fuel mass flowing through the injector would be approximately 4% lower with the model fuel than the reference fuel. This is due to the mass flow rate of the fuel through the injector being proportional to the square root of density by the Bernoulli equation. (Payri et al. 2000)

$$\dot{m}_f = \rho_f \cdot C_d \cdot A \cdot \sqrt{\frac{2 \cdot \Delta P}{\rho_f}} \qquad \therefore \dot{m}_f \ \alpha \ \rho_f^{\frac{1}{2}}$$

These characteristics would result in the model fuel having a leaner local air-fuel ratio than the reference fuel. This is to some extent offset by the difference in the stoichiometric air-fuel ratio which is higher for the model fuel. This results in the local equivalence ratio being about 2% leaner with the model fuel than the reference fuel. (Schaberg, 2005)

3. Literature review

3.1. Combustion imaging

The ability to photograph combustion within an engine has been something that engineers have been trying to achieve almost ever since engines were first invented. Of course this involves some way of having optical access into the combustion chamber. Many techniques have been tried, usually involving extensive modifications to the engine. Transparent windows somewhere in the cylinder head are common, but more complicated techniques involving glass pistons and engines have been used. There are modern test engines commercially available with glass cylinders and pistons for direct combustion imaging. Some AVL designs are shown below as an example.

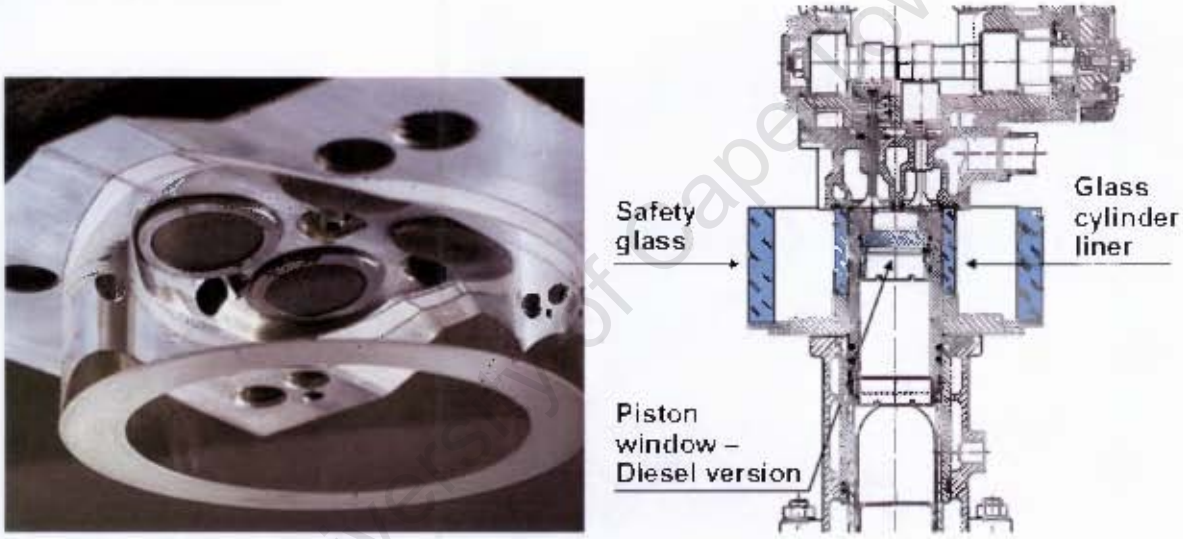

Figure 3-1: Glass engine techniques

The examples show to what extent the combustion chamber is altered. This affects the geometry and more significantly, the heat transfer characteristics of the combustion chamber. This casts doubt over the results generated in these engines with respect to its relevance in a standard engine.

A relatively new method developed by AVL as an alternative to conventional methods is the endoscope technique. The key feature is the use of small optical components which can be installed in a standard engine. Werlberger and Cartellieri (1987) presented the first paper on the subject of engine combustion imaging by means of endoscopic high speed photography. The primary author of this paper works for AVL and went on to be involved in the

development of the VisioScope. He has been of great assistance in this project with support on setting up our system and understanding the results.

The endoscope is fitted with a specifically designed quartz window which protrudes into the cylinder head from the outside. Optical access is thus provided to the combustion chamber with the viewing point at the cylinder head flame face. The main advantage is that there is minimal interference to the combustion process. This opens up the possibility for realistic imaging of engine combustion phenomena and a good basis for further thermo-graphic analysis. As the endoscope is so small, a similar process can be used to illuminate the combustion chamber, thus enabling viewing of the injector spray, valve motion and any other related application. The concept is illustrated below. (AVL, 2001)

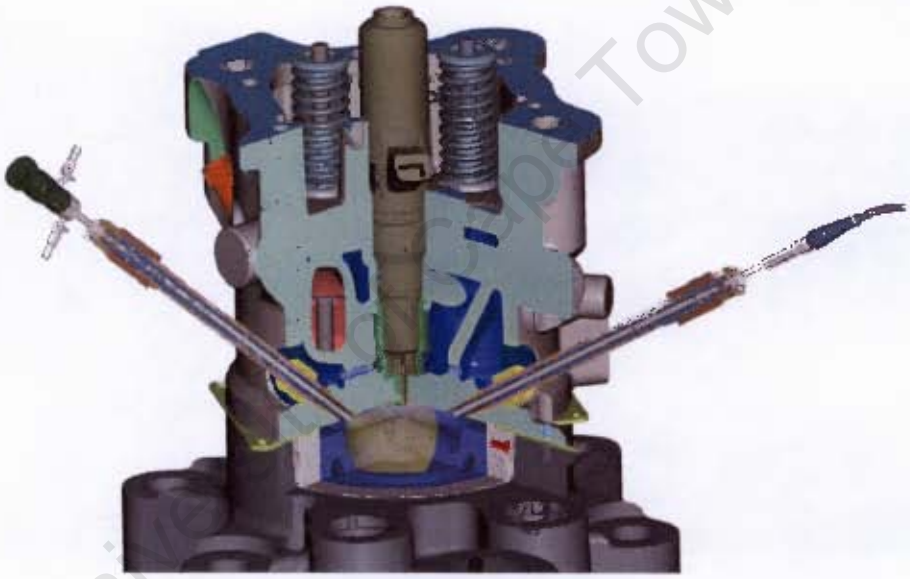

Figure 3-2: Endoscopic combustion chamber imaging system

The system has proved to be successful but is limited by a number of issues, as discussed in the previous chapter. The problem of soot deposits forming on the endoscope window is one of the main disadvantages of the method.

The system has been applied to both spark ignition and compression ignition engines and has been used in a number of publications since Werlberger and Cartellieri (1987).
Many of these investigations have incorporated image analysis by means of the two colour method which will now be discussed.

3.2. Image analysis by the two-colour method

As described in the previous chapter, the underlying theory of black body radiation was developed in the days of Einstein and has since been used in various applications as a method of determining temperature from a source of radiation. The two colour method was developed some 60 years later and one of the earliest automotive publications in this field was by Agnew (1961). His research involved the measurement of end gas temperature in a spark ignition engine using infrared radiation at two wavelengths. This research was a valuable step at the time in the process of understanding engine knock. In principle the method is very similar to the method used in this project for a diesel engine.

A study on the two-colour method applied to a direct injection diesel engine was presented by Matsui et al. (1979). It was realised that an optical method for flame temperature measurement in a diesel engine was the most effective because the temperatures are high and subject to rapid changes. This paper refined the method with improved verification of the emissivity of the diesel flame and calibration of the true absolute temperature.
The research made progress to establish the two-colour method as a reasonable temperature measuring method for diesel engines. The motivation behind this research was the desire to explore the combustion mechanism in diesel engines and furthermore the formation mechanism of nitrous oxides and soot. Radiative and convective heat transfer are other critical parameters that require the accurate measurement of temperature to be investigated.

With the advent of better optical access using endoscopes the method received a lot of attention and has been used in a number of further publications. Hampson and Reitz (1998) used the method to investigate the effect of split injections. Split injections had been found to reduce soot and NOx emissions and the two-colour method was used in this investigation to aid the understanding of the soot formation process. Multidimensional combustion and soot modelling was used to enhance the interpretation of the experimental results. The study concluded that good agreement was found between computed and measured cylinder pressures, heat release, soot and NOx emissions. They also found good qualitative agreement between the in-cylinder temperature and soot concentration (KL) fields obtained from the endoscope images and those obtained from multidimensional modelling.

A further study (Bakenhus and Reitz, 1999) compared single and split injections using the two-colour method. The flame temperature profile gives a very good indication of where nitrous oxides form as this process requires high temperature. The soot concentration results were used to determine the conditions that resulted in high soot emissions. The study looked at different parts of the combustion chamber and shed light on strategies that affect the key diesel emissions, soot and NOx. Injection timing and the number of split injections were the main parameters investigated.

At a similar time a study was conducted on heavy duty DI diesel engines using the two-colour method. (Shiozaki et al, 1998) This study also made use of the temperature and soot information to optimise soot and NOx emissions, since flame temperature has a direct effect on engine NOx characteristics. Two and four valve per cylinder engines were compared and combustion imaging was used to better understand the corresponding effects.

The main use of the method has been in research on engine optimisation and emission formation. An example of the two-colour method being used to compare different fuels can be found in a publication by Azetsu (2003), where fuels of varying aromatic content were analysed. The method was found to be particularly suitable for comparative research as the certainty of absolute values is of less importance than the relative results.

When a number of fuel properties are different and have been shown to produce different emission and performance results, it can be expected that the two-colour method should be able to distinguish between the fuels. This study therefore focuses on the two-colour method as a technique for comparing fuels and to what extent they can be distinguished.

The following section briefly outlines some work that has been done on the subject of the two-colour and other methods being used to compare synthetic and conventional diesel.

3.3. Comparing synthetic and conventional diesel

A number of research projects have been conducted to compare synthetic diesel to various other diesel specifications. A synthetic fuel was compared to other fuels meeting the various US diesel specifications with a view to determine the effect on exhaust emissions. (Schaberg et al, 2000) A significant reduction in all legislated emissions was observed, even when compared to the high quality CARB specification diesel. The reduction in soot was generally much larger than the reduction in NOx. A large reduction in hydrocarbon and CO emissions was also noted.

A very recent study was conducted to determine the emission performance of synthetic diesel and blends with optimised engine calibrations. (Schaberg et al, 2005) Vehicle emission tests showed HC and CO emissions reduced by over 90%. PM dropped by 30% while NOx was largely unchanged. These tests were conducted in a modern diesel passenger vehicle. Engine bench tests showed soot reductions of 30 – 60% with NOx reduction of up to 10%.

A significant finding was that synthetic fuel blends yielded emission reductions that were generally greater than their blending ratio. Remarkably, a 50% synthetic fuel blend yielded similar emission results to neat synthetic fuel.

Optical tests were also carried out in this study to investigate the combustion properties of the synthetic fuel. The engine was fitted with a quartz piston and combustion was photographed by means of a high speed video camera. OH chemiluminescence was measured, but no temperature or soot concentration information was published. The optical results reflected the better ignition quality of the synthetic fuel, but also showed better vaporisation characteristics and a more uniformly distributed flame structure.

At high load the effect of ignition quality appeared less significant than at low load. The OH chemiluminescence results confirmed an earlier relative onset of sooting combustion between the two fuels at low load than at high load.

Extensive testing with a modern passenger car DI diesel engine was also done by Payri et al. (2000) to compare synthetic diesel to a European reference diesel. The emission results were very similar to other tests, noting significant improvements on HC, CO, CO_2 and soot, while NOx emissions remained largely unchanged. A significant improvement in indicated efficiency was recorded as about 4%. This stems from the reduction in fuel mass injected for

maintaining the same IMEP. Thus it was concluded that the synthetic fuel resulted in a slightly better Specific Fuel Consumption. This was also observed by a decrease in exhaust $C0_2$ volume concentration. However, due to the low density of the synthetic fuel, an increase in volumetric fuel consumption in the vehicle tests were recorded as about 3%. It was noted therefore that the low density of the synthetic fuel is not fully compensated for by the higher energy content.

A study of the combustion rates of the fuels showed the synthetic fuel as having a faster combustion process. This is due to the low evaporation temperature and high cetane number of the fuel. This effect was more significant at low loads

Azetsu et al. (2003) did a study on the effect of aromatic components in fuel in the context of diesel engines. It was concluded in this study that the flame temperature and amount of soot in the flame increased with increasing amounts of aromatic components in the fuel. This study made use of the two-colour method to determine these results.

Ng et al. (2005) used the two-colour method in a comparative investigation between a synthetic bio diesel and conventional diesel. No flame temperature information was published, but the soot concentration results were presented. The synthetic diesel was found to have higher soot concentration levels than the reference diesel in the early stages of combustion; however these levels were lower towards the end of combustion in the after burn stage. It was also found that the synthetic fuel produced lower engine out soot emissions. The authors suggested that the reason for the high initial soot formation was the shorter premixed burn phase resulting in poor mixing. It was further concluded that the more rapid soot oxidation of the bio diesel was due to its low sulphur and aromatic content.

4. Experimental Setup

4.1. Ricardo Hydra Engine

Most of the experimental work in this project was done on a single cylinder Ricardo Hydra research engine. This engine was configured as a direct injection diesel engine making use of a modern Bosch high pressure fuel injection system. More specifically it incorporates a high pressure fuel pump capable of maintaining high fuel pressure, a fuel rail and a 4-hole electronic Bosch fuel injector. The cylinder head has two valves and the injector comes in at an angle from the side. The basic specifications of the engine are tabulated here:

Table 4-1: Specifications of the Ricardo Hydra Engine

Bore	mm	80.26
Stroke	mm	88.90
Swept Volume	cc	450
Compression ratio	-	16:1
Fuel injection system	-	Common rail - DI

In a previous MSc project by Ratshikuni (2003) the combustion chamber was modified to resemble a modern passenger car engine. This involved changing the shape of the piston bowl and reducing the compression ratio. The cylinder head was also modified to gain optical access. Two sleeves were inserted to house an endoscope and an illuminating probe simultaneously. Careful attention was paid to positioning these such that the best possible views of the combustion chamber could be obtained. Particularly the system is designed to allow the endoscope to protrude deep into the piston bowl and look up at the injector sprays.

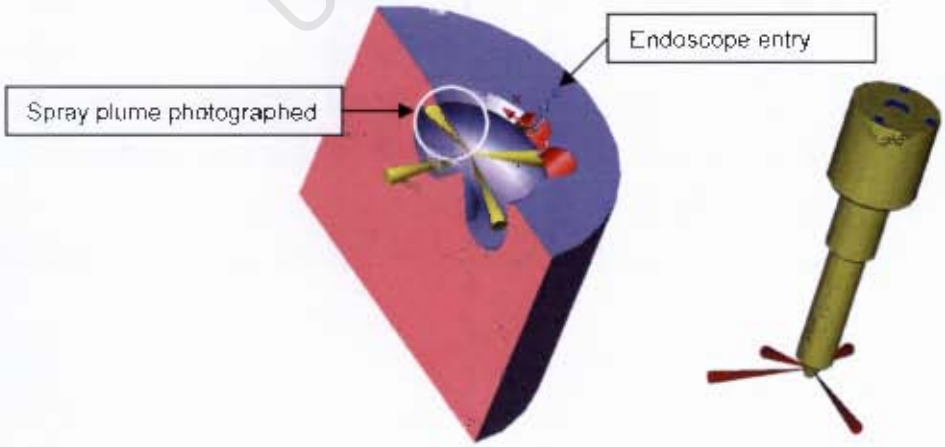

Figure 4-1: Piston Bowl and injector layout

The combustion chamber is therefore effectively in the piston bowl which is offset due to fact that the injector is not in the centre. While this system attempts to replicate a modern combustion chamber, it is acknowledged that it can be further improved by a four valve layout and a vertical injector placed in the centre. Details of the combustion chamber layout will become very relevant in the following chapters where it is important to understand what the combustion images are representing relative to the combustion chamber. Photographs of the underside of the cylinder head and the modified piston bowl are shown below:

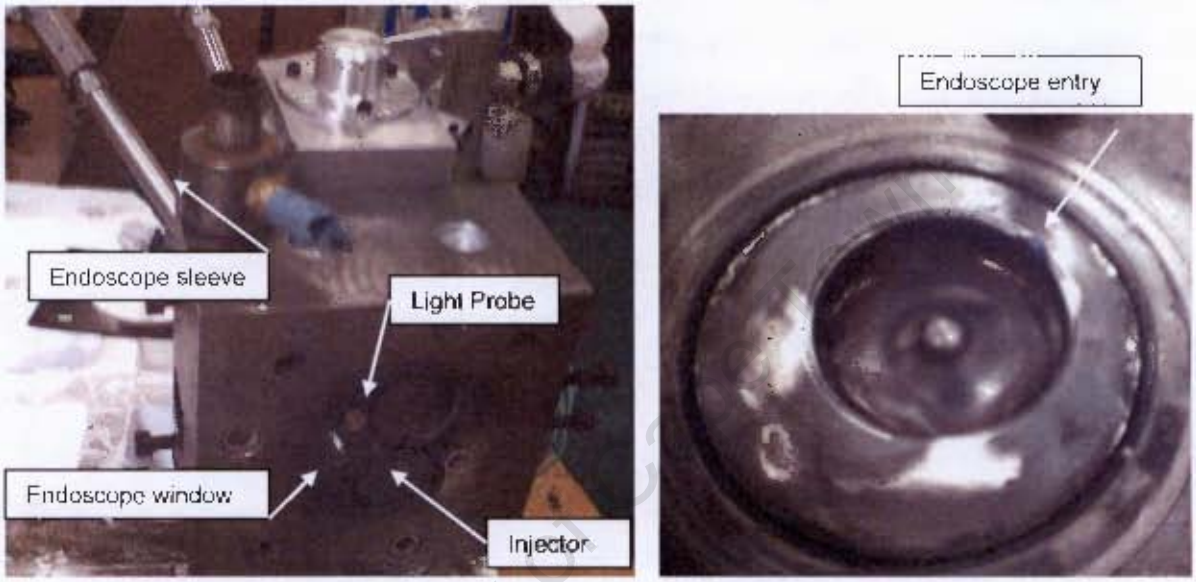

Figure 4-2: Modified Hydra cylinder head and piston

The optical access is designed to allow the endoscope and its protective window to be removed easily. This is necessary to clean the soot deposits on the window which form remarkably quickly in this engine. The endoscope is fitted in a protective sleeve with a quartz window at the end which is then inserted into the engine access sleeve and fastened. A compressed air line is attached to the endoscope for cooling as it is exposed to the engine combustion temperatures. A lens with adjustable focus and the CCD camera are fitted directly on top of the endoscope and held in place by an adjustable arm. In the second sleeve a light probe can be fitted to illuminate the combustion chamber. This is only used when looking at the liquid spray, but for thermo graphic combustion analysis no external lighting is used.

The layout of the optical access points, camera and light probe is illustrated in the photograph overleaf.

Figure 4-3: Optical setup

The engine itself is coupled to a DC dynamometer which is capable of motoring the engine or absorbing the torque. An extensive list of equipment is set up to control and measure the operating parameters of the engine. Before these are described in detail, an overview of the test cell and main components is shown below:

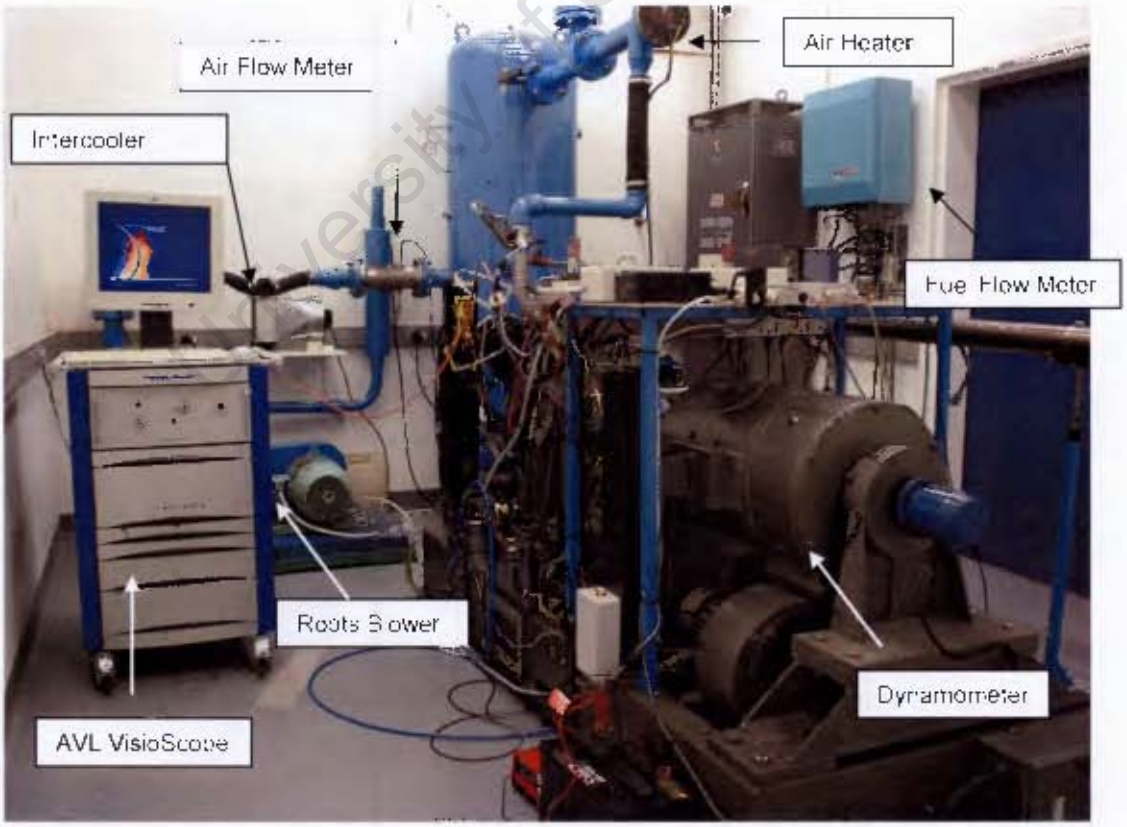

Figure 4-4: Hydra Engine Test Cell

The injector is controlled by a Bosch electronic engine management system similar to that found on a modern car. Access to the ECU is facilitated by means of a desktop computer whereby the engine maps can be read and altered. Parameters such injection duration, injection timing, fuel pressure and pilot injection can be adjusted by changing the map values on the computer. Adjustment of the injection duration on the map is how the engine load is varied. The details of these settings are given in the following chapter.

The pressure and temperature of the air supplied to the engine can be accurately controlled. A roots blower is used to simulate turbo charging by compressing the air. The air passes through an air cooler and laminar air flow meter before feeding into a large surge tank. This effectively eliminates any pulsing generated by the positive displacement roots blower, as well as damping the pulses from the engine to minimise the effect on the airflow measurement. The pressure in the tank is controlled by venting excess pressure to atmosphere prior to the air flow meter. Pressure is measured in the inlet manifold by a sensitive piezo-resistive pressure transducer. An air heater is fitted prior to the inlet manifold with a temperature controller capable of holding a set temperature to an accuracy of 1°C.

The fuel flow rate is measured by a gravimetric fuel flow meter (AVL 730), which calculates fuel mass flow rate from the change in mass of a fuel reservoir over a set time period.
This is effectively a mass flow meter which is useful for testing fuels of different density as required in this project. Fuel temperature is controlled by a water cooled heat exchanger and the room temperature is adequately controlled by an effective air conditioning system.

The engine torque is measured by a load cell on a lever arm attached to the dynamometer. Cylinder pressure is another critical parameter to determine the indicated engine load and this is measured by a water cooled piezoelectric pressure transducer. The cylinder head was modified in this project to incorporate this device and it resulted in a significant improvement in the quality of the pressure data compared to a previous uncooled system. The details of this modification and the pressure transducer are given in Appendix 2.

The engine speed and crank angle measurement is done by means of an AVL light pulse crank angle encoder which is set to a resolution 0.1 crank angle degrees. This signal is also used by the AVL VisioScope to accurately trigger the camera at the required times.

4.2. Data Acquisition

The AVL Indiset 620 data acquisition system was used to capture the signals emanating from the cylinder pressure transducer and the crank angle encoder simultaneously. The injector current, manifold pressure and torque signals are also fed into the AVL Indiset 620. This system works in conjunction with a desktop computer and AVL IndiWin software. While the engine is running the pressure can be displayed in real time on a graph relative to the engine crank angle and with the injector signal superimposed. Furthermore the pressure data is used to calculate the Indicated Mean Effective Pressure (IMEP) and the rate of heat release. The system can also be set to acquire the data over a set number of cycles and save a set of data which is averaged over this number of cycles. The relevant statistical figures are also then displayed. This results in reliable measurement of **IMEP, torque, engine speed, injector timing, cylinder pressure, boost pressure** and **heat release** at different operating points. It is accurate enough to distinguish between the effects of different fuels at the same operating points. The following section will detail how the IMEP can be cross checked between the torque and pressure data.

Other engine parameters are displayed on the control panel and are recorded manually as required. These include a range of temperatures: **air, fuel, oil, water, inlet manifold** and **exhaust gas**. The fuel consumption is measured over a set time period and displayed on a separate panel. The inlet air temperature control is also incorporated into the control panel.

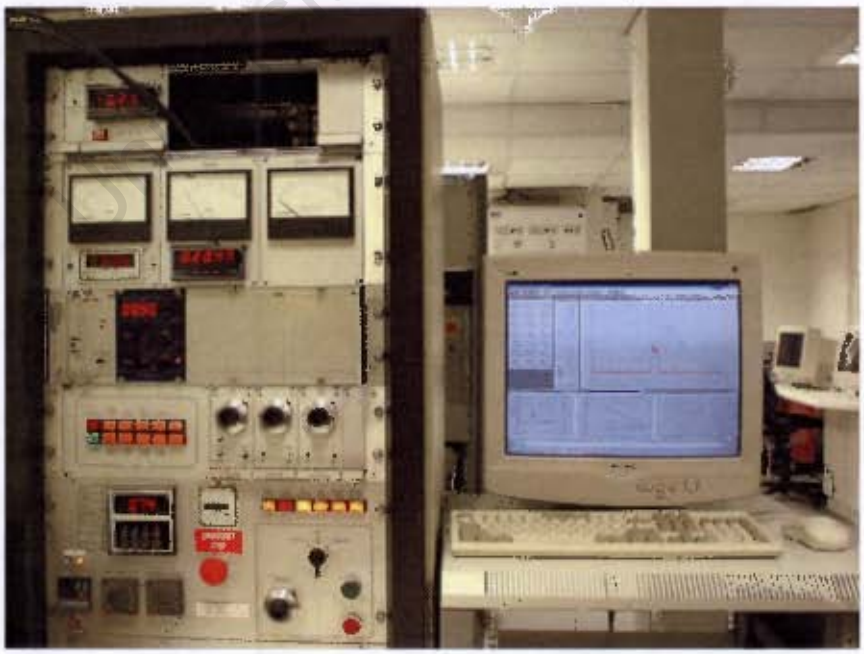

Figure 4-5: Control panel and AVL Indiset 620 data acquisition system

4.3. AVL VisioScope

This section briefly outlines the technical setup of the VisioScope. The theory behind the system's image analysis method is discussed in detail in chapter 2. The system incorporates a desktop PC and an electronic control unit mounted on a portable trolley. It requires a data input from the crank angle encoder from which it calculates the engine speed and triggers the camera at the appropriate crank angle degrees specified by the user through the software interface. The defining feature of the VisioScope kit is the three endoscopes, each with the objective lens looking in different directions, 0°, 30° and 60°. This enables a complete range of views from a particular access point. These endoscopes are designed specifically for combustion imaging by virtue of the fact that they are air cooled. Compressed air is supplied at the top to a channel within the endoscope shaft and exits through small holes at the bottom lens. The air thus cools the endoscope itself and the quartz housing window before travelling up the housing sleeve and exhausting to atmosphere.

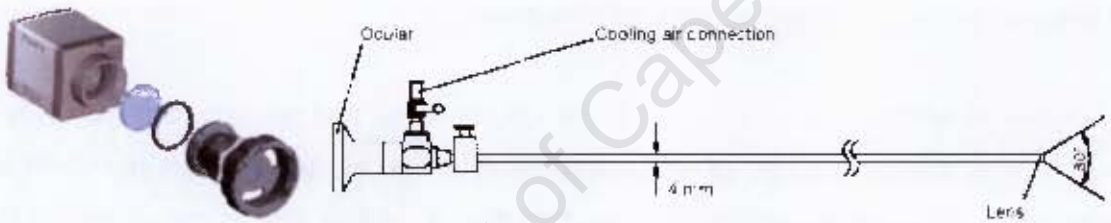

Figure 4-6: CCD camera, edge filter, lens and combustion endoscope

A lens with an adjustable focus length is fitted to the top of the endoscope. When images are to be used for thermo graphic analysis, the edge filter needs to be fitted to the CCD camera as shown in the above figure. The ThermoVision software is calibrated for the specific endoscopes and lenses supplied. Care must be taken to ensure that the correct calibration file is used for the chosen setup of lens and endoscope. More specific operational details are given in Appendix 1.

The camera speed is sufficient to capture one image per engine cycle. The software is however very neatly designed to take a range of images at over number of cycles and put them together in a video sequence. This is adequate for the purpose of comparative analysis; however the gradual soot formation on the endoscope window needs to be considered.

A cold light system with the option of a flashlight is triggered in conjunction with the camera and can be used to illuminate a fuel spray, for example.

4.4. Combustion Bomb

In a previous MSc project by Miller (2003) a constant volume Combustion Bomb was developed at the Sasol Advanced Fuels Laboratory. The bomb is designed primarily for optical access to combustion events and is used in this project to complement the work done on the Hydra engine in an effort to verify the combustion imaging results. Development of the bomb was largely incomplete at the time of this project and significant work was done by the author to commission it. The design details of this are presented in Appendix 3.

The Constant Volume Combustion Chamber (CVCC) is manufactured from stainless steel and capable of containing a pressure of up to 300 Bar. It is designed with numerous access points around its periphery where accessories can be fitted according to the user's requirements. In this project these included a pressure transducer, thermocouples, spark plug and the inlet and exhaust valves. The other points which can contain a turbulence fan, fuel injector and optical windows were plugged. The two faces of the bomb can accept a large optical window or fuel injectors as required. In this project the one face had the fuel injector in the centre and the other was a large optical window, 100mm in diameter. This gives a direct view of the injector. The window is made of Sapphire (Al_2O_3) and is about 25mm thick. The bomb is heated by eight cartridge heaters to a temperature representative of the average wall temperature in an engine. The bomb is insulated to minimise heat loss.

The principle of operation is to pressurise the bomb with a gaseous fuel mixture of Acetylene, Nitrogen and 21% excess Oxygen. A spark is then triggered to initiate the pre combustion charge which rapidly raises the pressure and temperature in the CVCC. As the pressure drops due to heat loss, the high pressure diesel injector is triggered at a user defined chamber pressure. Due to the excess oxygen in the initial mixture, the liquid fuel will auto-ignite, much like it would in a conventional diesel engine. As this occurs in front of a large window, the entire injection event can be photographed. This is a significant feature because in the engine setup only a small portion of the combustion chamber can be photographed.

The fuel injector is a Bosch unit from a modern diesel passenger car and has six holes. It is supplied by a corresponding automotive high pressure fuel pump and common rail, where the pump is driven by an auxiliary electric motor. The system is controlled electronically by a custom made program in LabVIEW™. Therefore the system is controlled via a desktop PC and the pressure trace and injection signal is then acquired by another computer.

The setup is shown in the pictures below:

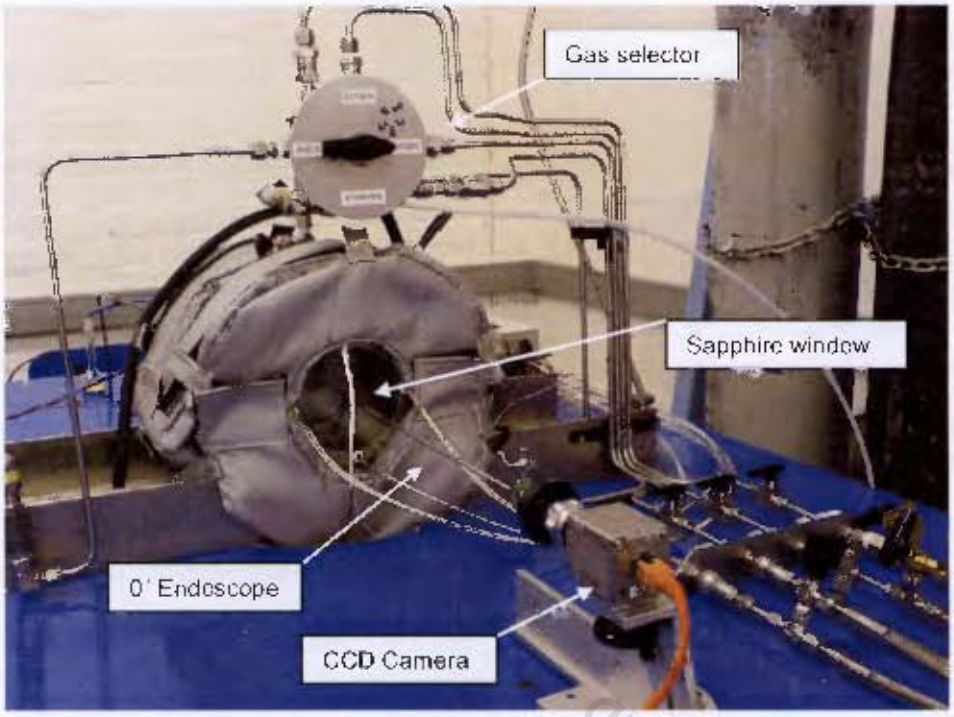

Figure 4-7: Optical setup of the Combustion Bomb

The figure above shows the bomb window and camera setup. The endoscope is still used because for thermo graphic analysis, the system is calibrated to include the optical effect of the endoscope. The figure also shows the inlet system and gas selection valve.

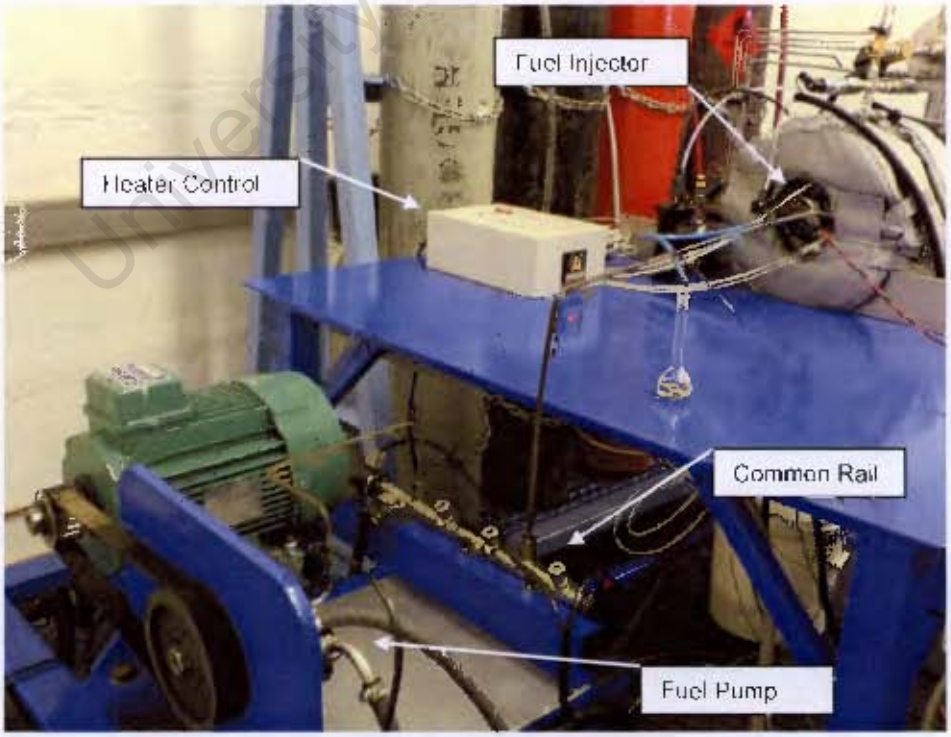

Figure 4-8: Diesel rig setup of the Combustion Bomb

The control interface of the operating program is shown below:

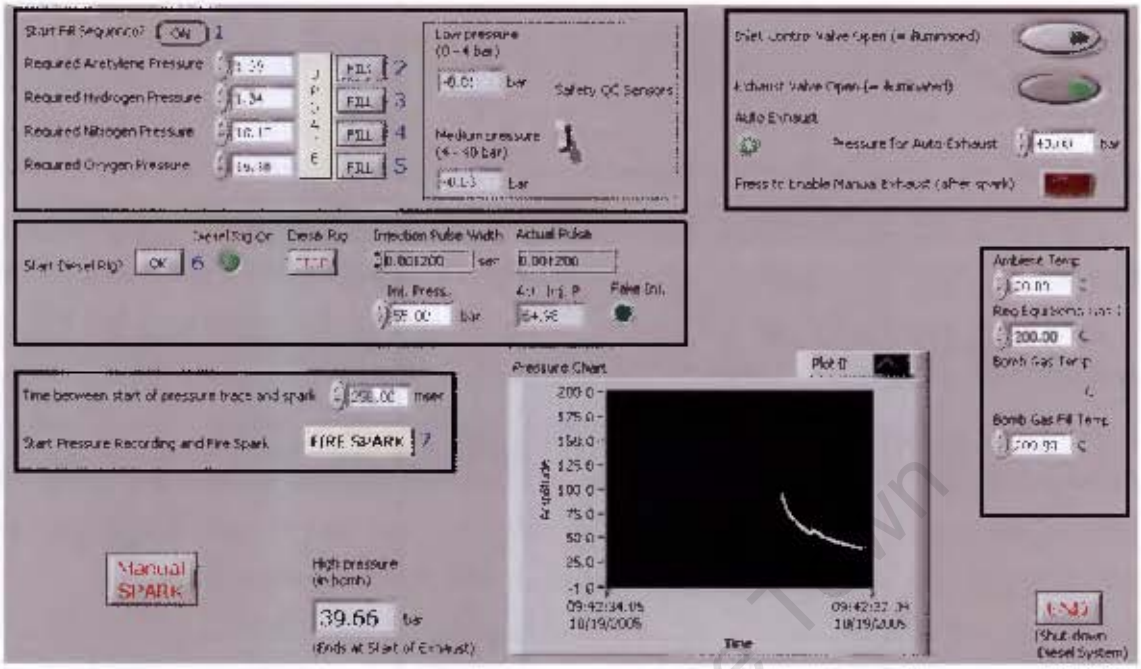

Figure 4-9: Bomb control interface in LabVIEW™

A separate program and computer is used to acquire and record the data. The pressure trace is displayed on the screen and an option is given to save the data as a spreadsheet.

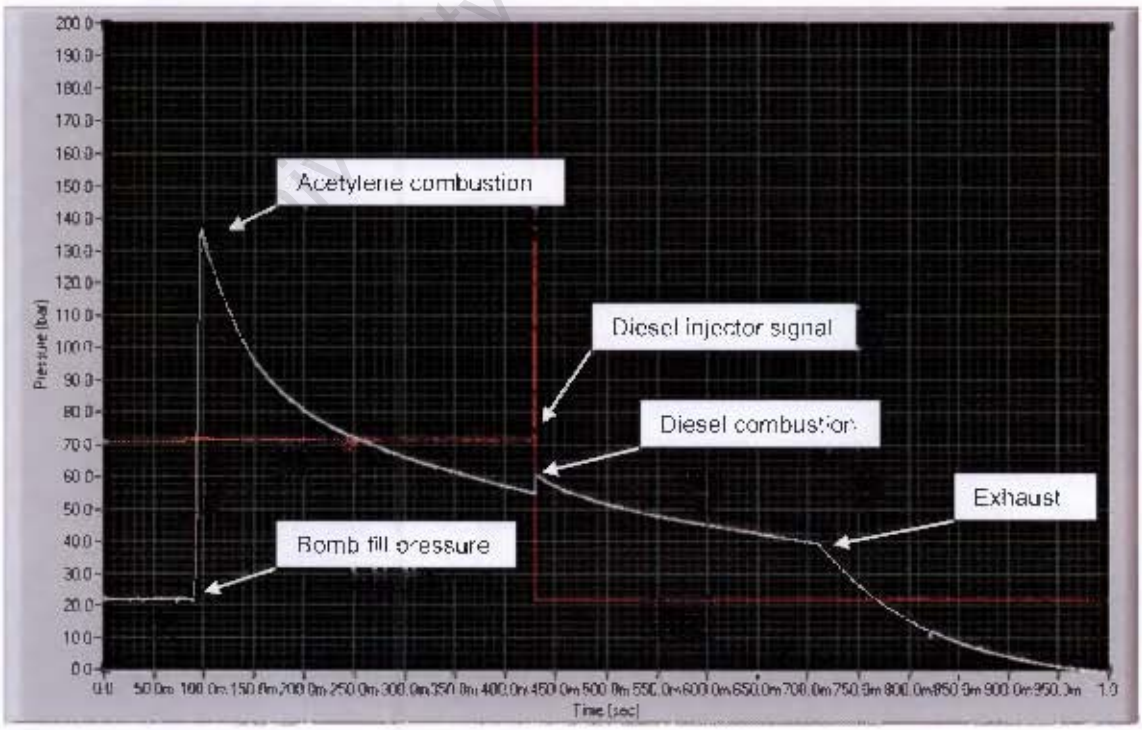

Figure 4-10: Example of the data acquired from a bomb experiment

5. Experimental Procedure

5.1. Hydra engine load verification

In a diesel engine the load or power output is determined by the amount of fuel injected, and thus it is difficult to define a specific point of 100% load. Traditionally it is done by increasing the fuelling until the exhaust smoke level reaches a set limit. More commonly in modern engines load is limited by cylinder pressure or exhaust gas temperature. In this project the maximum load point was determined experimentally by gradually increasing the fuel injection duration at a set speed and recording the IMEP and fuel mass flow rate. It was noticed that the engine load (IMEP) increased linearly with fuel mass flow up to a certain point where it became non linear. This occurs where the additional fuel injected is not being completely burned and results in excessive smoke formation and inefficient combustion.

This point can be clearly seen on the graph below. 100% load was defined as 1ms injection duration at 1500rpm for the purposes of this project. This point falls just before the graph becomes non-linear. A nominal boost pressure was used in an effort to avoid test results being dependant on atmospheric pressure. From this point on the engine load settings will be described as a percentage relative to the 100% load defined here.

Table 5-1: Main engine parameters for the defined 100% load point

Fuel	Inj Timing	Engine Speed	Boost Pressure	Inj Duration	IMEP	Fuel Flow	Rail Pressure
type	°BTDC	rpm	bar (absolute)	µs	bar	kg/hr	Bar
Euro	*10*	*1500*	*1.152*	*1000*	*9.45*	*1.04*	*500*

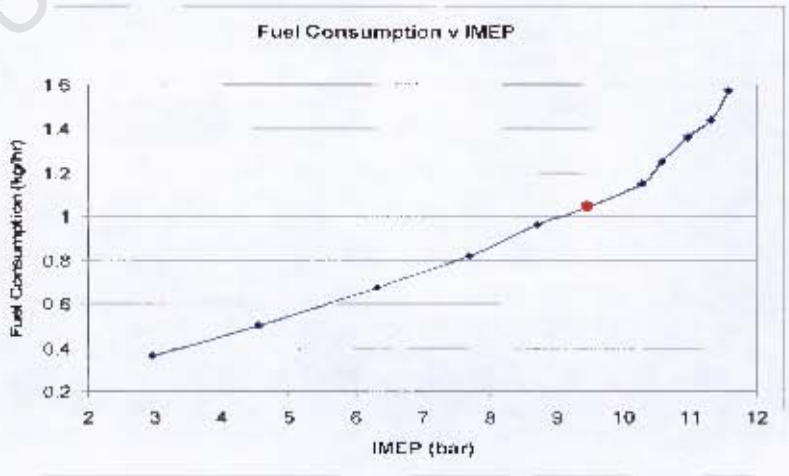

Figure 5-1: Experiment to determine 100% engine load

5.2. Hydra engine IMEP verification

Indicated Mean Effective Pressure, abbreviated as IMEP, is a measure of the average pressure exerted on the piston over an engine cycle. The signal acquired from the cylinder pressure transducer is averaged over 88 engine cycles and an IMEP value is calculated by the AVL Indiset. The torque signal from the load cell on the engine dynamometer is captured in a similar way. Mean Effective Pressure can be related to torque by a simple relationship. 'Indicated' implies that mechanical friction losses in the engine are not taken into account, whereas 'Brake' implies that friction has been accounted for.
The torque signal from the load cell is measuring the net shaft torque and can therefore be considered the brake torque. Brake Mean Effective Pressure can then be calculated:

$$BMEP = \frac{4\pi T_b}{V_d} \qquad \text{(Equation 5-1)}$$

Where: T_b = Brake Torque
V_d = Displaced Engine Volume

The Hydra test engine has the ability to motor the engine at a set speed. If this is done at the same speed as the running test, the torque measured is a result of mechanical friction. Thus the Frictional Mean Effective Pressure can be calculated:

$$FMEP = \frac{4\pi T_m}{V_d} \qquad \text{(Equation 5-2)}$$

Where: T_m = Motored Torque

Using these two results, IMEP can be calculated:

$$IMEP = BMEP + FMEP \qquad \text{(Equation 5-3)}$$

This result can be used to verify the IMEP obtained from the pressure data and is a useful cross check. If the systems are performing correctly, a very close correlation of the two results should be observed. However, the IMEP derived from the torque data should be slightly lower as the extra friction of the piston rings due to the combustion pressure is not present when the engine is motored. This procedure was followed for each engine test.

5.3. Hydra engine test procedure

The engine test procedure was designed to test the differences between the two test fuels at typical diesel engine operating points. Bearing in mind that the main purpose of the project is to evaluate the image analysis technique, it was decided to keep the number of variables to a minimum. The testing procedure entails a single carefully controlled speed point. The inlet pressure and temperature are also carefully controlled at a single point. The main variable introduced was engine load. Test sequences were then repeated at different injection timing.

Four load settings were defined based on the initial load verification test described in the previous section. Injection duration of 1ms of the reference fuel defined 100% load. Each engine test sequence comprised the following four load settings:

Table 5-2: Fixed engine test settings

Engine Load	*Injection Duration*	*Engine Speed*	*Manifold Pressure*	*Manifold Temperature*	*Water Temperature*	*Oil Temperature*	*Fuel Temperature*
%	µs	rpm	bar (absolute)	°C	°C	°C	°C
50	650	1500	1.152	50	85	110	19
70	750						
85	850						
100	1000						

Using the test sequence and settings shown above, five tests were conducted with varying fuel types and injection timing. It was decided to include a variation in injection timing to compensate for the earlier ignition of the model fuel due to its high cetane number. By doing this the cetane effect can be isolated from other effects when it comes to the image analysis.

Table 5-3: Engine test sequence

Test Batch	*Fuel Type*	*Injection Timing*	*Test Description*
		°BTDC	
Ref 1	*EN590*	*10*	*Base reference test*
Model 1	*LEMF*	*10*	*1st test with comparative fuel*
Model 2	*LEMF*	*9.2*	*2nd test - Injection timing set for equivalence of start of combustion*
Model 3	*LEMF*	*8.4*	*3rd test - Injection timing retarded one step further*
Ref 2	*EN590*	*10*	*Repeat of base reference test to quantify repeatability of equipment*

In summary each test batch is conducted at four load points, resulting in a total of twenty separate engine test runs. For each test run a complete set of engine data is recorded and a number of image sequences captured as described in the following section.

5.4. Hydra engine imaging procedure

In order to capture combustion images, the following procedure was followed.
The engine is run at the desired settings until all temperatures and controlled parameters have stabilised at the correct values or within a suitable range. Engine test data is first recorded at each operating point, and then the imaging process can be conducted.

The engine has to be stopped in order to remove the probe blank and insert the endoscope sleeve. The camera is then attached and the engine can be motored up to the set speed.
This process from stop to restart can be done in approximately one minute so the effect of engine cooling can be considered to be not overly significant.
To minimise the effect of window sooting, the injection is enabled simultaneously with the start of the image capture sequence. The engine map that controls the engine is constrained to the single injection duration and timing value which results in a seamless start up and a smooth transition from motoring to torque absorption. A slight speed variation occurs here but it does stabilise before the image sequence actually begins. The engine can run for about 10 seconds at 100% load before the images are noticeably affected by window soot. The sooting effect is considerably diminished at lower engine loads.

A number of image sequences were captured to investigate all possible insights that the optical setup can provide; both quantitative thermo-graphic data and qualitative visual data.
The primary interest is to capture a range of images from the start of combustion to the end of injection. This range was extended to obtain information on the combustion phase after the end of injection. These results would form the basis of the investigation, but for completeness a number of other tests were conducted to add value to these results.

It is inevitable that the endoscope window which is exposed to the combustion gasses in the cylinder will be blackened by soot deposits. This effect will to some extent alter the data obtained from the images and cast some doubt over those results. It follows that some testing to quantify this effect would be desirable. The best way to do this is to repetitively capture an image at the same point for a period of time from when the lens is clean to when the lens completely covered in soot. The results from these images will show a steady decline in temperature due to the soot built up on the lens. If this is done at each load point and for each fuel, comparisons can be drawn based on the rate of sooting under the various conditions. Some additional testing involving combustion chamber illumination was included

to examine the injector spray formation and the start of sooting combustion. The table below contains the settings of the seven different image capturing procedures that were followed in this investigation and the relevant camera settings of each. Each series of images were conducted at each of the four load points for each fuel. Each series is described in more detail below the table.

Table 5-4: Image capture procedure and settings

	Start	*Stop*	*Sample interval*	*Exposure*	*Gain*	*Endoscope*	*Lens*	*Illumination*
	°CA	°CA	°CA	µs		°	mm	
Series 1	***Sequence of images for range temperature analysis***							
	-1	20	0.2	30	low	60	25	None
Series 2	***Sequence of images for correction of sooting effect***							
	5	10	0.5	30	low	60	25	None
Series 3	***Single repeated images for temperature verification and sooting determination***							
	2.6	2.6	100	30	low	60	25	None
Series 4	***Single repeated images for temperature verification***							
	10	10	10	30	low	60	25	None
Series 5	***Sequence of images to determine burn duration***							
	25	65	1	30	low	60	25	None
Series 6	***Sequence of illuminated images for spray comparison***							
	-7	2	0.2	60	High	60	25	Flash
Series 7	***Sequence of illuminated images to investigate auto-ignition***							
	-2.5	1	0.1	60	High	60	25	Flash

Series 1 attempts to capture as many images as possible in sequence from the start of combustion to well after the end of injection. Images were captured at intervals of 0.2 crank angle degrees (CAD), which results in five images for every CAD. It was noticed that at the 50% load point, there was negligible soot deposits on the endoscope window. Thus at this load point series 1 was conducted using a sampling interval of 0.1 CAD, effectively ten images per CAD. Soot deposits increase dramatically at higher loads and these effects will be seen in the results. In an attempt to minimise this effect, series 1 was conducted in two steps. Firstly a range from -1 to 10 CAD was captured. At this point the engine was stopped; the endoscope window was removed, cleaned and re-inserted before the engine was restarted. With a clean window the image range from 10 to 20 CAD was captured. The overlap of the 10 CAD images can be used to determine the effect of the window sooting at this point. As mentioned before, while the cleaning of the endoscope window sounds like an elaborate procedure, it can actually be done very quickly.

To facilitate good statistical averaging of data, each sequence was repeated three times.

Recall that there are 4 load points for each of the 5 fuel tests, a total of 20 engine test points. Series 1 was conducted at each point, three times resulting in 60 image sequences.

Series 2 is an image sequence from 5 to 10 CAD taken at half degree intervals. This range can be captured very quickly and therefore the effect of soot build up can be considered negligible here. These results can be used to verify the corresponding points in series 1 and gauge to what extend the images in series 1 are affected by soot deposits.

Series 3 is the most effective investigation of the effect of soot deposits on the endoscope window. This sequence captures the same image, 2.6 CAD, repetitively 100 times over. While this lengthy capturing process takes place, the window gradually soots up until the light transmission is effectively completely blocked. These results can be used to determine a soot deposit rate and is effectively also a measure of in-cylinder soot formation. Comparison of these results between the different load points and different fuels will be very insightful.

Series 4 is an investigation of the 10 CAD point. Images are captures at this point ten times to get a good average of the data at this point to enable a cross check of the other series data should it be necessary.

Series 5 is a sequence from 25 to 65 CAD taken at a rate of a single image per CAD. This was conducted for qualitative interest to determine when the last visible signs of combustion took place. This can be used to compare the burn duration of the different fuels and different load points.

Series 6 is a detailed qualitative look at the injector spray prior to auto-ignition. Using in-cylinder flash light illumination, images of the fuel spray were captured form the start of injection to the start of combustion. Taken at 0.2 CAD intervals this provides a detailed sequence of the spray development. Due to the different density, viscosity and vaporisation properties of the two test fuels, it would be interesting to see if there are any noticeable differences in the spray patterns.

Series 7 is a detailed look at the onset of sooting combustion. Using flash light illumination and capturing 10 images per CAD, this sequence aims to reveal exactly where and when the first signs of sooting combustion can be seen.

Some of this testing is done for purpose of verification and cross checking. The results presented will include only the relevant features of these procedures.

5.5. Combustion Bomb testing procedure

As far as possible the conditions in the Combustion Bomb should be similar to those in the engine for the tests conducted in this project. In the engine injection occurred at a cylinder pressure just below 55 bar and the injection duration ranged between 0.65 and 1 ms. It was decided to do the bomb testing using an injection duration of 1ms and occurring at a bomb pressure of 55 bar. The initial mixture of gasses needs to be calculated such that the temperature at 55 bar is also representative of that in the engine. The initial combustion needs to peak at a considerably higher pressure than the injection pressure to ensure that the combustion of the gasses is complete before diesel is injected. A theoretical model developed by Miller (2003) was used to calculate a gas mixture that would be suitable for this project. As the bomb and model are still in an early stage of development, the accuracy of the predicted temperature cannot be established at this stage. However the bomb will accurately and repeatedly inject at 55 bar and this was considered adequate for the imaging comparison required in this project.

The gas mixture and settings used for all the bomb experiments is given in the table below:

Table 5-5: Bomb gas mixture and settings

Gas	Accumulative gauge pressure	Wall temperature	Injection pressure	Rail pressure	Injection duration
	bar	°C	bar	bar	ms
Acetylene	1	130	55	980	1
Nitrogen	10.5				
Oxygen	16.5				

Prior to filling of the pre-charge gasses, the bomb is flushed with nitrogen and exhausted to atmospheric pressure. The bomb is then filled with acetylene to the set pressure according to the table above. Nitrogen and oxygen are then filled consecutively to the accumulative pressures indicated. Once the bomb has been filled a manual inlet needle valve is closed to seal the bomb. The high pressure diesel pump is started and the spark can then be fired which starts the automatic process of diesel injection, camera trigger, data acquisition and exhaust at the appropriate times.

The data collected from an experiment is in the form a pressure trace from when the spark is fired until the exhaust valve is automatically actuated after both combustion events.

The VisioScope will also capture a single image at a preset point in the diesel combustion process.

5.6. Combustion Bomb imaging procedure

While the optical access to the Combustion Bomb is vastly superior to that of the engine, the limitation is that there is only one combustion event per experiment. Therefore the imaging procedure will contain considerably less images than the engine test procedure because only one image can be captured in each experiment. It is also acknowledged that the images are captured through a thick sapphire window which could have a small effect on the transmissivity of the endoscope system which is not included in the calibration.
An external triggering system was developed as the AVL Visioscope is designed specifically for an engine and thus requires a crank angle encoder signal to operate its internal camera trigger system. The external system makes use of the injector signal and a delay timer to trigger the camera momentarily after injection with a delay set by the user. The design details of this system are given in Appendix 3.

The trigger has a range of 0 – 10ms after injection. As the injection duration is 1ms, this delay allows the camera to cover the entire injection range and a significant time after injection. The delay can be adjusted by manually turning a dial and setting it to a desired value. A sequence of 14 images was captured from the start of combustion. The delay was incrementally increased, initially in very small steps as the flame developed. Images were then taken in slightly larger increments until combustion was nearly complete. The last two images were taken at large increments to capture the combustion of the injector sac volume which was clearly visible in the bomb.

An arbitrary scale of 1 – 20 was used on the manual dial, where 1.75 was used as the start of combustion. This corresponds to a delay of 1.15ms after the injection signal. The last image at point 20 corresponds to approximately 4ms after the injection signal. The 14 images taken are represented in the table below to show the arbitrary dial scale and the calibrated associated time delay values in ms from the injection signal.

Table 5-6: Image sequence settings for the Combustion Bomb

Dial setting	1.75	2	2.5	3	4	5	6	7	8	9	10	11	15	20
Delay (ms)	1.15	1.19	1.25	1.32	1.47	1.62	1.78	1.92	2.10	2.24	2.39	2.51	3.30	4.12

This sequence was conducted for the two test fuels and each image was repeated. A total of 56 experiments were conducted and the same number of images is therefore available for investigation.

5.7. Image data analysis procedure

Series 1 of the Hydra Engine imaging procedure contained 60 sequences of images. The 50% load points contain 212 images in each sequence, and all the other load points contain 107 images in a sequence. Considering that each test sequence was repeated three times, a total of 7995 images were captured in series 1. The CCD camera uses an array of 640 x 480 pixels which results in 307200 pixels in each image. When the pictures are analysed for flame temperature, each pixel is assigned a temperature value. This would result in approximately two thousand, four hundred and fifty six million data points in series 1 alone.

It follows that the data analysis procedure of the images needs to be carefully considered. Unfortunately the AVL ThermoVision V1.1 software which was used in this project does not offer access to the detailed pixel information, but it processes and presents the information in the following way:

The images are analysed by using the AVL software and three processing steps are conducted. Each image is firstly calibrated, then processed for flame temperature and thereafter processed for soot concentration KL values. Each step can be applied to an image sequence and then each image in that sequence will be processed automatically.
To access the numerical data, a histogram can be generated with parameters set by the user and exported as a text file. This effectively condenses the information of the individual pixels into categories; however the spatial information of where these pixels are is lost.
The flame temperature data was set up as follows:

The starting point was set to 2000K and the end point to 2800K with 16 intermediate steps. The histogram gives a table of neatly spaced columns of 50K from 2000K to 2800K and contains values representing the number of pixels in each temperature category.

These data can be imported into a spreadsheet. The three repeated sequences can then be averaged and smoothed. To further condense the data into a form suitable for comparison purposes, the final data output are columns containing the number of pixels above a threshold temperature. The threshold temperatures start at 2350K and increase in increments of 50K up to 2800K. These data can then be represented on a graph for each test batch. For direct comparison of the test fuels, they can be displayed on the same graph.

A similar procedure is used to analyse the data obtained from the soot concentration images. A histogram is set up to display data in the KL factor range 1 – 15 at 1 KL increments. Each column thus represents the number of pixels at the corresponding KL factor, which can then be modified to represent the number of pixels above the corresponding KL factor.

The resulting output is useful information, but is heavily dependant on the flame area by virtue of the fact that it represents a number of pixels above a temperature or KL threshold. This gives an accurate overview of the image as a whole, but it offers not spatial insight to the flame structure or specific areas of the flame.

Based on the abilities of the software available, the images were analysed and as much numerical data as possible was extracted. These results are presented and will be discussed later with reference to the limitations of the software and possible ways of better representing the numerical image data.

6. Results

6.1. Hydra engine test results

Prior to capturing optical data from the Hydra engine, each engine test point was tested thoroughly with both fuels and the main results are presented here for each test batch.

Table 6-1: Results for base reference test

Ref 1	Fuel:	Main engine parameters					IMEP cross check				
Inj timing	EN590	IMEP	Fuel mass	Injection	Energy	SOC	Torque	BMEP	Motored	FMEP	IMEP
°BTDC		(indiset)	flow rate	duration	in			(load cell)	Torque		(calc)
10	Load	bar	kg/hr	µs	J/cycle	°BTDC	Nm	bar	Nm	bar	bar
1	50%	5.11	0.55	933	523	1	12.08	3.37	6.22	1.74	5.11
2	70%	6.7	0.76	1033	722	1.2	17.57	4.91	6.35	1.77	6.68
3	85%	7.88	0.91	1133	865	1.3	21.69	6.06	6.33	1.77	7.83
4	100%	8.99	1.05	1278	998	1.5	25.48	7.12	6.25	1.74	8.86

Table 6-2: Results for 1st test with comparative fuel

Model 1	Fuel:	Main engine parameters					IMEP cross check				
Inj timing	LEMF	IMEP	Fuel mass	Injection	Energy	SOC	Torque	BMEP	Motored	FMEP	IMEP
°BTDC		(indiset)	flow rate	duration	in			(load cell)	Torque		(calc)
10	Load	bar	kg/hr	µs	J/cycle	°BTDC	Nm	bar	Nm	bar	bar
1	50%	5.12	0.54	933	526	1.7	12.25	3.42	6.26	1.75	5.17
2	70%	6.74	0.75	1033	730	2	17.89	5.00	6.24	1.74	6.74
3	80%	7.86	0.84	1133	818	2.3	21.87	6.11	6.20	1.73	7.84
4	100%	8.91	0.96	1278	935	2.6	25.47	7.11	6.22	1.74	8.85

Table 6-3: Results for 2nd test with injection timing set for equivalence of SOC

Model 2	Fuel:	Main engine parameters					IMEP cross check				
Inj timing	LEMF	IMEP	Fuel mass	Injection	Energy	SOC	Torque	BMEP	Motored	FMEP	IMEP
°BTDC		(indiset)	flow rate	duration	in			(load cell)	Torque		(calc)
9.2	Load	bar	kg/hr	µs	J/cycle	°BTDC	Nm	bar	Nm	bar	bar
1	50%	5.14	0.53	944	516	1	12.11	3.38	6.47	1.81	5.19
2	70%	6.71	0.73	1033	711	1.3	17.66	4.93	6.41	1.79	6.72
3	80%	7.76	0.85	1122	828	1.4	21.29	5.95	6.29	1.76	7.70
4	100%	8.9	0.96	1267	935	1.5	25.34	7.08	6.22	1.74	8.81

Table 6-4: Results for 3rd test with injection timing retarded one step further

Model 3	Fuel:	Main engine parameters					IMEP cross check				
Inj timing	LEMF	IMEP	Fuel mass	Injection	Energy	SOC	Torque	BMEP	Motored	FMEP	IMEP
°BTDC		(indiset)	flow rate	duration	in			(load cell)	Torque		(calc)
8.4	Load	bar	kg/hr	µs	J/cycle	°BTDC	Nm	bar	Nm	bar	bar
1	50%	5.1	0.62	944	506	0	12.10	3.38	6.26	1.75	5.13
2	70%	6.66	0.72	1022	701	0.4	17.47	4.88	6.33	1.77	6.64
3	80%	7.83	0.83	1122	808	0.6	21.55	6.02	6.28	1.75	7.77
4	100%	8.87	0.96	1267	935	0.8	25.05	7.00	6.32	1.77	8.76

Table 6-5: Results for repeated base reference test to quantify repeatability of equipment

Ref 2	Fuel	Main engine parameters					IMEP cross check				
Inj timing	EN590	IMEP	Fuel mass	Injection	Energy	SOC	Torque	BMEP	Motored	FMEP	IMEP
°BTDC		(indiset)	flow rate	duration	in			(load cell)	Torque		(calc)
10	Load	bar	kg/hr	µs	J/cycle	°BTDC	Nm	bar	Nm	bar	bar
1	50%	5.06	0.55	933	523	1	12.03	3.35	6.29	1.76	5.12
2	70%	6.71	0.73	1033	694	1.2	17.56	4.90	6.35	1.77	6.68
3	80%	7.97	0.91	1133	865	1.3	22.29	6.23	6.18	1.73	7.95
4	100%	9.01	1.05	1278	998	1.9	25.93	7.24	6.20	1.73	8.97

The injection duration figures given in the tables are calculated from the injection signal emanating from the ECU and corrected for the mechanical response time of opening and closing of the injector solenoid. The Visioscope was used with the flash light to determine exactly when injection actually starts and stops. This information was then used to determine the opening lag time and the closing lag time of the injector. This has been incorporated in the above tables to indicate the actual injection duration which is also presented on the upcoming graphs.

The results of the IMEP cross check are also shown here and the details of this procedure were given in chapter 5.2. It can be seen from the results that both methods of calculating IMEP correlate well and hence instils confidence in the test equipment used. The increasing error with load is indicative of increasing piston ring friction. Furthermore the repeatability test shows no significant deviation or drift over the time period of the testing procedure.

The cylinder pressure data is represented on a set of graphs over the following pages in the form of a comparison between the reference fuel and the model fuel at the various injection timing settings. Each load point is represented on a separate set of graphs. Additional information contained in the graphs is the rate of heat release calculated from the pressure data and the corrected injection signal which represents the actual injection.

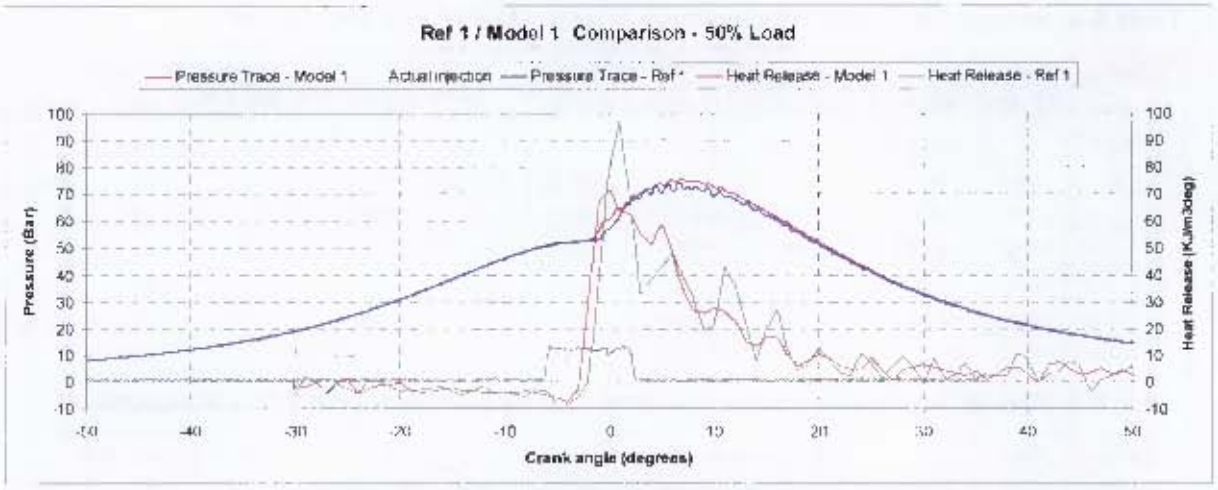

Figure 6-1: Ref 1 / Model 1 comparison at 50% load

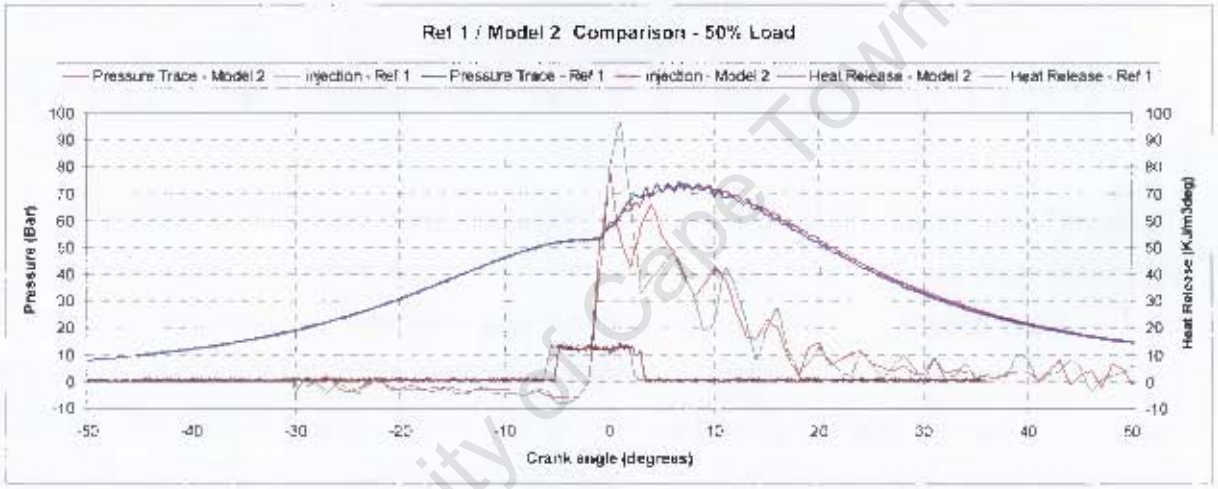

Figure 6-2: Ref 1 / Model 2 comparison at 50% load

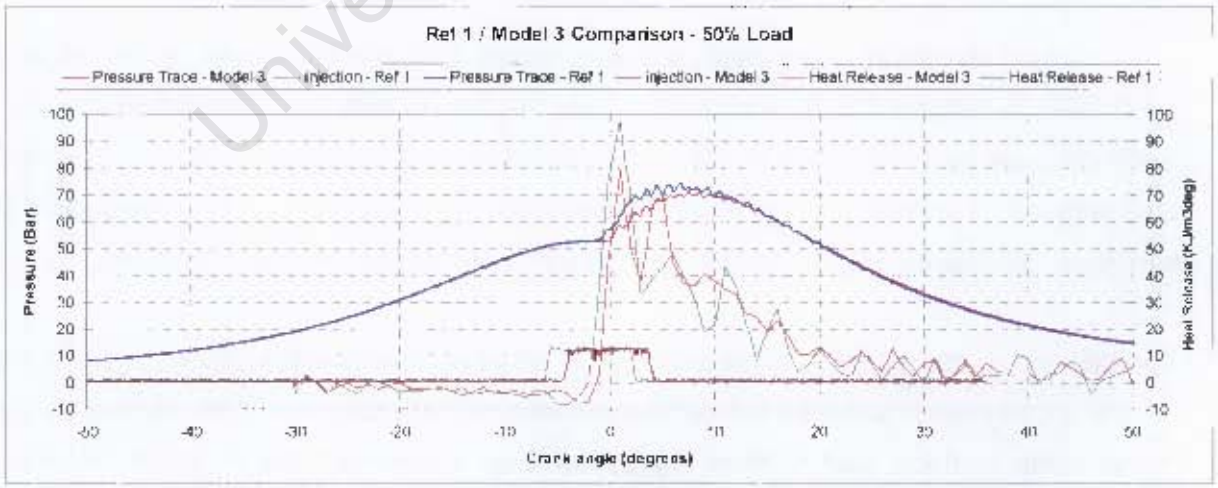

Figure 6-3: Ref 1 / Model 3 comparison at 50% load

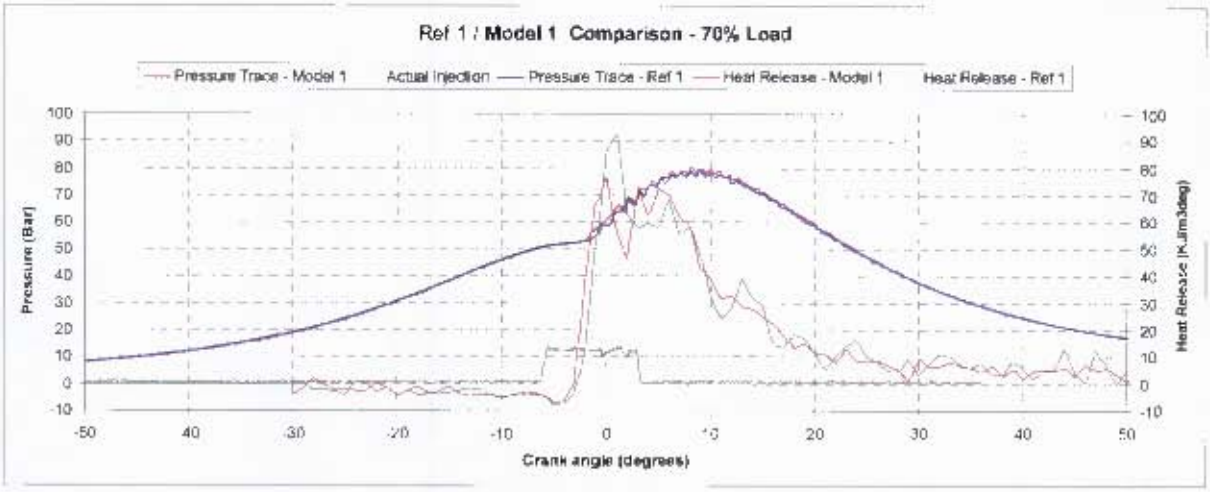

Figure 6-4: Ref 1 / Model 1 comparison at 70% load

Figure 6-5: Ref 1 / Model 2 comparison at 70% load

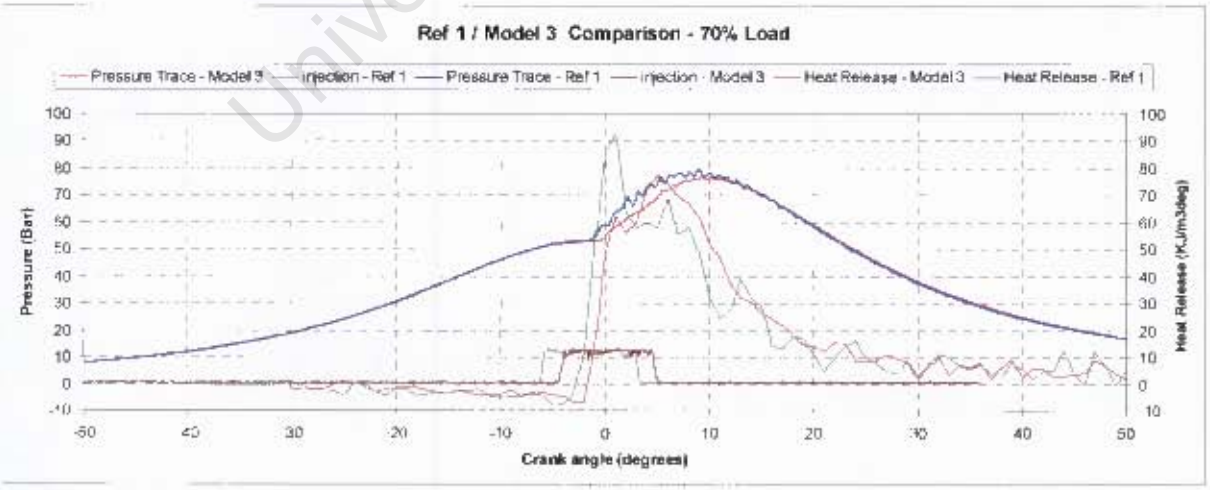

Figure 6-6: Ref 1 / Model 3 comparison at 70% load

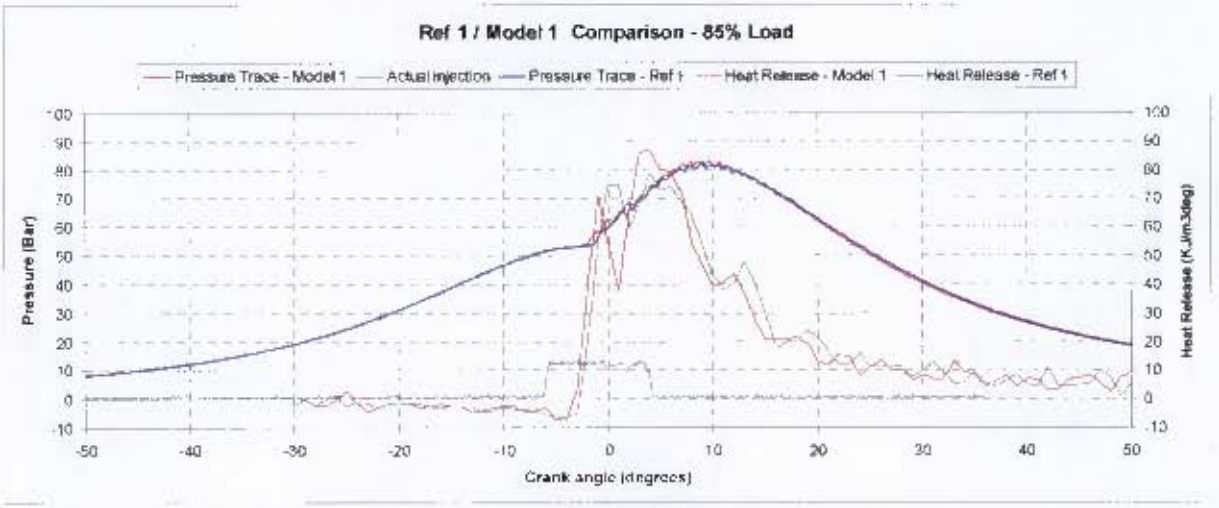

Figure 6-7: Ref 1 / Model 1 comparison at 85% load

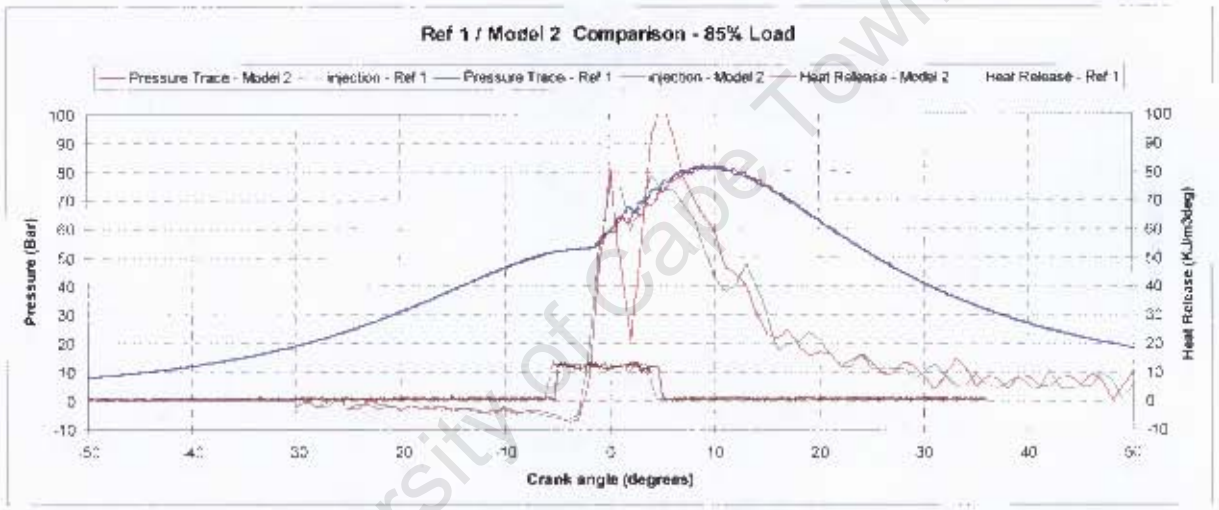

Figure 6-8: Ref 1 / Model 2 comparison at 85% load

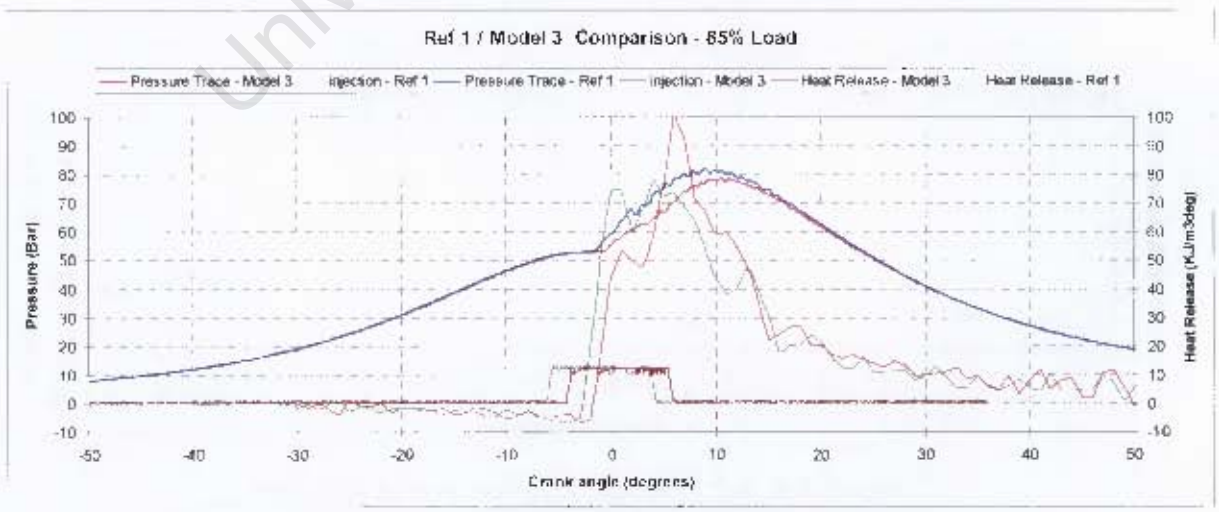

Figure 6-9: Ref 1 / Model 3 comparison at 85% load

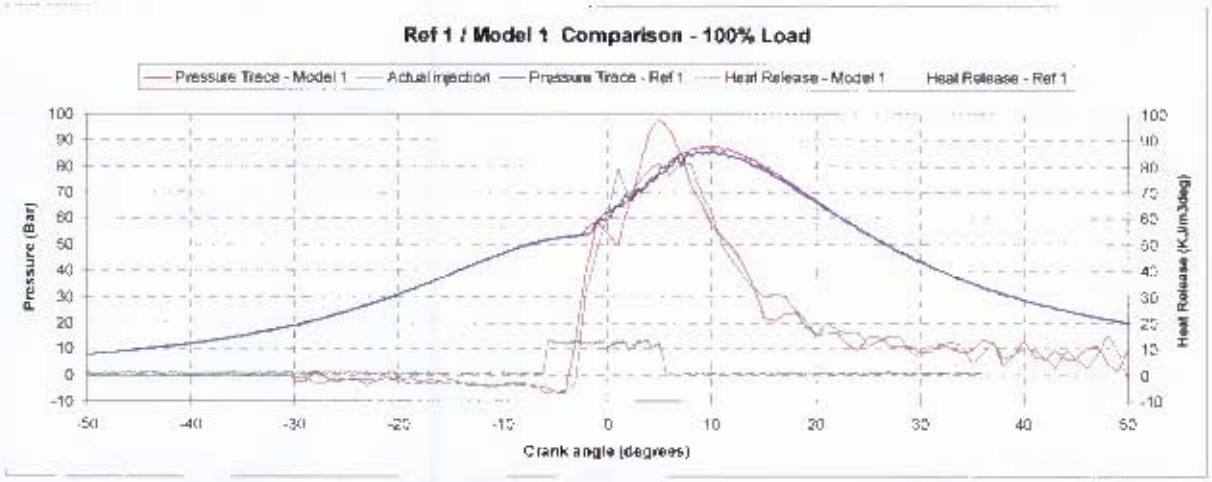

Figure 6-10: Ref 1 / Model 1 comparison at 100% load

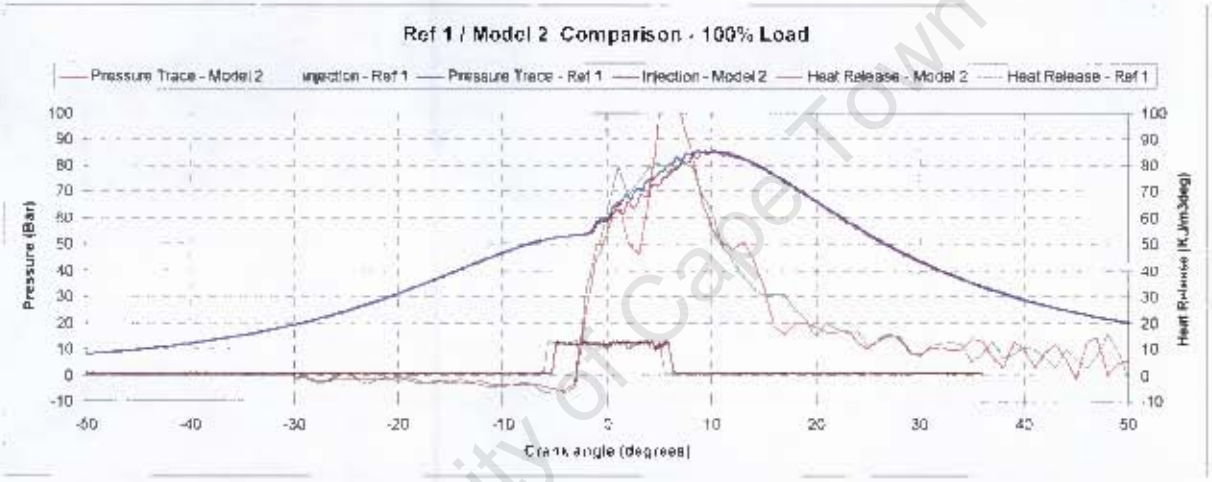

Figure 6-11: Ref 1 / Model 2 comparison at 100% load

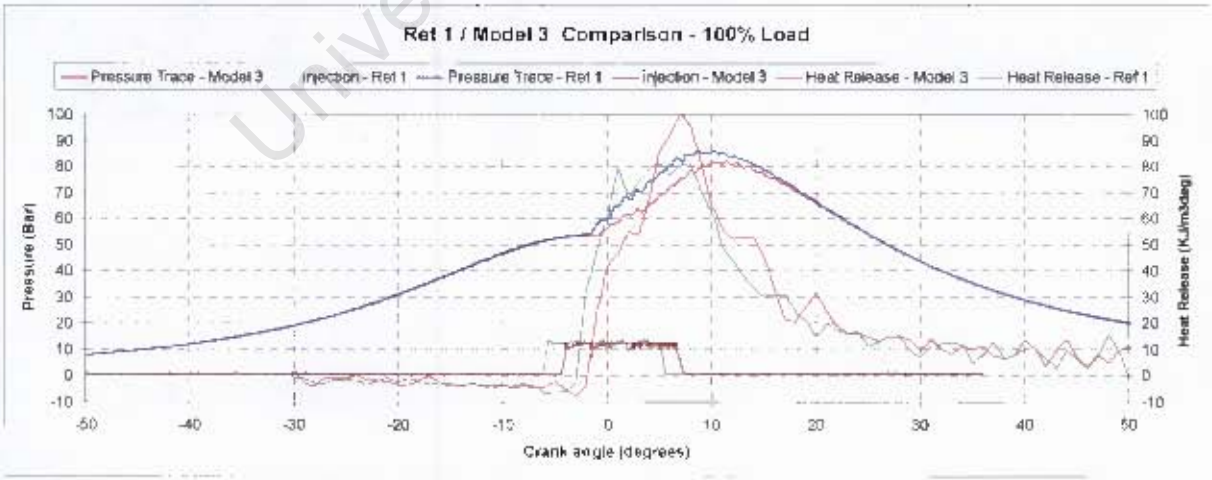

Figure 6-12: Ref 1 / Model 3 comparison at 100% load

6.2. Hydra engine image analysis results

Images were captured according to the procedure detailed in chapter 5.4 and all images from series 1 to 4 were processed to yield flame temperature and soot concentration information. Based on the raw image representing the soot luminosity, an image representing flame temperature and another representing soot concentration is generated.
An example of the resulting images is shown below for the two test fuels at 85% load and 3.4 crank angle degrees.

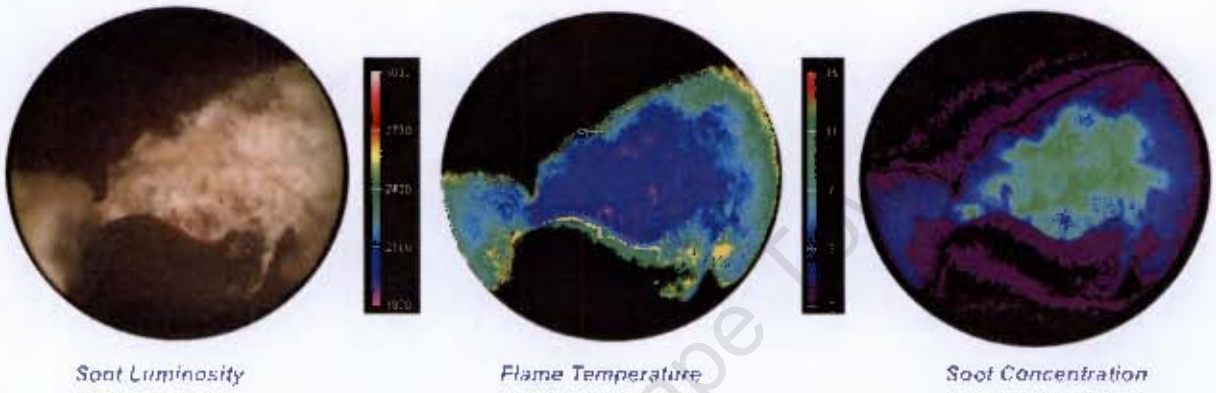

Figure 6-13: Processed images of the reference fuel at 85% load and 3.4 CAD

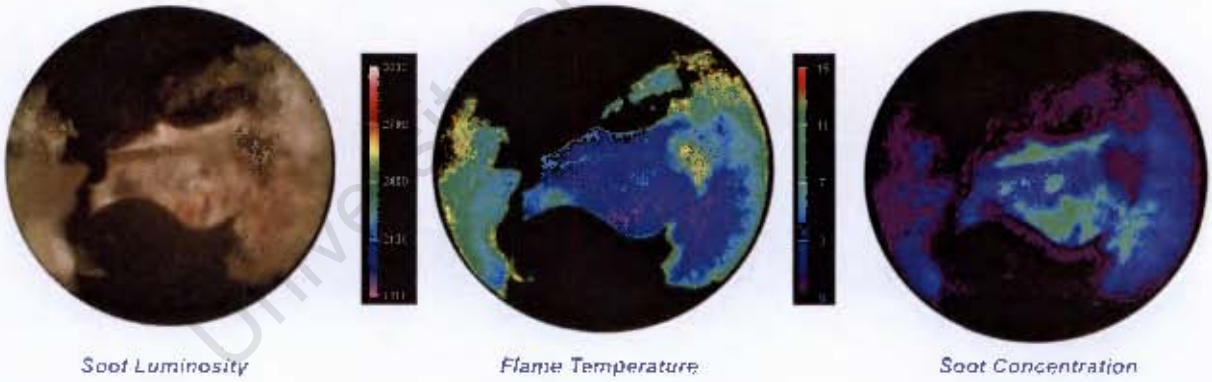

Figure 6-14: Processed images of the model fuel at 85% load and 3.4 CAD

The images reveal some degree of variation between the two fuels at identical operating points, however the images are best analysed numerically, as detailed in chapter 5.7.

Graphs representing the flame temperature results of the data collected in series 1 are presented overleaf for the four load points. Each graph contains all the fuels tested on the same set of axes for a specific load point. Although the data has been averaged and smoothed, cycle to cycle variation within the engine will still be evident in the data.

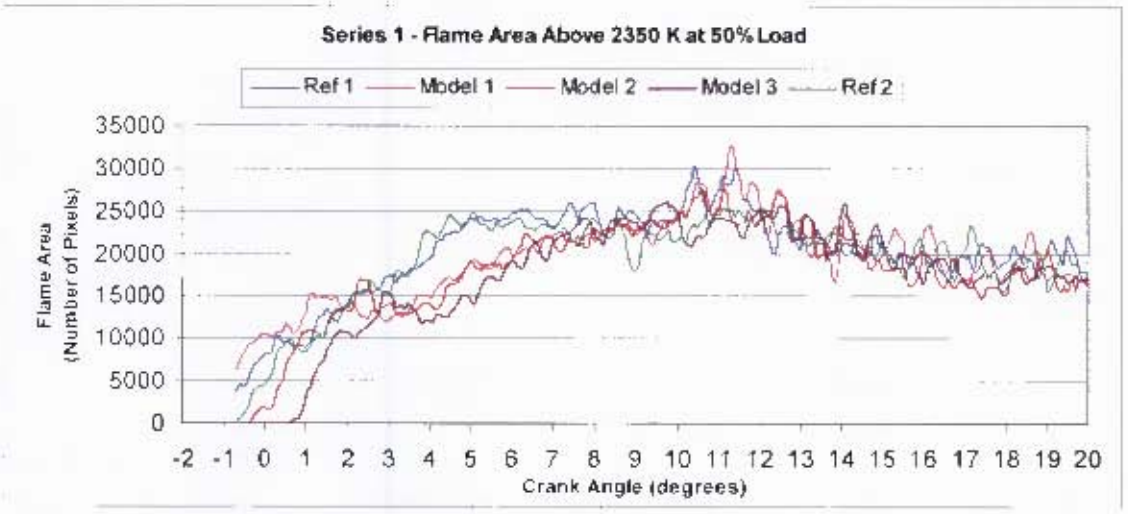

Figure 6-15: Range of flame area above 2350K at 50% load for series 1

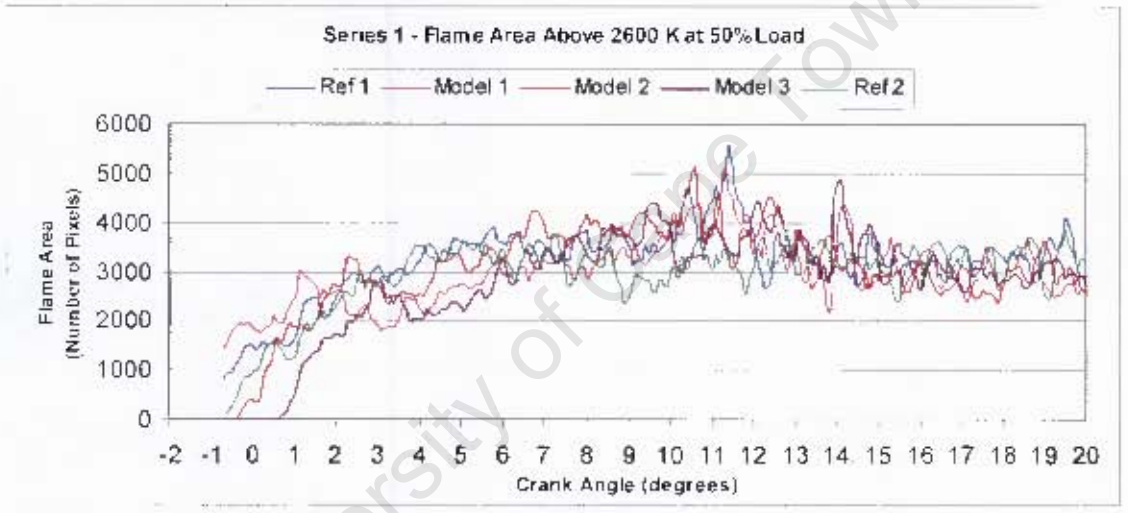

Figure 6-16: Range of flame area above 2600K at 50% load for series 1

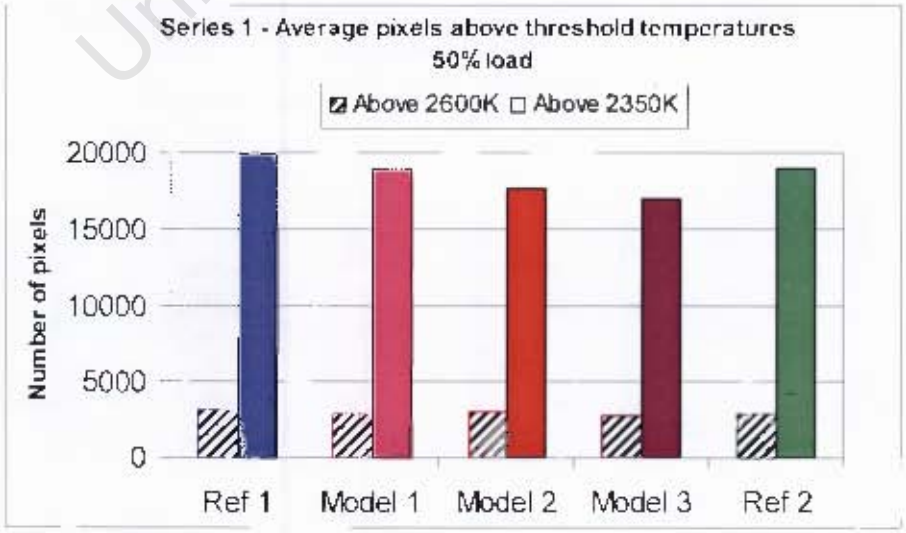

Figure 6-17: Average number of pixels across range at 50% load for series 1

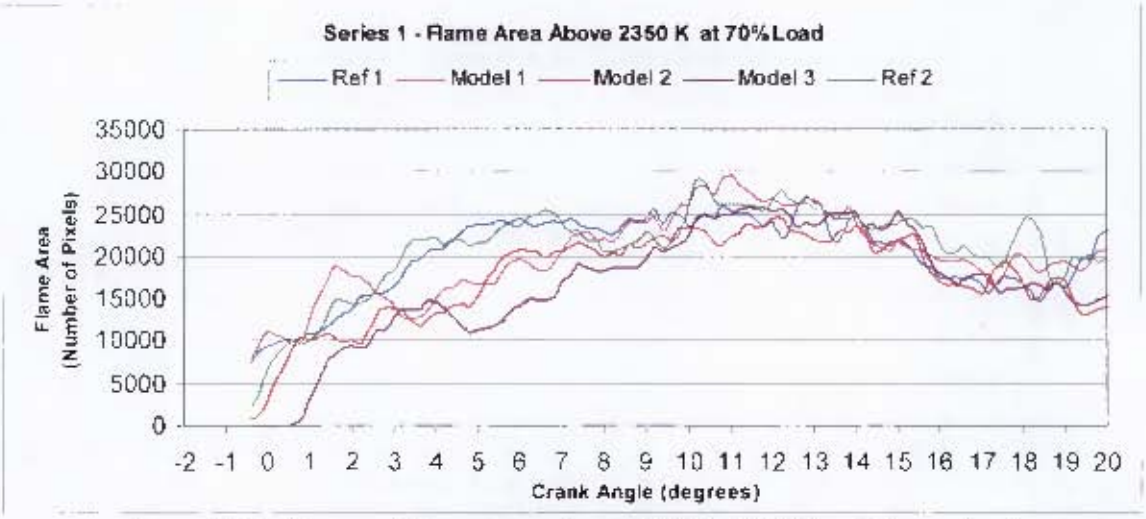

Figure 6-18: Range of flame area above 2350K at 70% load for series 1

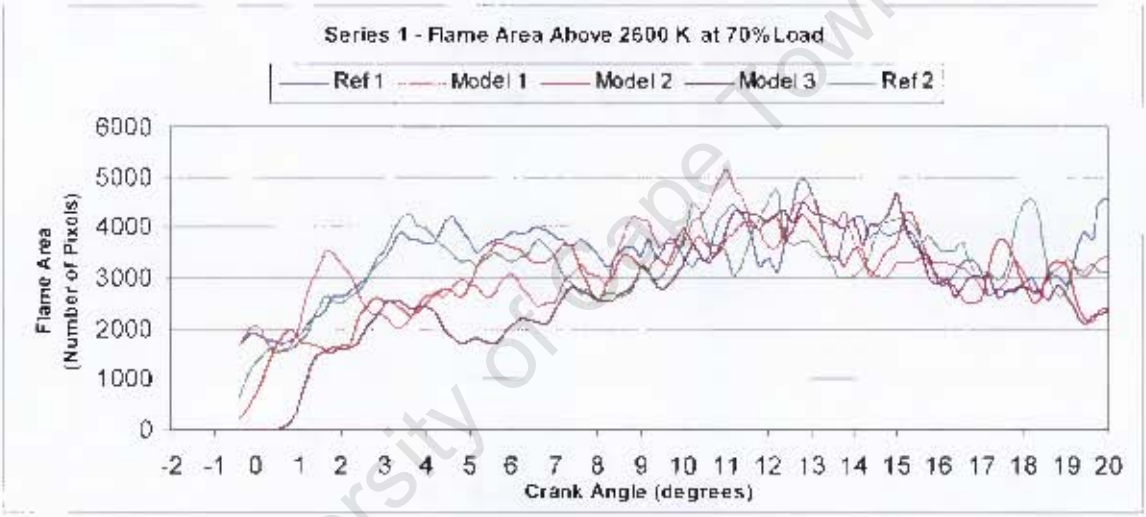

Figure 6-19: Range of flame area above 2600K at 70% load for series 1

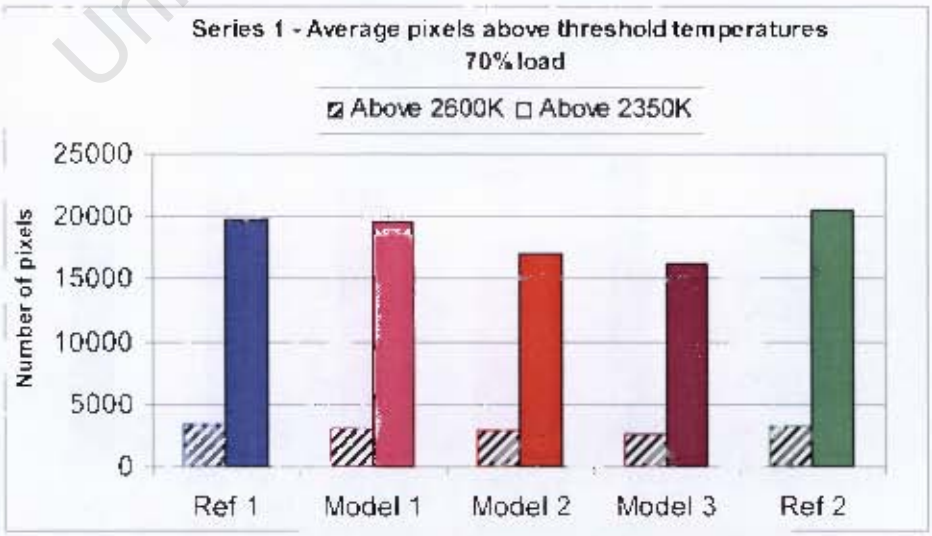

Figure 6-20: Average number of pixels across range at 70% load for series 1

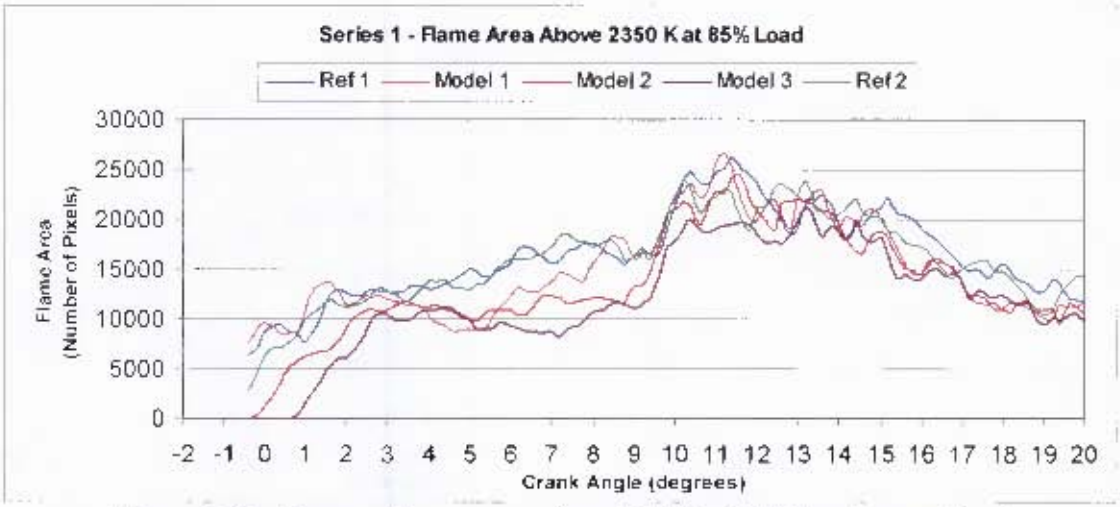

Figure 6-21: Range of flame area above 2350K at 85% load for series 1

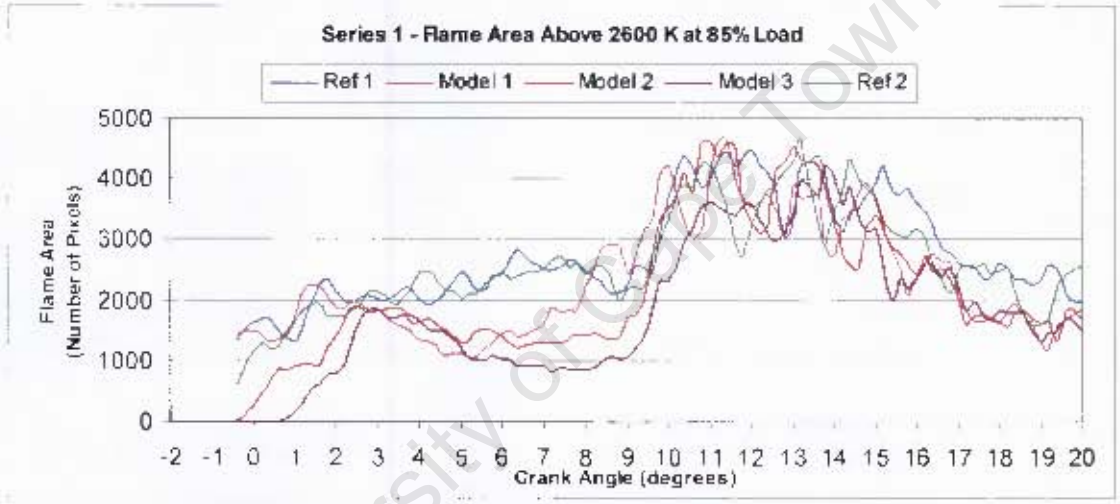

Figure 6-22: Range of flame area above 2600K at 85% load for series 1

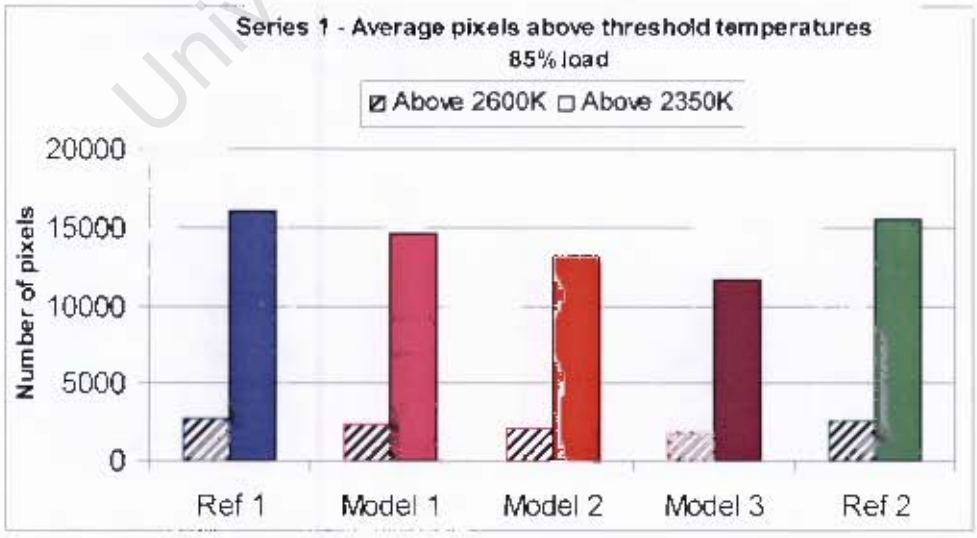

Figure 6-23: Average number of pixels across range at 85% load for series 1

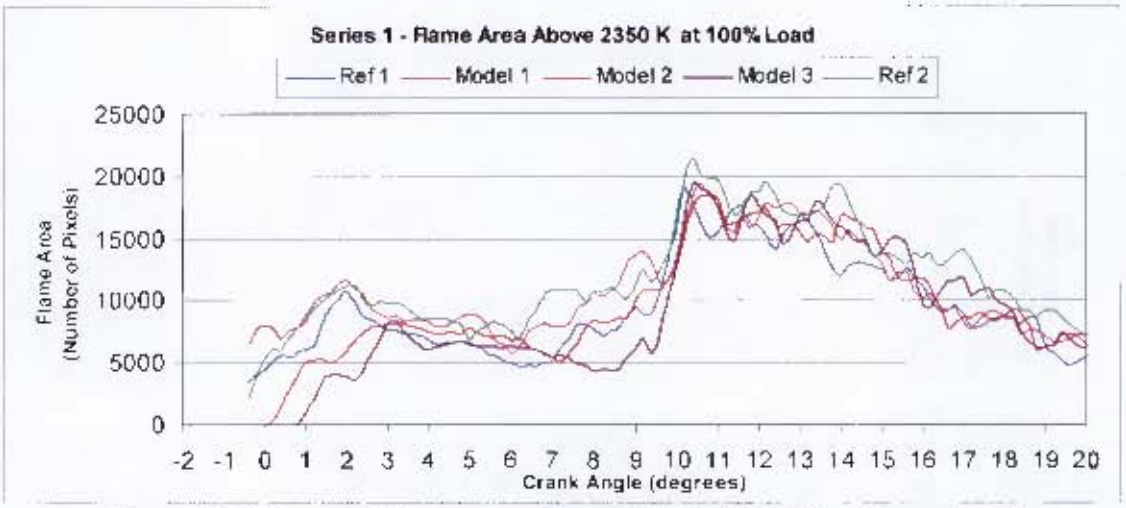

Figure 6-24: Range of flame area above 2350K at 100% load for series 1

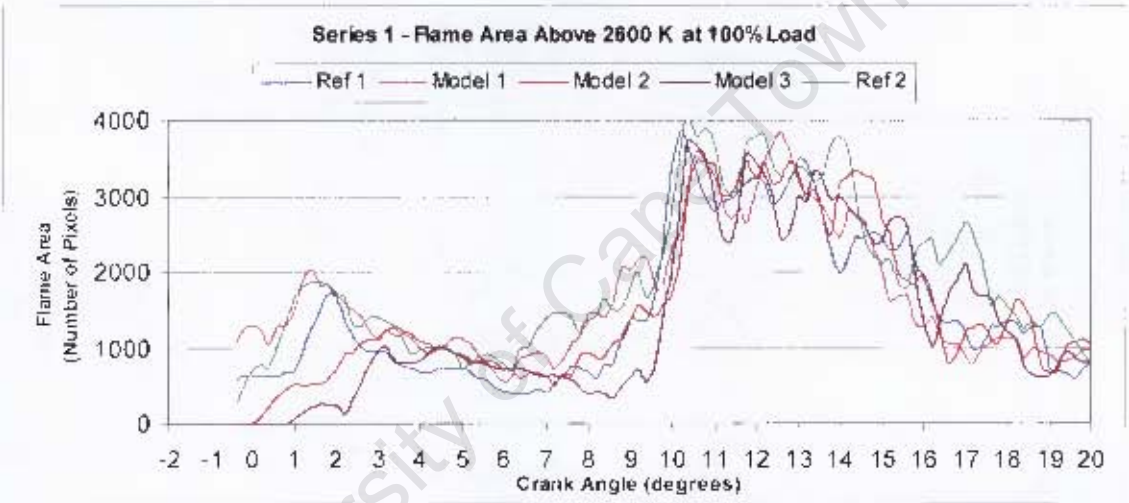

Figure 6-25: Range of flame area above 2600K at 100% load for series 1

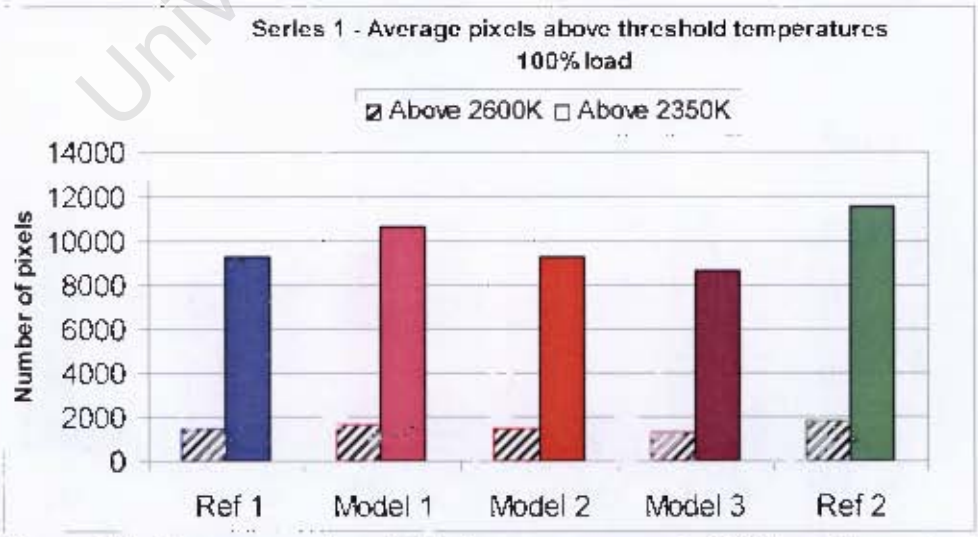

Figure 6-26: Average number of pixels across range at 100% load for series 1

It is very noticeable in the flame temperature results that as the load is increased, the effect of the soot on the endoscope window becomes more significant. The higher load results show a clear step in the data at 10 CAD where the window was cleaned. This effect is negligible at the 50% load point and very significant at 100% load. The soot deposits on the window have the effect of reducing the temperature values obtained by the two-colour method.

The soot concentration results for series 1 are presented in a similar way in the following graphs. A soot concentration threshold of KL = 11 has been used and can be considered a very high soot concentration level.

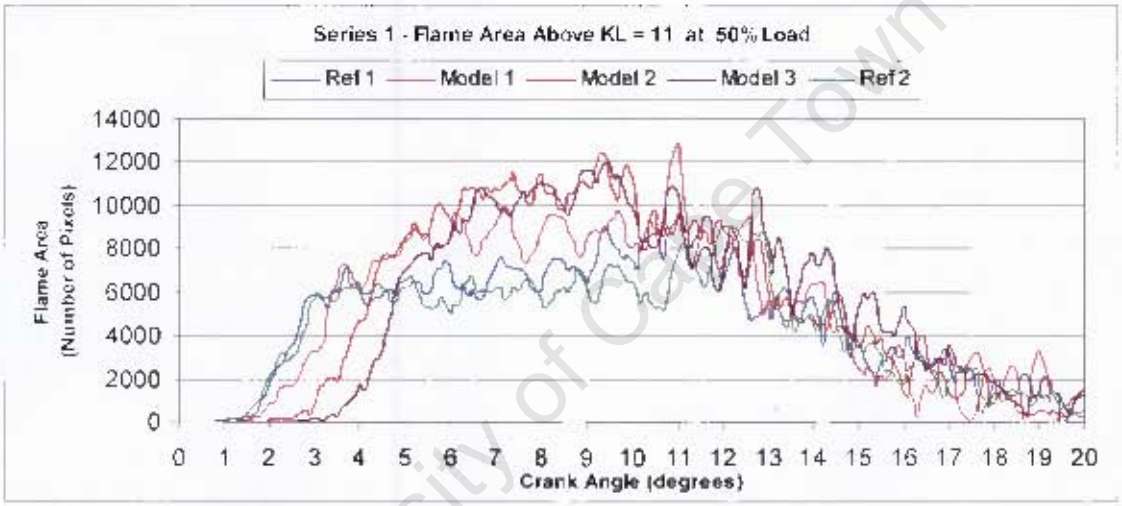

Figure 6-27: Range of flame area above KL = 11 at 50% load for series 1

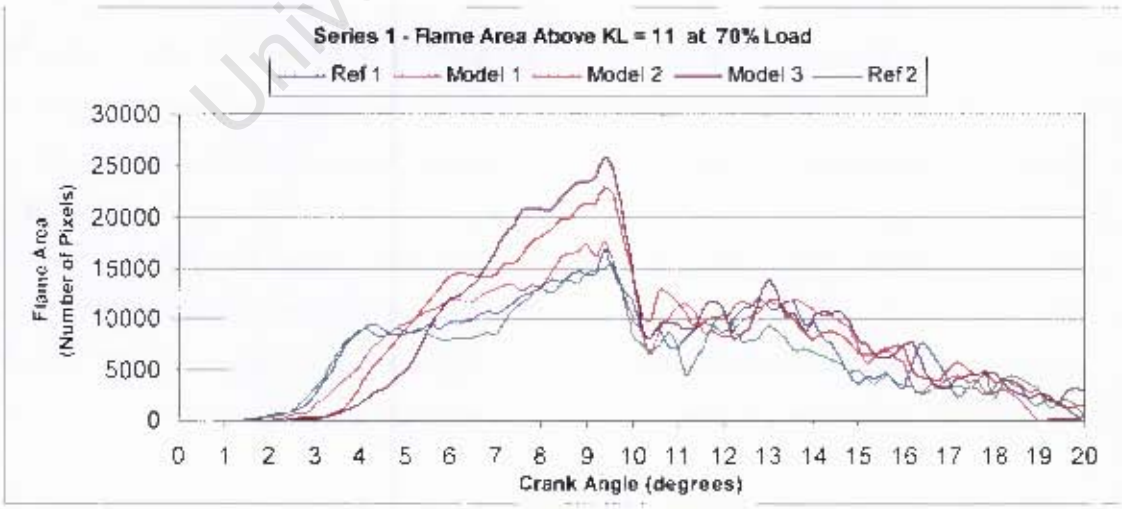

Figure 6-28: Range of flame area above KL = 11 at 70% load for series 1

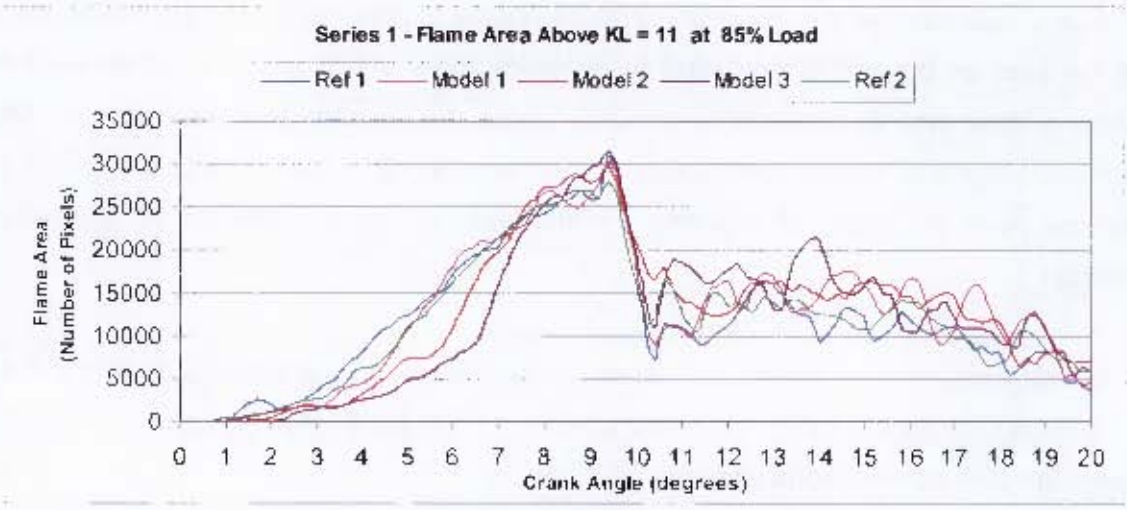

Figure 6-29: Range of flame area above KL = 11 at 85% load for series 1

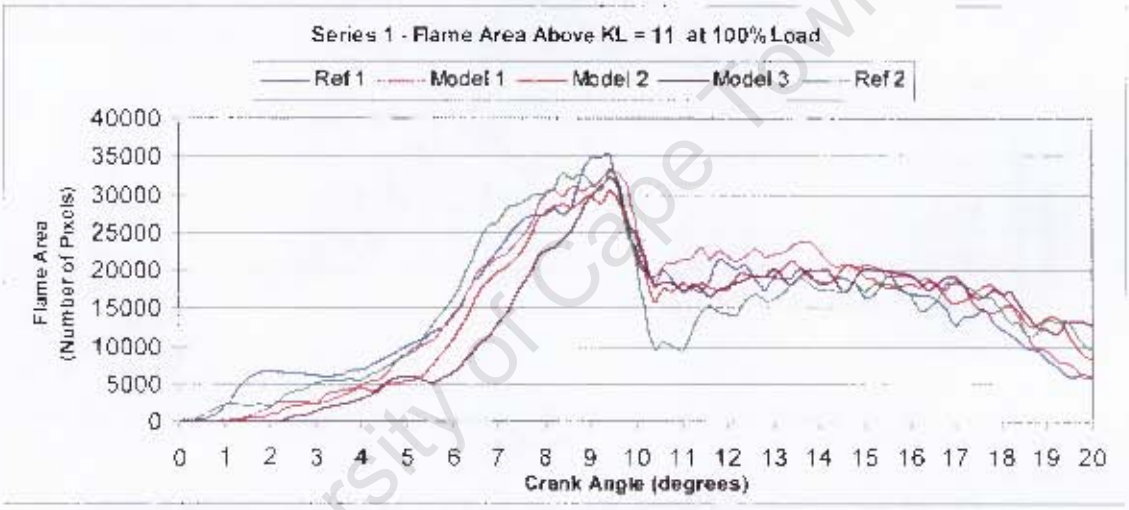

Figure 6-30: Range of flame area above KL = 11 at 100% load for series 1

The soot concentration results shown that soot deposits on the endoscope window have the effect of increasing the apparent soot concentration measured. It also follows that areas of relatively low temperature register a high soot concentration. The 70% load point shows a significant soot deposit effect, whereas the temperature results at this point revealed this to a lesser extent. This confirms the point made in the theoretical background that the soot concentration results of the two-colour method are more sensitive to the transmissivity of the window than the temperature results are. This is evident in these results with the possible exception of the 50% load point which remains unaffected by soot deposits.

In all cases there are areas where significant differences are detected between the two test fuels and these will be discussed in detail in the following chapter.

To summarise the results of series 1 the flame area above the relevant thresholds were added up and averaged over the number of images taken. These results therefore represent the entire range of crank angle degrees as one average data point and can thus be used to compare the fuels over the range of load points. These results are presented below.

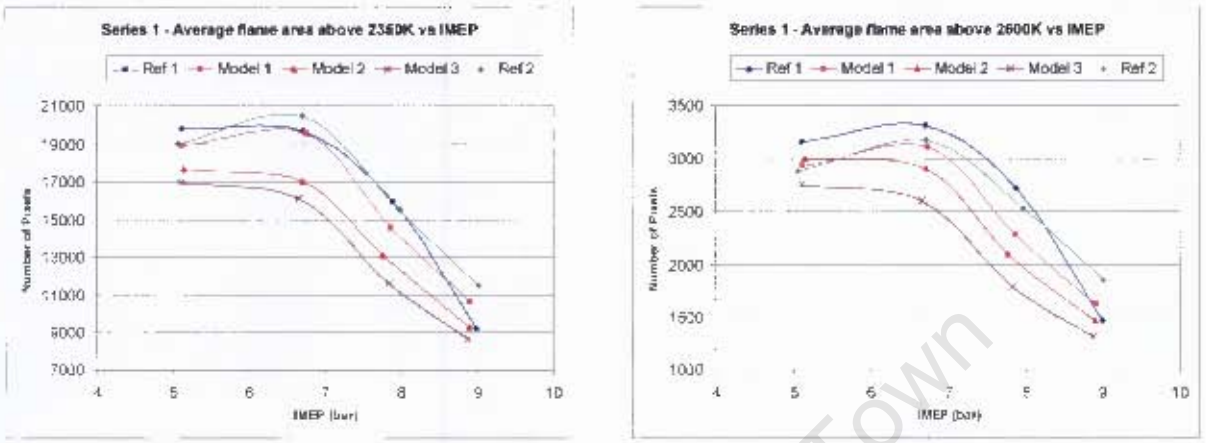

Figure 6-31: Summary of flame temperature results for series 1

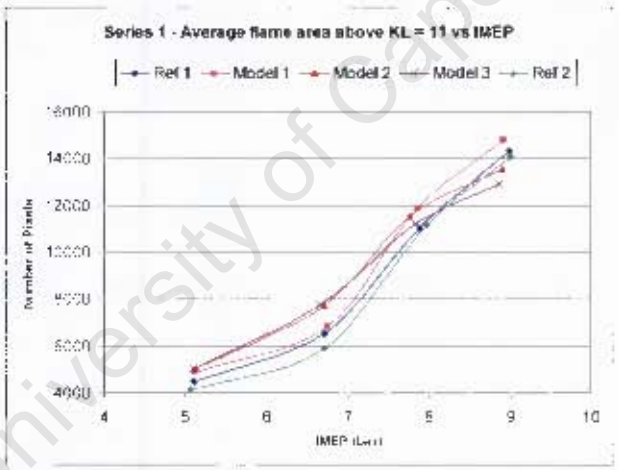

Figure 6-32: Summary of soot concentration results for series 1

An increase in combustion temperatures with load should be expected; however this trend is offset by the soot deposits on the endoscope window. An increase is evident between the 50% and 70% load point. but then a significant drop-off in the temperature results is realised at higher loads. This can be attributed to window soot deposits. Similarly the rise in the soot concentration results is accelerated by window soot deposits.

Series 1 represents the main focus of the investigation in the Hydra engine. The subsequent series of testing were done to add value to these results and to understand them better. Selected interesting parts of these results will now be presented.

The effect of soot deposits on the endoscope window

The graphs presented below represent 100 consecutive images taken at the same point. The raw data for each test batch is presented along with a dotted line indicating the average of the first 10 repetitions, which can be considered a representative true value. The linear trend line gives an indication of the rate at which the temperature is apparently decreasing due to fouling of the endoscope window over the course of the experiment. The gradient of these lines vary significantly between the different fuels and increases with engine load.

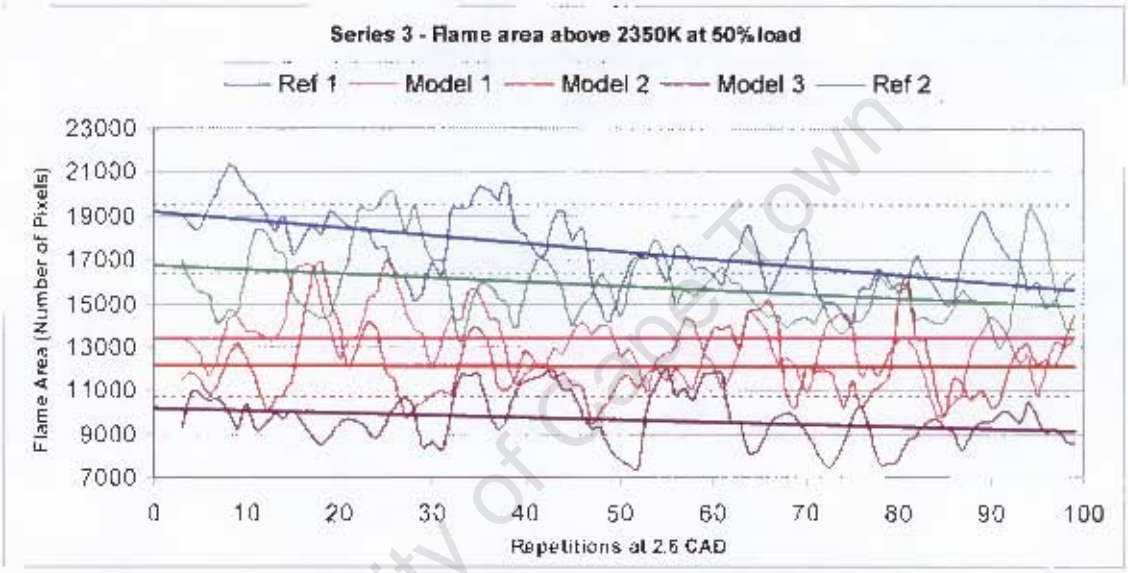

Figure 6-33: Repetitive temperature results at 2.6 CAD at 50% load for series 3

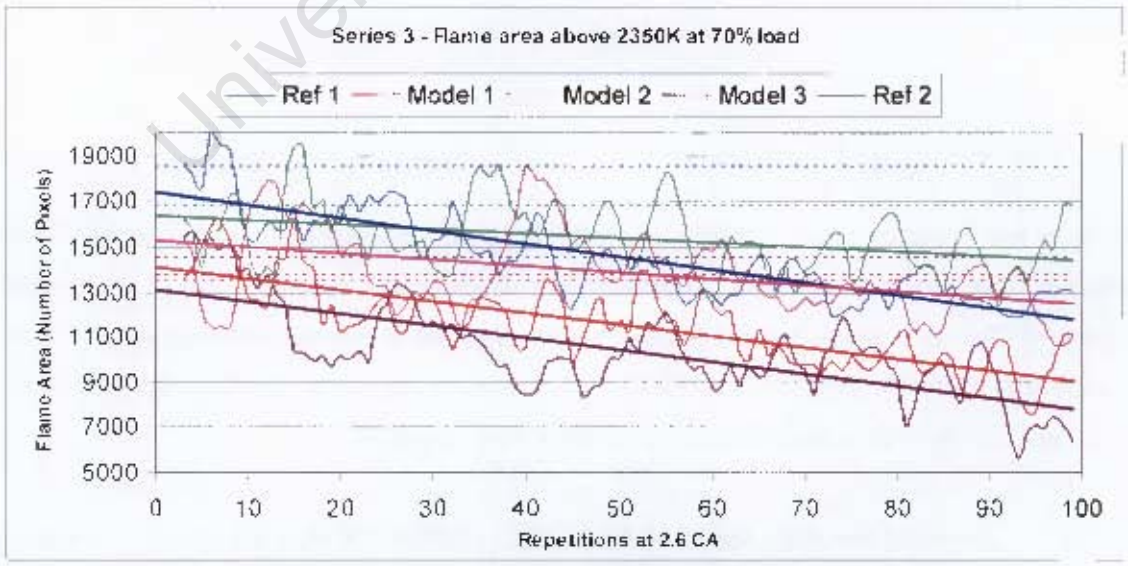

Figure 6-34: Repetitive temperature results at 2.6 CAD at 70% load for series 3

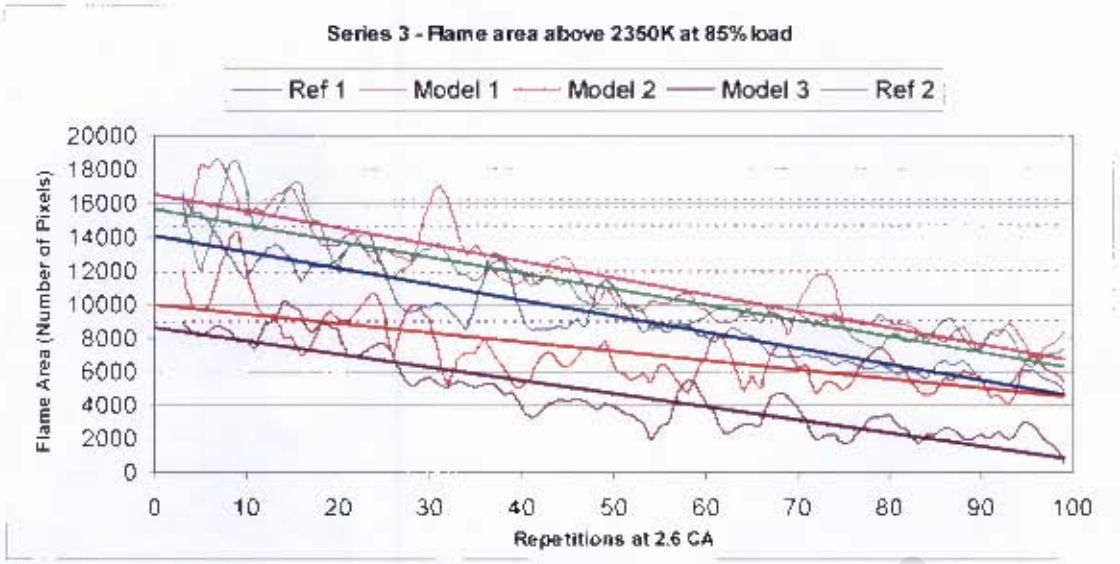

Figure 6-35: Repetitive temperature results at 2.6 CAD at 85% load for series 3

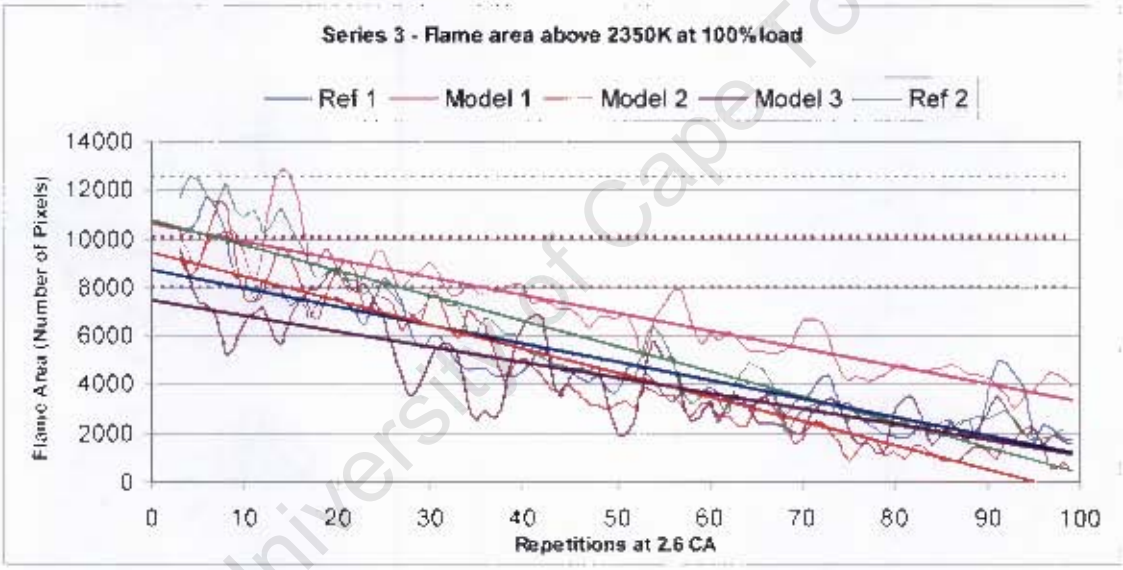

Figure 6-36: Repetitive temperature results at 2.6 CAD at 100% load for series 3

The most notable result here is that the model fuel shows no effects of soot deposits at 50% load. Furthermore the rate of window sooting at 50% load is significantly less than the higher load points. This was evident in the previous results and is confirmed by these tests.

Visual comparison of spray formation and start of sooting combustion

Series 6 and Series 7 use illuminated photography to look at the injector spray formation and the start of combustion. A selection of these images is presented overleaf and discussed in chapter 7.2.

Figure 6-37: Selected images from series 6 comparing the injector spray formation

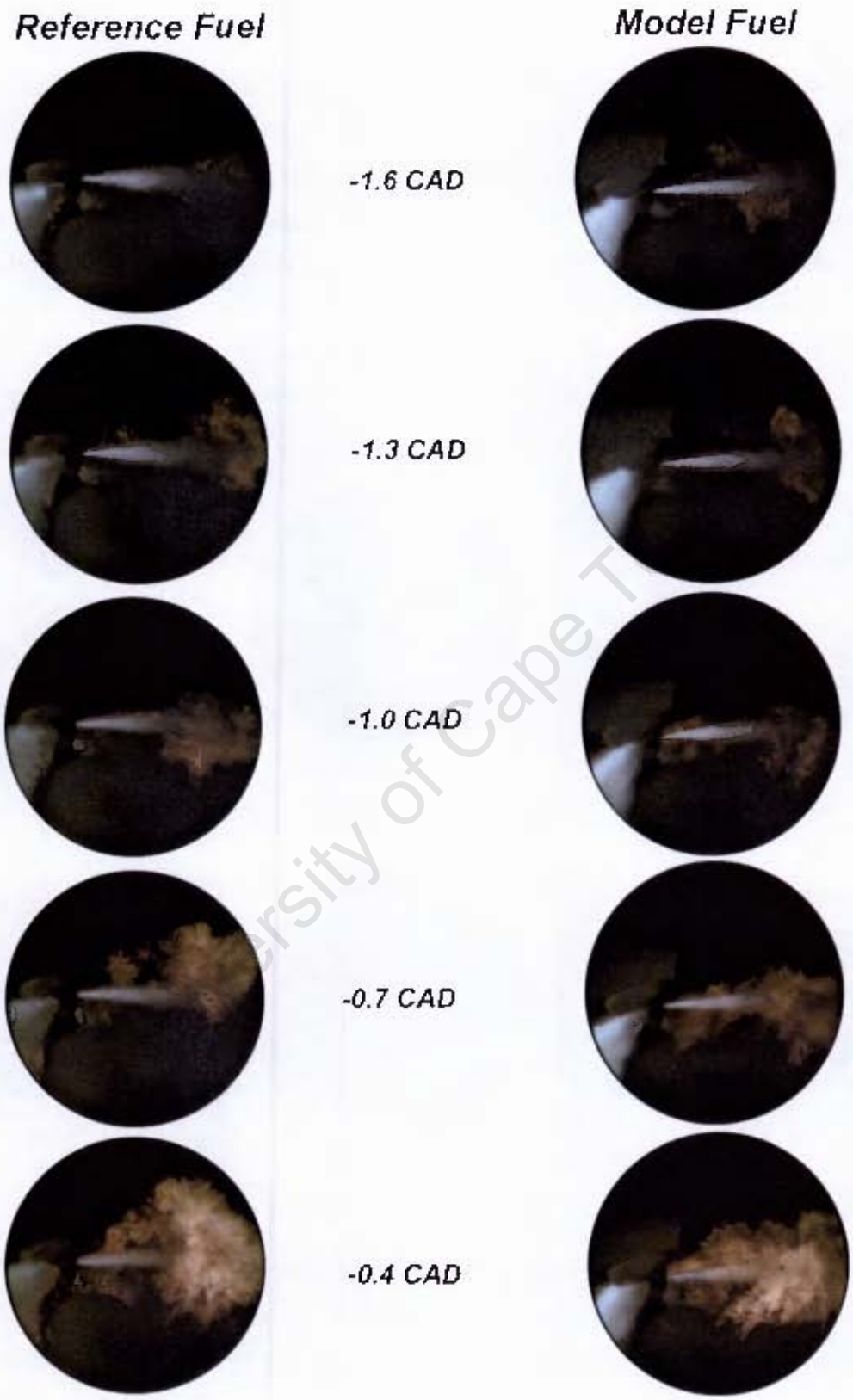

Figure 6-38: Selected images from series 7 comparing the start of sooting combustion

6.3. Combustion Bomb results

Images were captured according to the procedure detailed in chapter 5.6 which resulted in a sequence of images from the start of combustion to the end of combustion. The same method was followed as with the Hydra engine results and all images were processed to yield flame temperature and soot concentration information. The images from the bomb show a direct view of all six injector spray plumes, however they also contain some reflection from the stainless steel bomb walls. This is easily removed by a masking function prior to processing which eliminates the background reflection. An example of the processed bomb images at test point 6 (1.78 ms after injection signal) is shown below for the two test fuels:

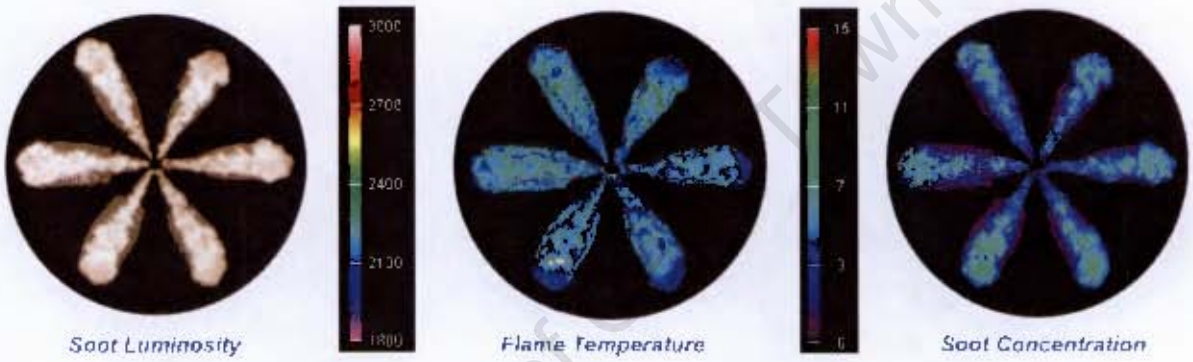

Figure 6-39: Processed images from test point 6 of the reference fuel

Figure 6-40: Processed images from test point 6 of the model fuel

A numerical analysis of all images as done for the Hydra engine results is presented over the following pages. These data are the average of two images per test point. The graphs are presented with error bars which indicate the difference between the two image results at each test point. As the results are dependant on flame area, the following analysis begins with a comparison of the total flame area of the images collected in the sequence.

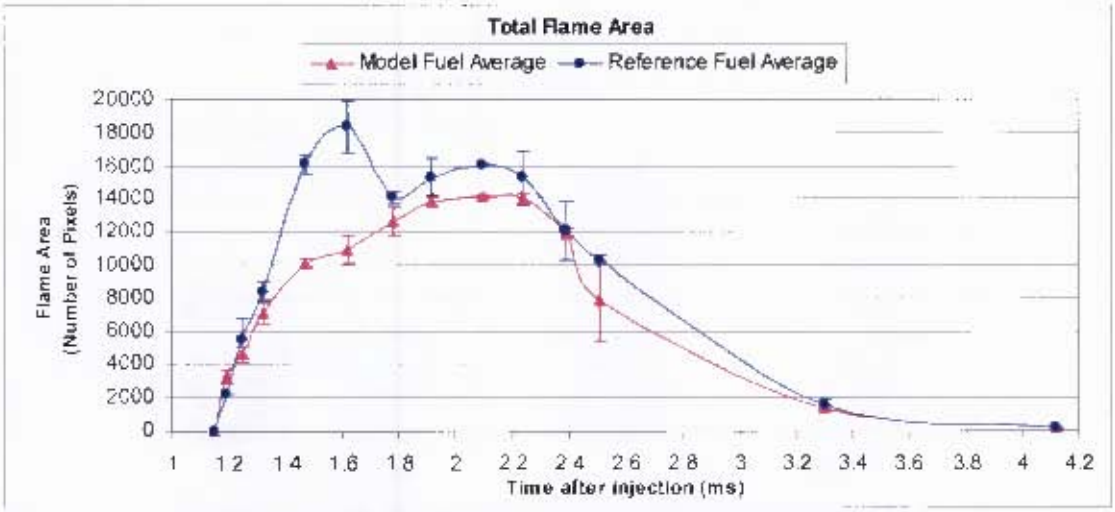

Figure 6-41: Total flame area of images in the range

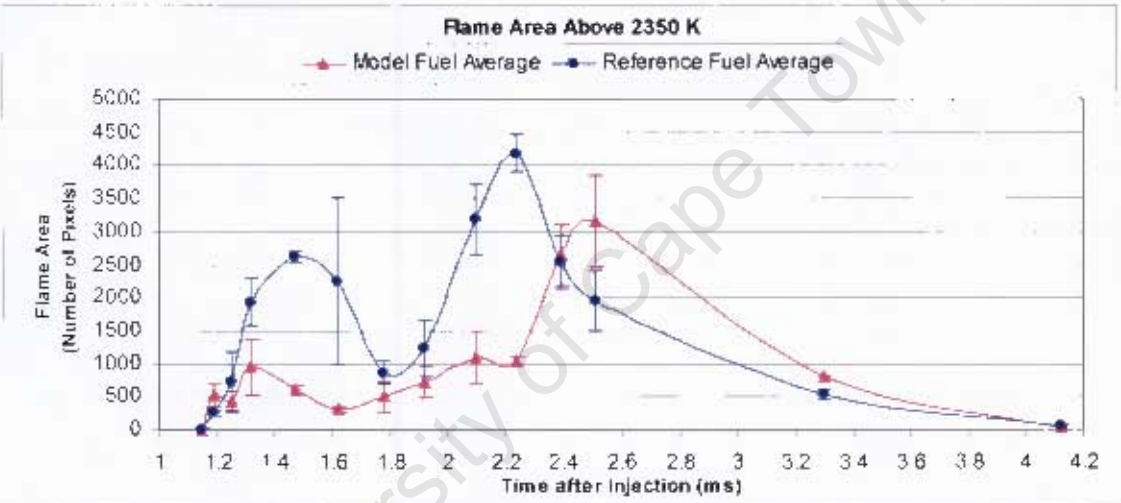

Figure 6-42: Range of flame area above 2350K for the Combustion Bomb

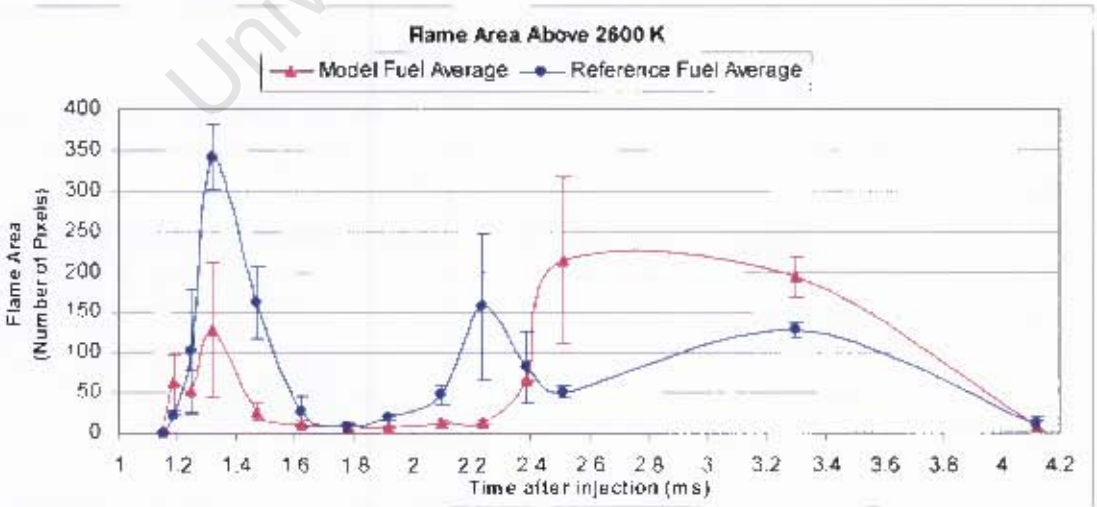

Figure 6-43: Range of flame area above 2600K for the Combustion Bomb

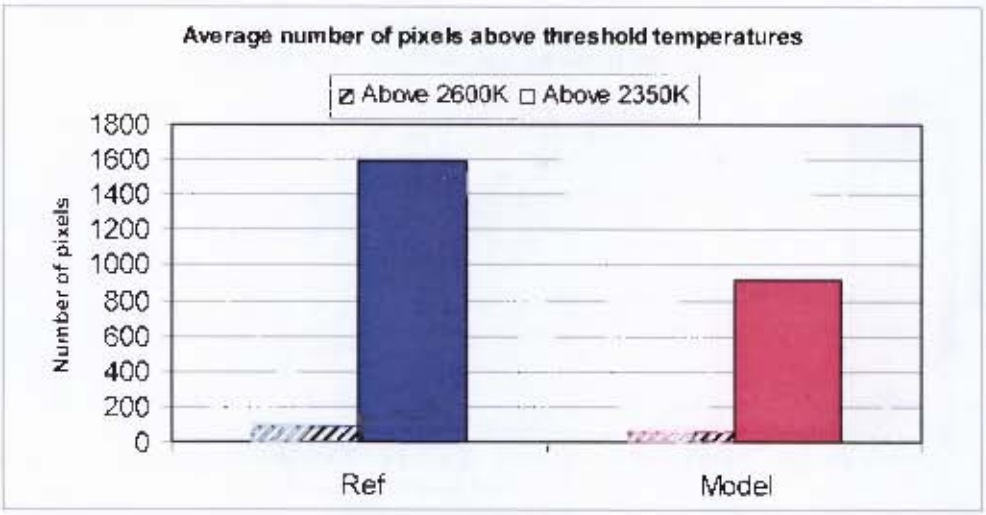

Figure 6-44: Average number of pixels above threshold temperatures across the range

The soot concentration results are presented in a similar way, using two threshold KL values. KL = 4 can be considered a low soot concentration level and KL=11 can be considered a high soot concentration level. The scale is better understood by examining the processed image example at the beginning of the section.

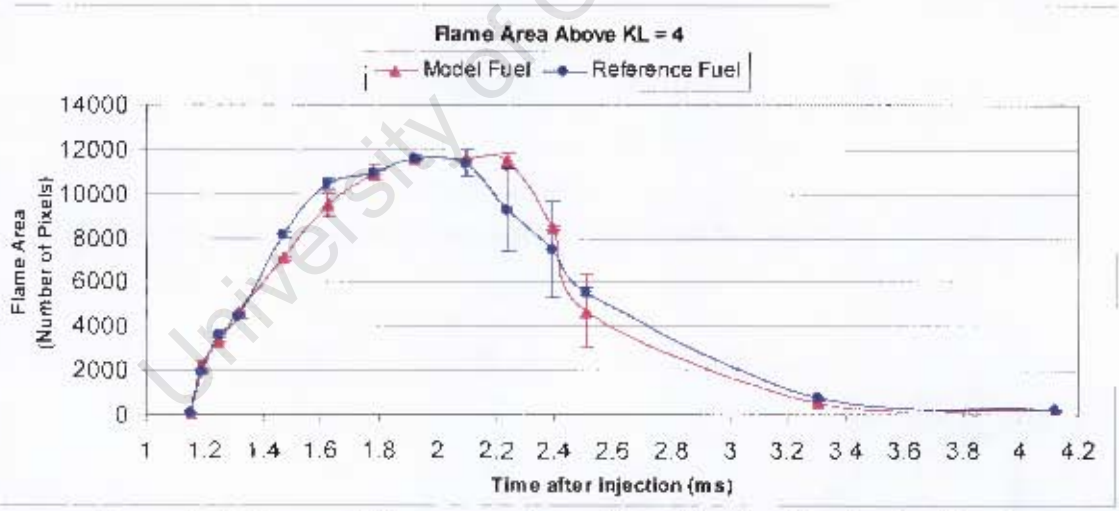

Figure 6-45: Range of flame area above KL = 4 for the Combustion Bomb

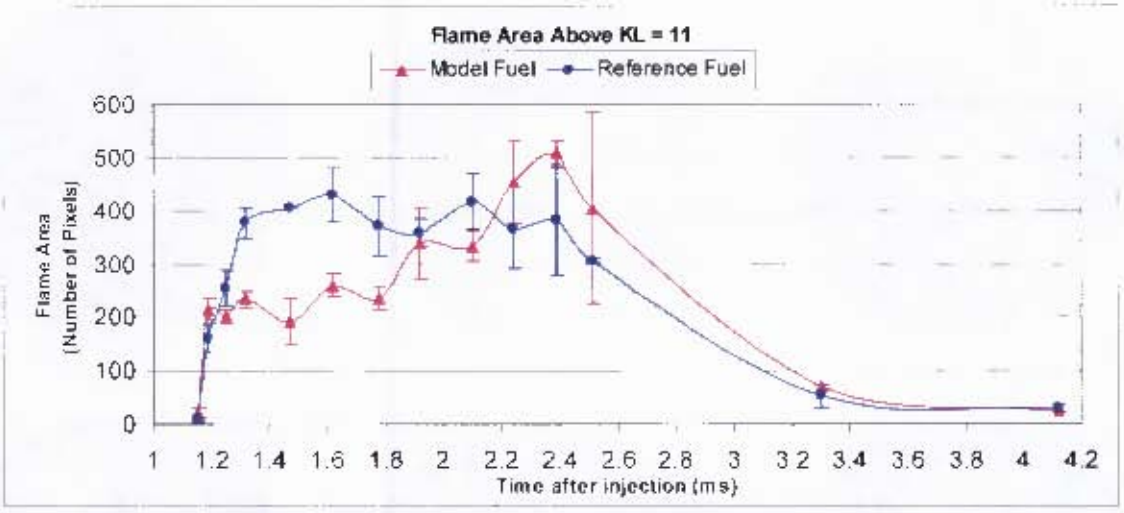

Figure 6-46: Range of flame area above KL = 11 for the Combustion Bomb

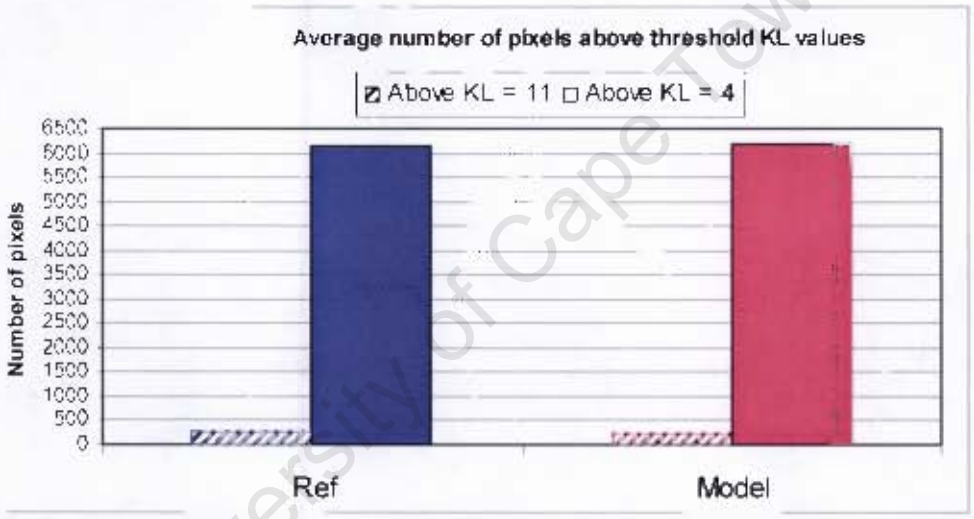

Figure 6-47: Average number of pixels above threshold KL values across the range

Due to the relatively small number of images captured in the combustion bomb, the sequence of images is shown over the following two pages for a visual comparison between the test fuels. All images in the sequence are included except for the first and last images which show a negligible amount of luminosity and have therefore been omitted from this visual comparison. Only one image per test point is shown and the images do correspond to the data points on the graphs. The time delay given in brackets below each image represents the time after the injection signal begins that the camera was triggered. The graphs indicating the range of images over time use this time scale as well.

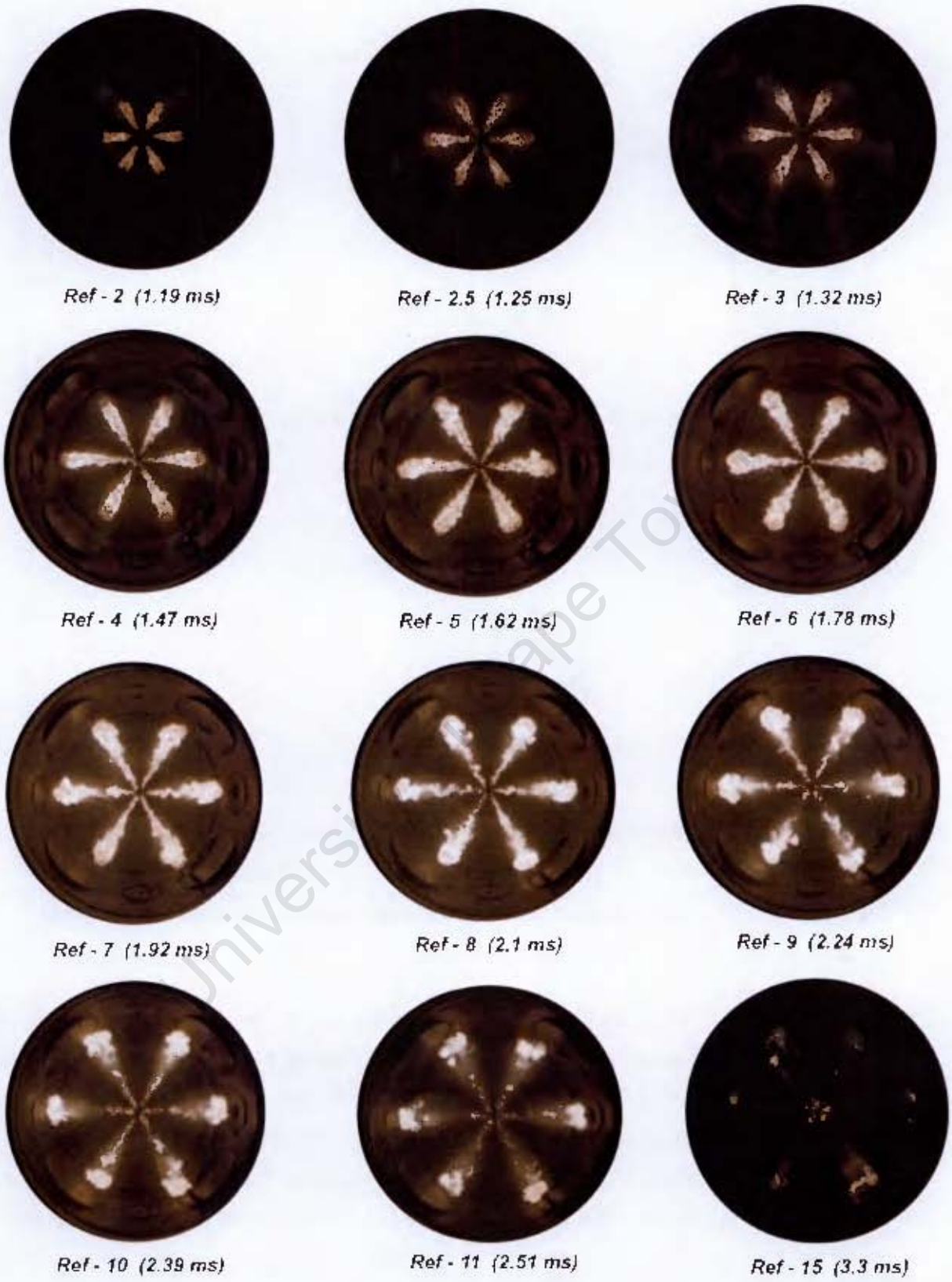

Figure 6-48: Sequence of images from the Combustion Bomb of the reference fuel

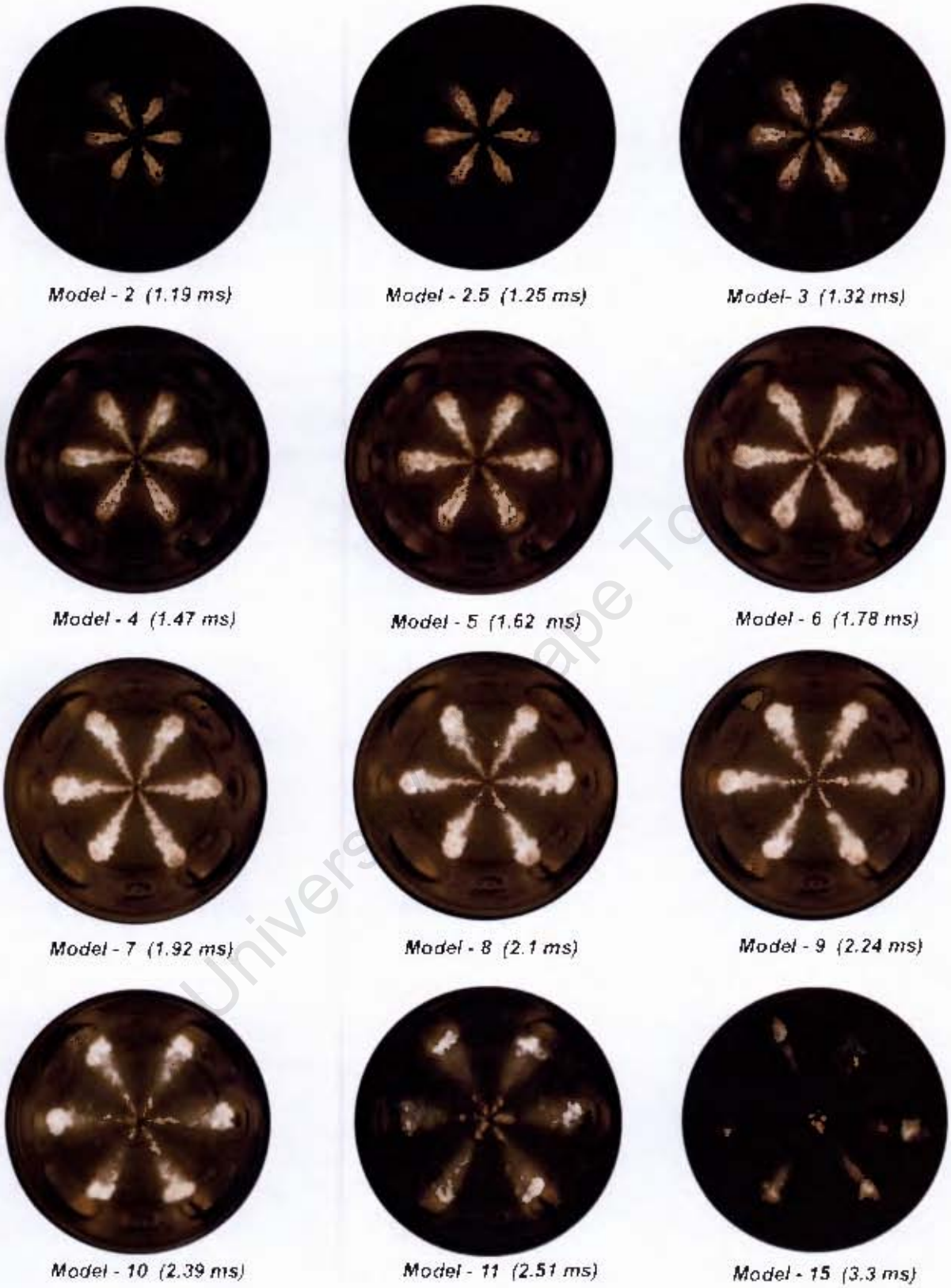

Figure 6-49: Sequence of images from the Combustion Bomb of the model fuel

7. Discussion of results

7.1. Discussion of Hydra engine test results

The engine test results highlight some of the main differences between the test fuels and show why the different timing settings were chosen. The higher cetane number of the model fuel resulted in start of combustion occurring 0.8 crank angle degrees earlier than the reference fuel. This is shown in the pressure graphs of section 6.1. Shortly after SOC, the model fuel consistently exhibits an apparent deviation in the pressure trace between TDC and approximately 5 degrees after TDC. This can be better defined as a region where the local rate of change of pressure following the onset of combustion of the model fuel is smaller than the local rate of change of pressure following the onset of combustion of the reference fuel. Due to the earlier combustion, the model fuel reaches a higher peak pressure and the pressure trace is also considerably smoother at the peak. This can be attributed to less fuel being available for premixed auto-ignition resulting in a longer controlled combustion phase. For this reason the rate of heat release is also consistently lower for the model fuel.

The second set of graphs represent a comparison of the reference fuel with the model fuel operating at a timing setting retarded by 0.8 CAD. This results in identical SOC times for the two fuels which reduces the effect of the model fuel's high cetane number to achieve a more representative comparison of other fuel properties. The dip in the pressure trace is still clearly present, representing the shorter premixed combustion phase, and now the peak pressure is very similar between the two fuels.

When the timing is retarded a further 0.8 CAD for the model fuel, a significantly lower peak pressure is realised. The dip in the pressure trace is consistent with the other data and the pressure trace is still smoother than the reference fuel.

The IMEP data shows a slight increase in power when running on the model fuel at low loads and slight loss of power at higher loads. However, the differences are very small but can possibly be attributed to the difference in density and viscosity between the fuels. A non-proportional fuelling response has been noticed before with similar fuels. (Friess et al., 2003) At low load the injection duration is very short and the lower viscosity of the model could result in lower pressure losses in the injector nozzle, thus increasing the injected quantity.

This effect would occur at small needle lifts when the injector is opening and closing. The slightly better vaporisation properties of the model fuel could also contribute to the low load IMEP advantage exhibited by the model fuel.
As the injection duration is increased there becomes a longer period of full needle lift where the effect of viscosity is less significant. The lower density of the model fuel would then become dominant as less fuel would be entering the combustion chamber over the set injection duration. Although the model fuel has a slightly higher energy content by mass, the lower density is expected to result in a net power loss. A close examination of the energy-in columns in the results tables will reveal that these results are consistent with the IMEP results. Energy-in is calculated from the fuel mass flow rate, engine speed and energy content of the specific fuel. At low loads the model fuel test results exhibit slightly higher energy-in figures, and indeed higher IMEP results. At higher loads the energy-in of the model fuel drops due to the lower fuel mass flow rate and consequently the IMEP drops as a result.

Fuel consumption by mass was lower in all cases for the model fuel; however at low loads the difference was very small. The difference increased with load. This result is expected because the injection duration remains constant between the tests of the two fuels and therefore a lower density would result in less fuel being injected over that period. As the injection duration is increased, so the difference in the injected quantities becomes greater. These trends are shown very clearly and consistently in the results.

In summary the engine test results are consistent with what should be expected based on the theory of the different fuel properties. The repeat test of the reference fuel demonstrates good repeatability of the test equipment. The results confirm that the experimental set up was sufficiently accurate to distinguish between the two test fuels.

7.2. Discussion of Hydra engine image results

The results show the effect of the model fuel's high cetane number very clearly by consistently indicating earlier combustion of the model 1 test batch. An unexpected, but very interesting result is the apparent dip in the model fuels temperature area results compared to the reference fuel in the early stages of combustion. This was first noticed in the cylinder pressure results and is consistently evident in the image analysis.

The model fuel shows early and high initial flame temperature areas due to the premixed combustion phase. The high cetane number would result in a shorter ignition delay and consequently less time for a premixed fuel mixture to form before auto-ignition. The premixed phase is therefore shorter. It appears that a drop in pressure and temperature is noticed once this is consumed before the diffusion combustion phase takes over. The results show that the model fuel has lower flame temperature areas than the reference fuel during injection, but these rise significantly after injection stops. In some cases the model fuel shows higher flame temperature areas than the reference fuel after injection stops.

As the injection timing is retarded, one would expect that cylinder pressure and temperature would decrease and that soot formation would increase based on conventional wisdom. In exhaust emission literature this effect results in the well known NOx-particulate trade off.
The temperature results consistently show that the model 1 test batch is greater than model 2 which is greater than model 3. The bar graphs are a good indication of the steady drop in the temperature results as the injection timing is retarded, and hence place a lot of confidence in these results. An increase in the soot concentration levels as injection timing is retarded is clearly noticed in the 50% and 70% load KL value graphs, which further strengthens this point and adds value to the results. At higher loads the results become less convincing due to the reasons discussed below.

The relative temperature results are consistent across the load range; however the flame area above the threshold temperatures decreases as load increases, contrary to what should be expected. This can largely be attributed to very high soot formation in the Hydra Engine at higher loads. The 50% load data can therefore be considered the most accurate and reliable as the effect of soot deposits on the endoscope window has been shown to be negligible here. The step in the data at the 10 CAD point is indicative of the soot deposit effect on the window because the window was cleaned at this point. It is very interesting to see how the

increase in load affects the sooting of the window and in turn how this affects the results of the two-colour method. As this project is an investigation of the method and not an in depth study of the fuels, the results have been left to show the window sooting effects. The results also show how the soot deposits affect the KL value results more than the flame temperature results. It would be advisable to try and limit the effect of window sooting by better combustion chamber design in future testing.

The results across the range make it difficult to conclude which fuel burns with higher flame temperature areas than the other, because this varied over the combustion process. Initially the model fuel is higher but then drops below the reference fuel. In the after burn phase of combustion the two fuels are very similar with the model fuel showing higher flame temperature areas in some cases. To summarise the results, the bar graphs present the data as a collective average across the entire testing range. These results consistently show that the reference fuel has a higher number of pixels above both threshold temperatures than the model fuel at all load points. The repeated reference fuel test also correlates well with the initial test, except at the 100% load point where the repeated test should be considered the more accurate one. A large drop in the flame temperature areas is noticed as the injection timing is retarded for the model fuel and this trend is consistently reflected in the results.

The image analysis results presented here are always an indication of flame area above threshold temperatures and hence are heavily influenced by flame area in the photograph. It can therefore be expected that a large degree of cycle to cycle variation would be reflected in the results. Even with a large number of data points with statistical averaging and smoothing, the results show a large degree of variation across the range. It is however encouraging that despite this, the detected difference between the fuels is larger than the deviation due to cycle to cycle variation. This confirms that the method is effective for the comparison of fuels, but could be improved by a high speed camera that could capture the full range over one cycle. The potential for a more in depth numerical analysis exists by accessing the raw data and comparing zones of equal flame area. The present system allows only a visual representation of the spatial flame temperature and soot concentration information.

A close study of figures 6-13 and 6-14 reveal that relatively low temperatures are detected in the area of the injector spray plume and higher temperatures occur further away from the spray. This can be explained by the onset of sooting combustion occurring at the head of the jet and the better mixing which occurs on the periphery of the combustion bowl. The soot

concentration image shows high soot concentration levels in the areas of low flame temperature. This is consistent with the theory that the rich fuel mixtures in the area of the injector spray result in high soot formation. As the soot burns and moves away from the fuel spray which is still driving in, the luminosity increases and consequently the flame temperature. The processed images presented are therefore consistent with conventional wisdom of the combustion process in a diesel engine. These images also reflect differences in flame area due to the turbulence in the combustion chamber. This is a weakness of the method as these differences become encapsulated in the results and are not entirely due to fuel property differences. This problem has been addressed in this project by collecting many images over the range and repeating them three times. It is then assumed that after statistical averaging and smoothing of the results that the effect of varying flame areas is less significant. The ability to process specific zones of images would further improve the results and is a feature of newer software developments by AVL, not available in this study.

The soot concentration results also show a distinct difference between the test fuels. The model fuel shows very high soot concentration levels after the premixed combustion phase. This result was also concluded by Ng et al. (2005) in the comparison of a synthetic bio diesel with conventional diesel using the two-colour method. The model fuel soot concentration results indicate further that the higher soot concentration levels than the reference fuel become similar and often lower in the after burn phase where it appears that the model fuel burns the soot more completely towards the end of the range. This is possibly due to the low aromatic content of the model fuel. This results in higher flame temperature areas and lower soot concentration areas with the model fuel at the end of combustion relative to the reference fuel, despite lower initial flame temperature areas. This observation is however not apparent in all of the data presented and is therefore not conclusive.

This observation could be used as a plausible explanation for the results presented in the literature review where similar model fuels were found to show significant improvements in both NOx and particulate engine out emissions. To reduce NOx emissions, one would expect lower peak cylinder temperatures, however to reduce particulate emissions one would expect that higher temperatures would be required to burn the soot more completely.
The results of this investigation would suggest that the model fuel achieved such desirable combustion properties more effectively than the reference fuel. The fact that this sort of in-cylinder combustion information can be revealed by this technique makes it a very promising method for further comparative fuel research.

The additional testing series in the Hydra engine revealed some interesting results. Many of these results were used to cross check the results of series 1 and are not actually presented individually. Series 3 proved to be an effective measure of the rate at which soot deposits form on the endoscope window and the corresponding effect on the measured temperature. While the results were not entirely consistent across the load range, the 50% load point results reveal quite convincingly that the model fuel showed no effect of soot build up on the window, where the reference fuel showed a slight drop in measured temperature as soot formed. It also appears that as the timing was retarded, the model fuel began to show effects of window sooting. At higher loads the sooting effect was similar between the fuels and significantly increased with load.

The visual comparison presented in figure 6-37 shows illuminated images of the fuel injector spray as injection begins. The brightness of the images is only a consequence of the flash light and the soot deposits on its lens. The interesting comparison lies in the shape of the injection plume. The model fuel appears to have a finer and more widely dispersed fuel spray. This is possibly due to faster vaporisation of the model fuel due to its distillation properties. This could result in better fuel mixing in the combustion chamber.

Figure 6-38 shows a similar investigation at the onset of sooting combustion. It is important to remember at this point that only sooting combustion is detected by this method and this is not representative of auto-ignition. The images show that sooting combustion begins in the vapours at the end of the injection plume and progresses around the periphery of the plume. Most of the flame area occurs at the end of the injector plume which develops into a large, round area of flame. No conclusive differences can be noted from the combustion; however the spray plumes seem to be slightly different. The spray plume of the model fuel appears to be more slender with a smaller cone angle. Considering that the white spray represented in the images indicate liquid fuel droplets, it can be speculated that the model fuel has vaporised more readily around the periphery of the spray plume. It is acknowledged that image analysis alone is not sufficient to be conclusive on these speculations.

At this point it is interesting to compare the images of the start of sooting combustion with figure 2-1 by Musculus and Cicone (2005) presented in the theoretical background. The images appear to be consistent regarding the area where sooting combustion begins. These images are also consistent with the Dec model for diesel combustion in a direct injection diesel engine. (Dec, 1997)

7.3. Discussion of the Combustion Bomb results

When analysing the results from the Combustion Bomb one must consider that there is no turbulence or swirl in the bomb as there would be in an engine. The large combustion chamber also reduces the effect of the spray plumes interacting with the wall. This is clearly shown in the images which show very neat and uniform spray plumes. The images make for an interesting visual comparison between the test fuels with the reference fuel being visibly brighter. It is also interesting to notice the combustion of the injector sac volume at the end of the image sequence. The numerical results from the bomb are presented in the same way as the engine results; however they are based on much fewer data points. The temperature results are very interesting and reveal information that is not as clear in the engine results, possibly due to turbulence.

It appears that large deviations in the temperature areas over the injection range could represent the different phases of combustion. The premixed combustion phase appears to be represented by a sharp rise in the initial temperature area results. This rise is larger and lasts longer for the reference fuel. The shorter premixed phase of the model fuel was discussed in the engine results section, but its effect is shown more clearly in the optical bomb results. Both fuels show a drop in the temperature area readings after some time and both rise again, possibly representing the mixing controlled combustion phase.
This is plausible considering the long injection duration of 1ms in the Combustion Bomb tests which is consistent with 100% load in the engine. The model fuel temperature areas remain lower than the reference fuel until injection stops. The model fuel registers higher temperature area results in the later stages of the range which is consistent with the trends observed in the engine. This adds credibility to the observation that although the model burns initially with lower temperature areas than the reference fuel, it appears to burn better in the latter stages of combustion. It is reasonable to speculate that this would result in better exhaust emission performance as suggested in the previous section.

The collective temperature results across the range are presented in a bar graph which is consistent with the engine test results. The model fuel has fewer pixels above the threshold temperatures than the reference fuel.

The soot concentration results show some trends that are similar to those seen in the engine. Initially the soot concentration of the model fuel is lower, but it rises above the reference fuel

as combustion progresses, although this appears to occur later in the bomb results than in the engine. Significantly the model fuel shows slightly lower soot concentration levels at the last data point than the reference fuel. It is encouraging that the Combustion Bomb results have to some extent verified the trends observed in the engine results and in literature.

7.4. Critique of the AVL image data analysis method

The results reveal that a great deal of information is contained in the images, and particularly in the processed images. Considering that each pixel in each image is assigned a specific temperature and KL value, it must be said that the presented method of extracting the numerical image data is disappointing. If the number of pixels above certain thresholds is the only numerical data that can be gained form this method, its usefulness for a detailed fuel comparison is considerably diminished.

If an array of data containing the temperature value of each pixel in the 640 x 480 image could be extracted, it would open up the possibility of significantly more detailed numerical comparison techniques. The following data analysis procedures would add considerable value to this method as a fuel comparison tool:

- A comparison of temperature and KL values within specific equal area zones of the flame. Spatial flame information could then be represented by generating average temperature or KL values for a number of zones in the spray plume. The effect of different flame areas would then be eliminated, thus directly representing true results.
- Numerical averaging of each pixel over a number of repeated images taken on different test runs. The current software can only do this for repetitions taken on the same test run.
- An image representing the difference in flame temperature or soot concentration between two fuels could be generated by subtracting the individual pixel values of two averaged combustion images of the test fuels.
- Representation of soot concentration directly as a volume fraction rather than the indirect KL value which is proportional to soot concentration.

A recently updated software package from AVL has the ability to do the abovementioned detailed data analysis, and is therefore essential to realise the full potential of the two-colour method as a technique for comparing fuels.

7.5. Comparison of the method applied in the engine and bomb

It is interesting to compare the virtues and shortfalls of the two-colour method applied to the engine compared to the Combustion Bomb. The main advantages and disadvantages of the two applications as experienced in this investigation are summarised below:

Advantages of the two-colour method applied to an engine:

- The ability to capture images consecutively over many cycles.
- Good statistical averaging over many data points.
- Very close proximity of the endoscope window to the flame.
- Genuine engine conditions.

Disadvantages of the two-colour method applied to an engine:

- Soot deposits form of the endoscope window over time and reduce its transmissivity.
- Turbulence and swirl in the combustion chamber vary the flame area from cycle to cycle resulting in erratic results.
- Only a small portion of the combustion chamber can be viewed.

Advantages of the two-colour method applied to the Combustion Bomb:

- The endoscope is not affected by soot deposits.
- No turbulence or swirl in the bomb results in very consistent images with similar and repeatable flame areas over a number of experiments.
- The entire combustion chamber can be viewed.

Disadvantages of the two-colour method applied to the Combustion Bomb:

- Only one image can be captured per experiment without a high speed camera.
- The endoscope is further away from the flame and on the outside of a thick sapphire window. Although sapphire has excellent light transmission properties, this could possibly cause a reduction in the measured flame temperature and soot concentration results.
- The combustion chamber is significantly larger than an engine resulting in a very small pressure rise due to the diesel combustion. This makes it difficult to compare and attach value to the resulting pressure data.
- Wall reflections from the stainless steel combustion chamber influence the image.

8. Conclusions

Based on the foregoing information and results, the following conclusions were drawn from this research:

- Combustion imaging can be conducted effectively in both an engine and Combustion Bomb in this laboratory and analysed by the two-colour method.

- This technique has proved to be effective for the purpose of comparing different fuels as significant differences were established in the results. Some of these differences can be explained by the fuel properties of the two test fuels, while some other differences observed hold possible new insight into in-cylinder combustion phenomena not yet fully understood.

- The optical results revealed that the reference fuel exhibited higher collective flame temperature areas over the combustion range; however the flame area at high temperature of the model fuel was found to be slightly higher in certain phases of the combustion range. Specifically this is at the start of combustion and generally after injection stops.

- The results obtained from the engine and the Combustion Bomb concur by demonstrating similar trends with respect to the difference between the two test fuels. The combustion bomb results verify the engine results to a large extent and hold additional useful information.

- A number of speculative conclusions were suggested in the discussion of the previous section regarding the differences observed between the two fuels. While this project is not a detailed study of the fuels themselves, these results confirm the potential of this method.

- The method of extracting the numerical image results used in this project contains little value compared to what can potentially be achieved with improved software abilities. The results presented are heavily dependant on flame area and reveal no spatial information of the flame structure.

- The ability to extract more numerical information from the processed images is limited by the lack of data access features of the software version used in this project. A more detailed fuel comparison could be achieved if the raw data assigned to each processed image pixel could be accessed.

- The engine test results are limited by soot deposits on the endoscope window. This is increasingly significant at higher loads.

- The combustion bomb results are limited by the relatively small number of images that can be collected in a reasonable amount of time.

9. Recommendations

While this project has been successful in achieving what it set out to do, it has highlighted areas that need to be improved to realise the potential of this method to compare and characterise different fuels more effectively using this technique.
On the basis of the above conclusions and results, the following recommendations are made to further improve the quality of the images and the data generated:

- Engine testing should be conducted at low loads only with the current system to limit the effect of soot deposits on the endoscope window.

- The combustion chamber design of the Hydra engine could be improved significantly to limit soot formation which would result in better flexibility of the optical system. It is recommended that the system be modified to represent a modern passenger car diesel engine. Specifically this would involve replacing the cylinder head with a four valve unit and a centrally placed injector and combustion bowl.

- Acquisition of ThermoVision Advanced V1.2 would improve the ability to process combustion images. Significantly it would enable images to be divided into specific zones of equal area and then process these zones separately. This would help to reduce the effect of cycle to cycle variation and differences in flame area. It also contains improved statistical functions and automation of the processing procedure. The ability to directly access the information contained in each pixel makes the potential data analysis unlimited.

- More data needs to be collected from the Combustion Bomb.
  This can be achieved by the acquisition of a high speed camera that is capable of capturing a sequence of images for each experiment. Alternatively consecutive experiments need to be conducted more quickly by an automated filling procedure.

- The repeatability of the bomb experiments can be improved by better metering of the fill pressures and a more accurate temperature control. The ability to accurately predict the temperature of the bomb at injection needs to be further developed.

10. References

Agnew W.G. (1961) *End Gas Temperature Measurement by a Two-Wavelength Infrared Radiation Method,* SAE Transactions, volume 69, pp 495.

AVL Austria (2001) *Spectral Flame Temperature Measurement Using the Two Colour Method*

Azetsu A. et al. (2003) *Effects of Aromatic Components in Fuel on Flame Temperature and Soot Formation in Intermittent Spray Combustion,* SAE Paper 2003-01-1913.

Bakenhus M., Reitz R.D. (1999) *Two-Color Combustion Visualization of Single and Split Injections in a Single Cylinder Heavy Duty D.I. Diesel Engine Using an Endoscope-Based Imaging System,* SAE Paper 1999-01-1112.

Cengel Y.A., Boles M.A. (1998) *Thermodynamics: An Engineering Approach.* (3rd edn.) McGraw-Hill, pp-767.

Challen B., Baranescu R. (1998) *Diesel Engine Reference Book* (2nd edn.) SAE International.

Dec J.E. (1997) *Conceptual Model of DI Diesel Combustion Based on Laser Sheet Imaging,* SAE Paper 970873

Ferguson C.R., Kirkpatrick A.T. (2001) *Internal Combustion Engines – Applied Thermosciences 2nd Edition*, John Wiley and Sons

Friess W., Herrmann H.O., Maly R.R., Schnell M., Schaberg P., (2003) *Reductions in Exhaust Emissions with GTL Diesel Fuel,* VDI-Berichte 1808

Hampson G.J & Reitz R.D. (1998) *Two-Colour Imaging of In-Cylinder Soot Concentration and Temperature in a Heavy Duty DI Diesel Engine with Comparison to Multidimensional Modelling for Single and Split Injections,* SAE Paper 980524.

Heywood J.B. (1988) *Internal Combustion Engine Fundamentals*, McGraw-Hill.

Kweon C., Okada S., et al. (2003) *Effect of Fuel Composition on Combustion and Detailed Chemical/Physical Characteristics of Diesel Exhaust*, SAE Paper 2003-01-1899, JSAE Paper 20030098

Matsui Y et al. (1979) *A Study on Time and Space Resolved Measurement of Flame Temperature and Soot Concentration in a D.I. Diesel Engine by the Two-Colour Method,* SAE Paper 790491.

Miller G. (2003) *Personal communication and unpublished work*

Millikan R.C. (1961) *Measurement of Particle and Gas Temperature in a Slightly Luminous Premixed Flame*, pp. 535

Musculus M. & Cicone D. (2005) *Imaging of Advance Low Temperature Diesel Combustion,* Sandia National Laboratories, CRF News, Vol. 27, No. 5.

Ng H, Ciatti S, Miers S, Biruduganti M, (2005) *Comparing the Performance of SunDiesel™ and Conventional Diesel in an LD Vehicle and Engines,* Argonne National Laboratory

Payri F, Arregle J, Fenollosa C, Belot G, Delage A, Schaberg P, Myburgh I, Botha J. (2000) *Characterization of the Injection-Combustion Process in a Common Rail D.I. Diesel Engine Running with Sasol Fischer-Tropsch Fuel.* SAE Paper 2000-01-1803.

Ratshikuni M. (2003) *Personal communication and unpublished work*

Schaberg, P.W., et al. (1999) *An Overview of the Production, Properties, and Exhaust Emissions Performance of Sasol Slurry Phase Distillate Diesel Fuel.* 2nd International Colloquium on Fuels, Technische Akademie Esslingen.

Schaberg, P.W., Myburgh I, Botha J.J. (2000) *Comparative Emissions Performance of Sasol Fischer-Tropsch Diesel Fuel in Current and Older Technology Heavy Duty Engines*, SAE Paper 2000-01-1912.

Schaberg, P.W. et al. (2002) *Exhaust Particle and Size Distributions with Conventional and Fischer-Tropsch Diesel Fuels*, SAE Paper 02FFL-216.

Schaberg, P.W. et al. (2005) *Emissions Performance of GTL Diesel Fuel and Blends with Optimized Engine Calibrations*. SAE Paper 2005-01-2187.

Schack, A. (1925) *Temperaturdifferenz Zwischen Flamme und Kohlenstoffteilchen,* Z.Tech. Phys, 6-10, pp. 530

Shiozaki T. et al. (1998) *The Visualization and its Analysis of Combustion Flame in a DI Diesel Engine,* SAE Paper 980141.

Signer M. et al, (1996) *European Programme on Emissions, Fuels and Engine Technologies (EPEFE) – Heavy Duty Diesel Study*, SAE Paper 961074.

Welberger P. and Cartellieri W.P. (1987) *Fuel Injection Combustion Phenomena in a High Speed DI Diesel Engine Observed by Means of Endoscopic High Speed Photography,* SAE Paper 870097.

Zhao H., Ladommatos N. (2001) *Engine Combustion Instrumentation and Diagnostics,* SAE International.

Appendix 1

Additional operating instructions for the AVL Visioscope.

The basic operating procedures for the hardware and software are detailed in the supplier's manual. The following essential details are not clear in the manual and have been established through experience gained in this project and support from AVL.
Some of the information here is specific to the Sasol Advanced Fuels Laboratory test rig used in this project.

1) Triggering the correct cycle

The Visioscope relies on accurate crank angle information to trigger the camera at the correct times as specified by the user. The Hydra engine is set up with an AVL crank angle encoder. This must be set to read at a resolution of 0.1° CA. The Trig and CDM lines must be connected to the light unit as indicated in the manual. The AVL Indiset 620 data acquisition system is also connected to this encoder via a separate cable.

In the Camera Control Dialogue, ensure that the trigger is set to 'light unit'

The trigger settings are done in the Light Unit Control dialogue:

The trigger can be set to 'Even', 'Odd' or 'Auto'. As the engine is operating a four stroke cycle. one cycle consists of two revolutions. The light unit cannot therefore ensure that it is triggering on the combustion cycle where the flames occur. If your record comes out completely black, it is because the camera has been triggered on the exhaust stroke.

Recommended procedure to avoid this:

Set the trigger to "EVEN"
Ensure that the AVL Indiset is running on oscilloscope mode
Take a small test record in the flame zone to determine if the cycle trigger is correct.
Unfortunately this first step is trial and error.
Once you have established whether the system is running on EVEN or ODD, you can continue testing on that setting provided that the AVL Indiset is not stopped. If you have to restart the Oscilloscope mode for whatever reason, simply switch over the trigger from ODD to EVEN or vice versa.

A tip to insure that the oscilloscope does not stop between lens cleaning breaks is to follow the shut down procedure below:

- Switch off injection
- Wind down speed to a stop quickly.
- Press the red STOP button immediately as the engine stops.

CAUTION: Without pressing the stop button, the engine will still tend to turn very slowly, even when the speed dial is at zero. This can be very dangerous when removing the endoscope.
Never leave an endoscope, plug or light probe in the engine unsecured. If the engine turns it will become a dangerous high speed projectile.

- When the endoscope is ready again, press the green START button
- Wind up the speed immediately
- The Oscilloscope should resume normally without user input.

If it needs to be manually started, the cycle trigger has been reversed.

There is however a function of the Light Unit that can determine the correct cycle automatically, but it requires a cylinder pressure signal to be connected to the ANALOGUE IN socket of the light unit. If this is available, set the trigger to 'Auto'.
I have found this to be unreliable and recommend the manual method described previously.

2) Endoscope Cooling

While the importance of endoscope cooling is clearly described in the manual, some further notes should be observed. There is a safety circuit to ensure that there is an adequate air pressure supply for the cooling of the endoscope when in use. This is wired to the emergency stop switch on the engine bed. There is a switch on the engine bed table to bypass this system when the Visioscope is not in use.

NB: This system only ensures that there is air pressure. You still need to manually open the endoscope tap to have air flow through the endoscope. To make this system 'fool proof' a safety system that requires air pressure and air flow will have to be developed.

It is advisable to have air flowing at all times when the endoscope is in the engine. Do not leave it in a stationary hot engine or let the engine run for extended periods with the endoscope in place. It takes about 30 seconds before the window is completely covered in soot, therefore it is unnecessary to expose the endoscope to combustion temperatures for any period exceeding this.
Even with cooling air, the endoscope gets quite hot.

3) Creating a reference image for ThermoVision:

The manual indicates that a dark level image should be used as a reference image for the ThermoVision image processing functions.

A dark level image is an averaged image which shows an image without flames in order to subtract the camera noise when there is no light displayed on the camera sensor. Camera noise is related to the sensor temperature of the camera in the test bed.

Create a record of dark level images after you have recorded the flame images with the running engine. This can be done either at exhaust TDC or at a crank angle when there are no flames in the combustion chamber. The following procedure is recommended:

- Name: Dark Record
- Set the recording start angle to -100 CAD
- Tick the "Single" checkbox
- Specify 25 repetitions

You now have a record of 25 dark images. Create a single averaged image from this by using the image processing function "Average from Repetitions"
Save this image as your reference image and use it for thermo graphic analysis of the images taken at the same time and operating settings. The Flame Temperature Measurement Program will ask you to specify a reference image.

4) Saturation and exposure

One of the critical requirements for thermo graphic analysis is that the images must not be saturated. Saturated zones will be calculated at a temperature of over 3000K.

It is however important that the exposure time be set as high as possible before saturation occurs. This needs to be done by trial and error to determine the best useable exposure for a particular setting.

Be careful to check all three colours for saturation. The intensity histogram gives an average of the colours which can be misleading. Red usually saturates first and should be checked. Alternatively the 'Detect Saturation' function can be used to display saturated zones in bright pink. This works even if only one colour is saturated.

As you mouse over the picture, the intensity for each colour is shown in brackets beneath the image An intensity of 4095 is saturated.

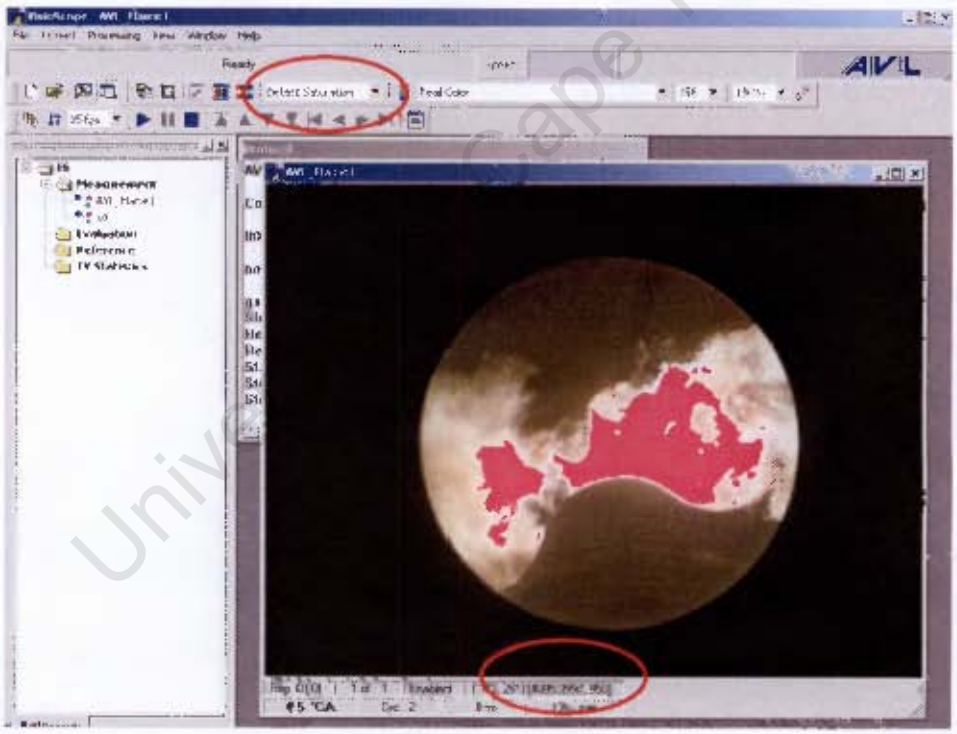

Figure A1-1: Detecting image saturation

5) Calibration

Be aware that there is a different calibration file for each combination of endoscope and camera lens. These files are on the Visioscope CD in folders indicating for which endoscope and lens they are for. Depending on your particular choice, copy the correct calibration file into the C-drive root directory of the computer.

This file is used when running the ThermoVision calibration function, which needs to be done for each record before the Diesel Flame Temperature function can be used.

When using the Diesel Flame Temperature function, you are presented with an option to 'Add detailed calibration info.' If ticked, this will add the calibration information to the protocol window of the temperature record. This is also saved as a text file amongst the images. This is recommended as you can then check if the correct calibration file has been used. It will indicate which endoscope and lens it is calibrated for.

NB: The calibration files issued with Visioscope Version 1.0 are inaccurate!

The older calibration file (V1.0) uses an intensity threshold of 800 instead of the more reasonable 64 of V1.1. (This is a bug of V1.0). With this high threshold many valid data points are disregarded, which skews the calibration statistics and leads to different calibration values and therefore a shift in the temperature field. The shift amounts to about 150 - 200°K. *(The calibration files in Version 1.2 are the same as Version 1.1.)* The error was discovered in this project and a comparison of the effect is illustrated below for the same flame image:

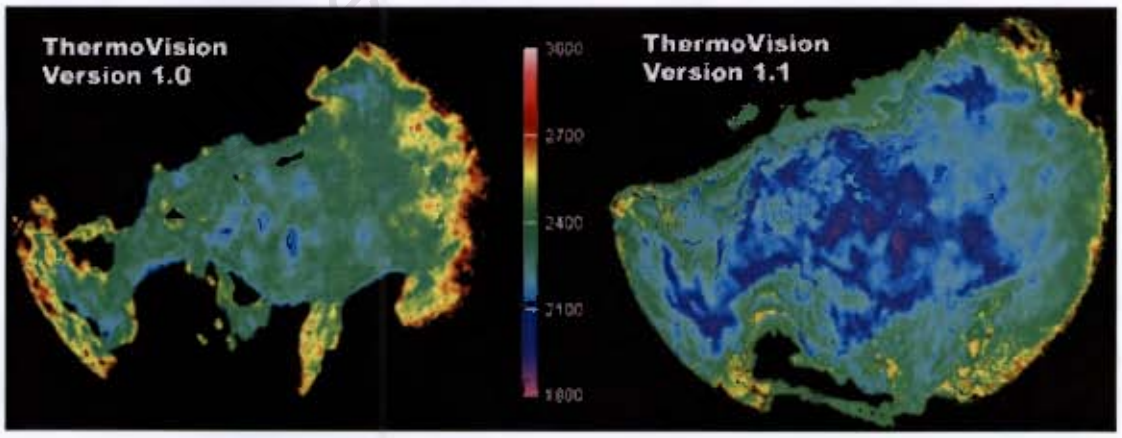

Figure A1-2: The effect of the bug in Thermo Vision 1.0

6) Dynamic Temperature Quantification

When using the Diesel Flame Temperature function, in the same dialogue box as the above calibration information, you are presented with an option: 'Dynamic Temperature Quantification' There is no reference to this in the manual.

This function does not affect the average temperature values but will change the extreme high and low values. As detailed in the next point, temperature values are averaged into 7 classes. The effect of Dynamic Temperature Quantification is that.

- The lowest values are raised to the nearest partial average
- The highest values are lowered to the nearest partial average

This will affect the histogram data and the temperature pictures. It is recommended not to use this function for normal analysis. An example of the effect is shown below:

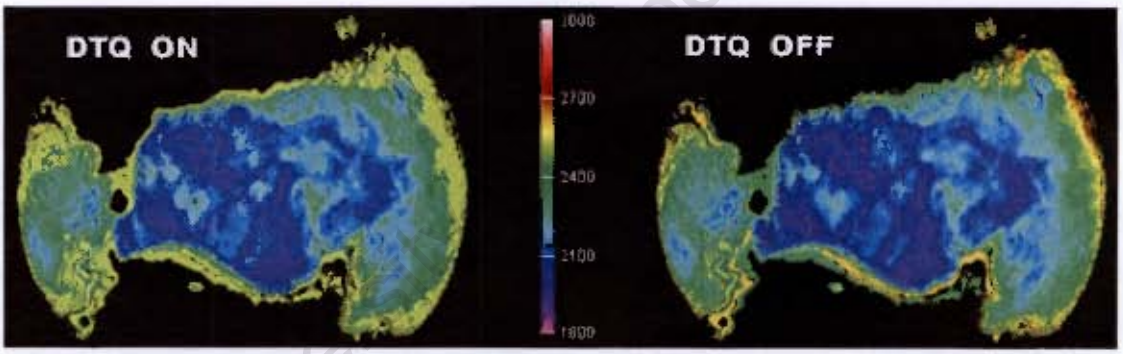

Figure A1-3: The effect of Dynamic Temperature Quantification

7) Understanding the ThermoVision temperature output.

Initially the Diesel Flame Temperature is displayed for each image in seven columns with the heading T1 to T7. This refers to the following:

- T1 indicates the mean temperature value in Kelvin of the coldest 15%
- T2 indicates the mean temperature value in Kelvin of the next 15%
- Continues as above
- T7 indicates the mean temperature value in Kelvin of the hottest 15%

8) Processing more useful data

The image processing Histogram function can be used on any image. You are asked to specify and starting point, ending point and number of steps. The output is the number of pixels at a certain intensity. This is arranged in columns depending on your input at the beginning.

For a temperature image this function can still be used. Although it still indicates intensity, it is actually working in degrees Kelvin. This is indicated nowhere in the manual or software. but has been confirmed by Peter Werlberger of AVL.

For example: Set the starting point to 2000. the end point to 2800 and specify 16 steps.
The histogram will give neatly spaced columns of 50°K from 2000 to 2800 and will contain the number of pixels in that temperature zone.
Similarly for soot concentration images, "intensity" actually refers to the soot concentration factor, KL.
Unfortunately this data cannot be exported directly to Excel™, but can be saved as a text file. This can then be imported to Excel™ by the process: Data > import external data > import data. Some rearranging will be necessary.

9) Using an external trigger

The triggering software of the Visioscope is specifically designed for an engine using information from a crank angle encoder. To capture an image in the Combustion Bomb, the camera needs to be triggered by a single pulse to capture a single image of the once off combustion event. The best way to do this is to develop an external trigger source and connect it as follows:
Unplug the cable 'CamTrig' from the Light Unit socket (X20)
Connect trigger signal to the cable CamTrig.
The signal must be TTL (transistor-transistor-logic), active high
A pulse of 5v and 1ms duration is usually used.

The measurement setup is: 0 Repetitions, Single ON

After pressing the record button, the camera will wait for 30 seconds in which time the signal must be activated to capture a single image. If no signal is received, the "Time out" error message will be displayed.

Appendix 2

Design modifications to the Hydra Engine

For the purpose of comparing fuels, the accuracy of the IMEP measurement is critically important. The AVL Indiset data acquisition system uses the pressure signal to calculate IMEP and thus relies on a smooth and accurate pressure trace. Previous to this project an uncooled Kistler pressure transducer was used and its performance was inadequate for reliable IMEP measurement.

1. Pressure transducer selection

A direct injection diesel engine results in a very high pressure and temperature environment for a pressure transducer to work in. It is highly recommended to select a water cooled piezoelectric quartz pressure transducer for best results.

AVL has a wide range of such instruments and some are specifically designed for heavy duty diesel engines. The following pressure transducer was selected for use in these tests:

AVL QH32C Quartz Pressure Transducer

Sensor for heavy duty application

Diesel/Gas engines

AVL	*Measurement Range*	*Sensitivity*	*IMEP Stability*	*Linearity*
	Bar	**pC/Bar**	**%**	**%**
QH32C	0....200	26.69	< 1.5	< +/- 0.2

2. Fitting the transducer in the engine

The smallest cooled transducer, as selected here, has a diameter of 10mm. This is significantly larger than the sleeve in the original Hydra engine design allows. In order to fit this pressure transducer, the cylinder head had to be removed and a larger sleeve designed.

The sleeve for the pressure transducer passes through the water jacket and enters the combustion chamber. A larger sleeve would require a larger bore though the cylinder head which had to be carefully designed so not cause a water leak into the combustion chamber.

The opening space in the combustion chamber is also limited as it is very close to the exhaust valve.

The original drawings were obtained from Ricardo to ensure that a larger sleeve could be safely incorporated into the cylinder head. The sectional drawing below illustrates how the sleeve passes through the water jacket.

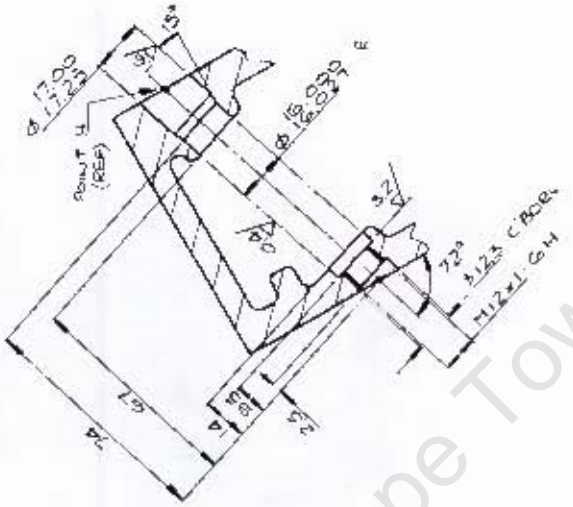

Figure A2-1: Original Cylinder head drawing

Figure A2-2: New pressure transducer sleeve

Given the constraints of the cylinder head a larger sleeve was designed and manufactured in Stainless Steel grade 316. The sleeve seals by means of a copper washer at the bottom and a double O-ring on the top. After careful machining of the cylinder head, the sleeve was fitted. With the sleeve in place, the pressure transducer can be easily fitted and removed.

The image below shows the sleeve and pressure transducer fitter in the cylinder head. Valve stem seals were sourced and fitted as they were not fitted as a standard item on the Ricardo Hydra. The design was successful and resulted in a vastly improved pressure signal. An example of the resulting pressure trace is also shown. It is however acknowledged that the pressure transducer still enters the combustion chamber at an angle. This results in a wedge shaped void between the pressure transducer and the cylinder head surface. Due to space constraints it is also exposed to the squish zone and not the piston bowl. These compromises result in the level of noise that is still apparent in the pressure trace.

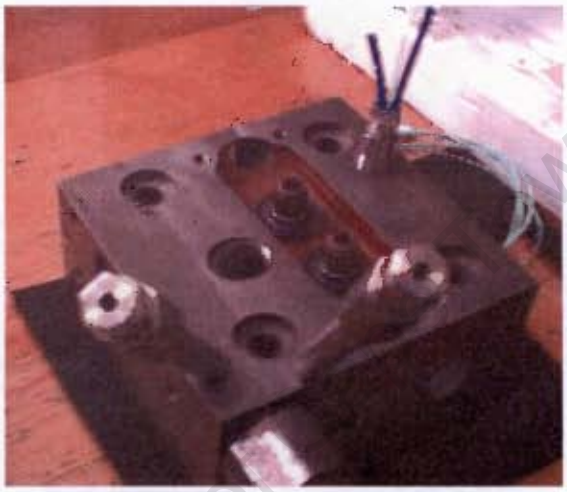

Figure A2-3: Modified cylinder head with optical sleeves and pressure transducer

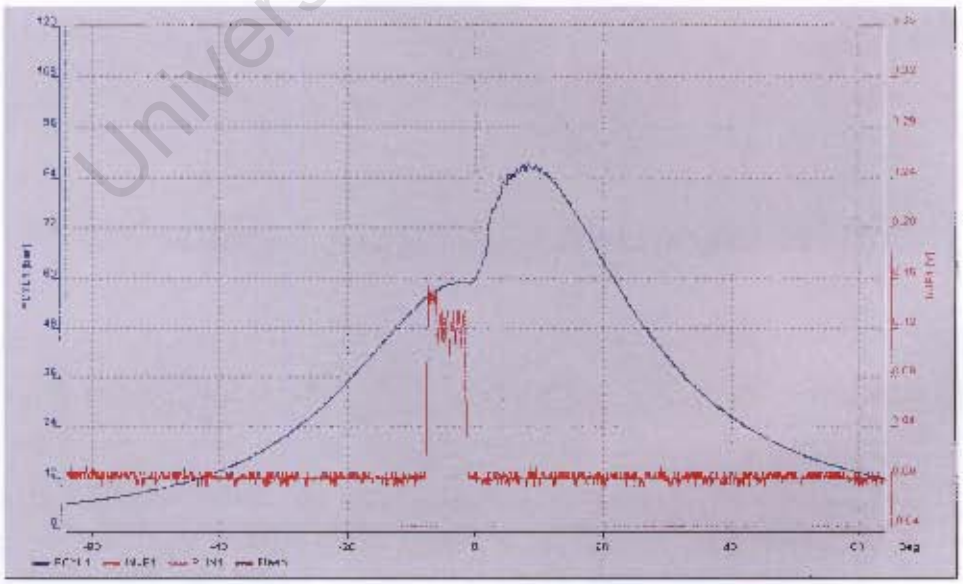

Figure A2-4: Example of the resulting pressure trace

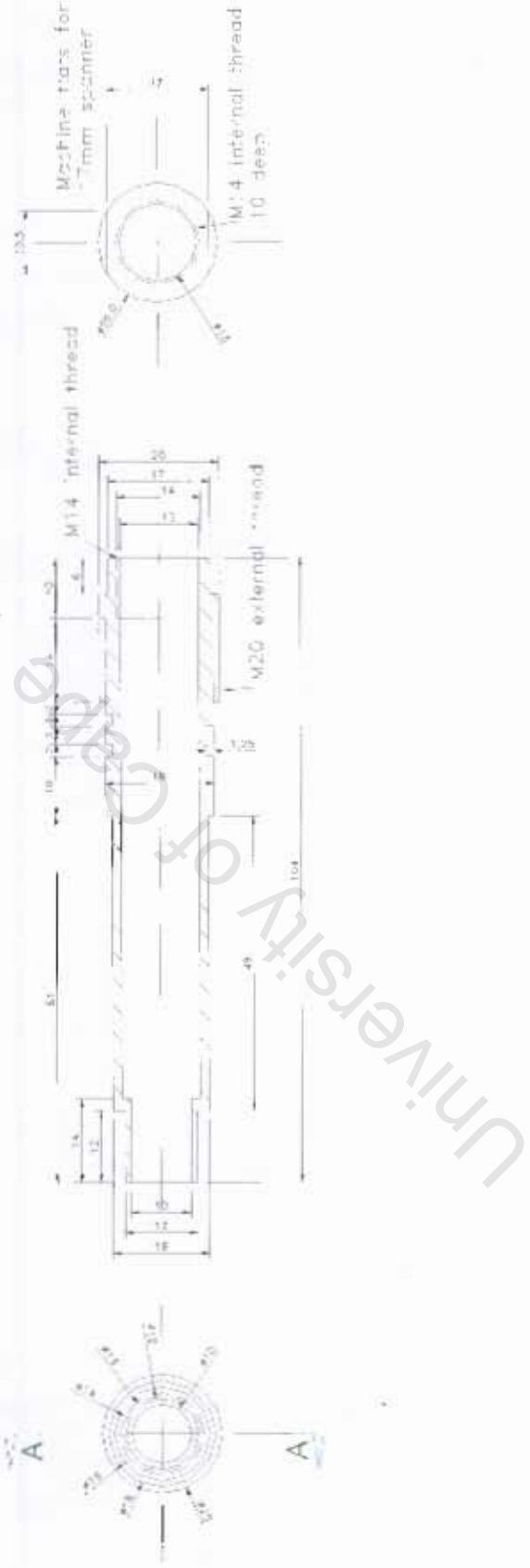

Figure A2-5: Detailed drawing of the pressure transducer housing sleeve

Appendix 3

Design modifications to the Combustion Bomb

The Combustion Bomb was designed and built at the Sasol Advanced Fuels Laboratory as a previous MSc project. This project was however incomplete at the time when it was required for the testing work in this project. This project therefore involved some design and a lot of final development work to commission the bomb in a suitably working order. The main tasks are described briefly below:

The bomb was relocated, set up and re-wired in a professional manner.

The exhaust valve was changed from a needle valve to a ball valve and proved to seal better and last longer. It remains however a weak point of the bomb as it requires maintenance periodically.

A five way gas selection switch valve was incorporated to streamline the filling procedure. This eliminated the need to manually couple the separate gas pipes to fill the bomb for each experiment. Although the process is still manual, it is now considerably easier and quicker to operate.

The control system of the electric motor driving the high pressure fuel pump was re-designed to eliminate electromagnetic noise that was interfering with the instruments.

An electronic system was required to trigger the camera as no crank angle encoder signal was available to input to the VisioScope. Furthermore the system had to be variable such that the camera can be triggered at incremental points during the diesel combustion process in order to capture a sequence of images.

An electronic circuit was designed and built which used the injector signal as an input. A variable resistor is used to adjust the delay after the injection signal before a trigger signal is given as an output to the VisioScope. This system proved to work very well and the 10ms range allows the entire combustion range to be captured.
An accurately marked manual dial with a time scale was fitted to the Combustion Bomb control panel which allowed for easy and repeatable adjustment of the delay.

The circuit diagram of the camera trigger device is given below.

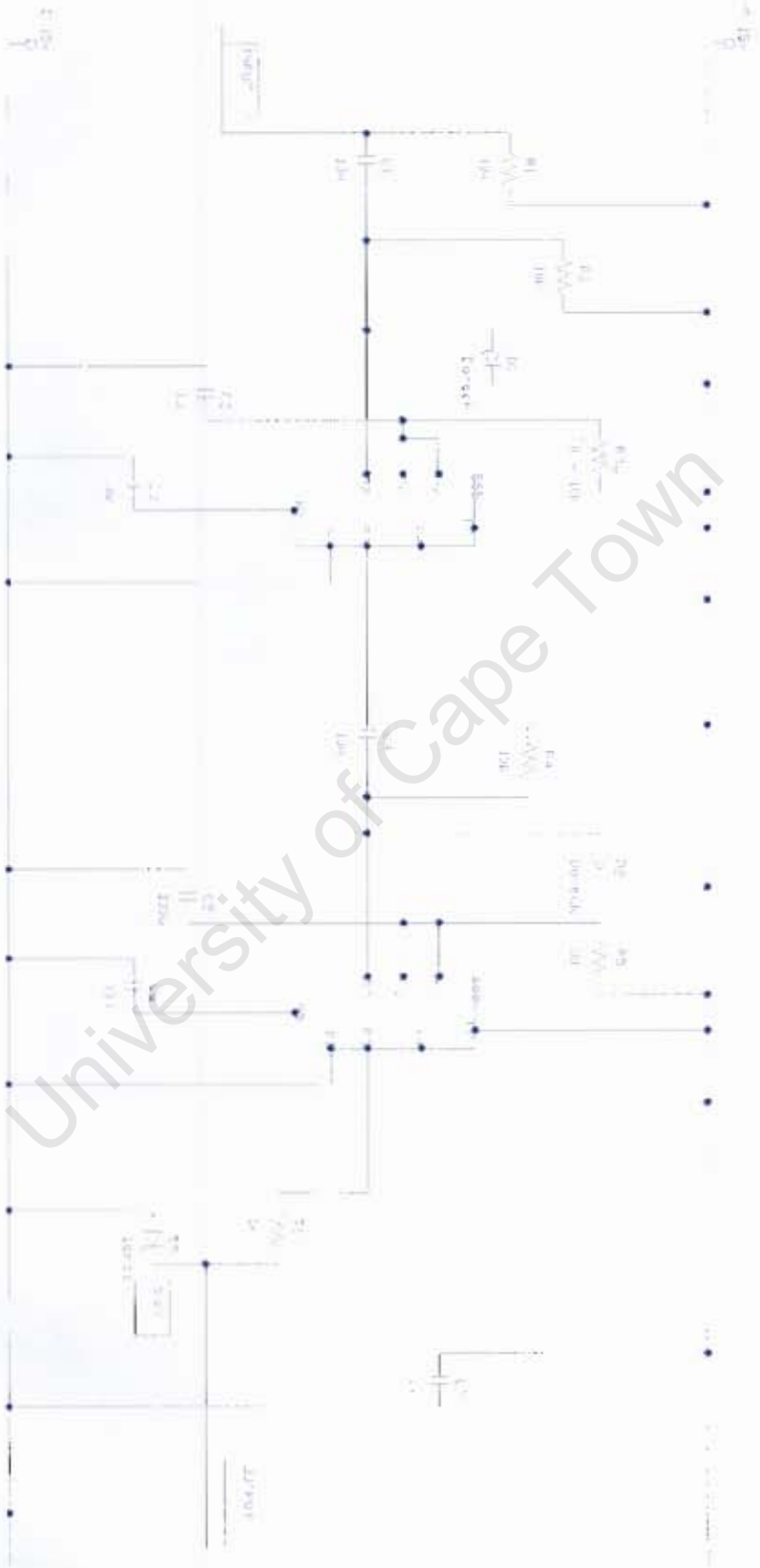

Figure A3-1: Circuit diagram for the Combustion Bomb camera trigger